Field Evaluation and Hyperspectral Imagery Analysis of Fire-Induced Water Repellent Soils and Burn Severity in Southern Idaho Rangelands

Charles D. Finley, Idaho State University, GIS Training and Research Center, 921 S. 8th Ave., Stop 8104, Pocatello, Idaho 83209-8104

ABSTRACT
This study utilizes spectroscopy and field analysis to classify and detect burn severity and fire-induced soil water repellency following a rangeland wildfire in Southern Idaho. To map the distribution of burn severity and water repellency, hyperspectral imagery was collected over the study site and classified with the Spectral Angle Mapper (SAM) and Mixture Tuned Match Filtering (MTMF) algorithms. Prior to the analysis, burn severity was assessed at the study area, and water repellency was evaluated with a mini-disc infiltrometer (MDI) and the water drop penetration test (WDPT). Field information was recorded with a GPS and used as training data for the spectroscopic classifications.

Analysis of the field data indicated significant increases in water repellency with respect to increasing burn severity, but repellency decreased in high severity areas. The SAM classification correctly classified low severity shrub and grass areas, as well as high severity grass areas with producer's accuracies between 74% and 92%, but the differentiation of moderate and high burn severity areas was ambiguous, resulting in producer's accuracies between 39% and 54%. A MTMF classification of soil water repellency resulted in a representative map of soil water repellency distribution. The analysis techniques conducted in this project signify spectroscopy to be beneficial for differentiating soil characteristics and fire severity classes in burned rangeland areas, where mostly bare, spectrally homogenous soils exhibit slight changes in reflectance.

KEYWORDS: remote sensing, fire, wildfire

Introduction and Background

Statement of Problem

Wildland fires are a naturally occurring phenomenon throughout the rangelands of the Intermountain West. The physiology of the vegetative communities and the hot, dry summer climate make the region extremely susceptible to fire. Frequent occurrences of dry lightning storms regularly ignite wildland fires in the rugged western country. Rangeland ecosystems have adapted to the frequent occurrences of fire in such manners as regulating the buildup and decomposition of litter and organic matter (DeBano et al., 1998). Wildland fires have been documented to increase forage production of rangeland grasses by reducing the cover of sagebrush and other shrubs (Raper et al., 1984).

As a result of the natural occurrence of fires, vegetative communities exhibit fire regimes, which refer to the nature of fire occurrences over time in an ecosystem, as well as the short and long-term effects (Smith, 2000). Natural and human-influenced alterations like climate change, invasive species, and increased fuel loads can lead to variations in an environment's natural fire regime, often resulting in an increase of severe fire events. These events, whether accelerated or naturally occurring, can destroy litter accumulation and organic layers on forest and rangeland floors, and induce or enhance soil water-repellency, which leads to increased soil erosion, watershed degradation, flooding, and debris flows (DeBano, 2000). Severe fires can alter entire ecosystems by wiping out vegetation stands, displacing and killing wildlife, inflicting damage to organic soil layers, restricting plant regeneration, and forcing the environment to deviate from its original fire regime (Odion et al., 2004).

A significant factor influencing erosion, sedimentation events, and watershed processes after wildfires is the presence of water repellent layers within the soils. Past research has indicated that the formation of soil water repellency after fires is a result of several factors, including fire behavior, temperature and burn severity (DeBano, 2000). The severity of a wildland fire describes the consequences of a fire on the soils, vegetation, and ecological processes of the affected area (DeBano et al., 1998). Though the comprehensively described severity of a wildland fire includes its effects on soil, the post-fire soil characteristics and subsequent ecological and physical processes are a causal effect of the temperature and intensity at which vegetation, litter, and organic material burns. Therefore it is important to assess the components of burn severity and soil water repellency independently of one another, as well as comprehensively. The independent assessment of these factors is necessary for susceptibility modeling of wildfire areas, particularly in assessing debris flow and increased sedimentation risks, which are common problems associated with wildfire-affected areas.

This project consists of two components: a field regimen that assesses the severity, or ecological alteration of the landscape, caused by a rangeland wildfire, and its cause-and-effect relationships with fire-induced soil water repellency. This study also develops a method to extract spectral signatures of burn severity classes and water repellent soils from high spectral resolution imagery to classify and map these parameters in a rangeland wildfire setting at a landscape scale. The use of hyperspectral imagery for mapping soil effects of wildfires in rangeland areas provides a detailed window into the subtle changes of spectra among ground targets in arid landscapes. Certain fundamental problems have been noted by past researchers when applying remote sensing techniques in arid areas; these include a high background soil reflectance that crowds out the contribution of vegetation and other spectra (Okin et al., 1999b), and the tendency for desert vegetation of the same species to often have high spectral variability (Okin et al., 2001). Through field assessments of wildfire burn severity and soil water repellency, coupled with statistical tests, and subsequent hyperspectral spectroscopy analysis, this research project evaluates the effects of fire-induced soil water repellency in a rangeland environment. The two hypotheses of this study are (a) water repellency will be evident to the highest degree in areas of moderate burn severity and (b) hyperspectral spectroscopy will discern water repellent soils of varying degrees, as well as wildfire burn severity classes, in a rangeland wildfire area.

Past studies of relationships between wildfire severity and soil water repellency have indicated higher repellency is found in moderate burn severity areas due to extended burn times and temperatures (Davis and Holbeck, 2001; DeBano, 2000; Lewis et al., 2004). The majority of the described research, however, has been conducted in Rocky Mountain West forested ecosystems, where the dominant vegetation is pine and conifer stands, and soils tend to be shallow, rocky, and poorly developed. This study was conducted in the Clover fire area of the southern Idaho rangelands, within which the primary vegetation is sagebrush and grass and the soils are composed of loamy sands to clays, typically derived from basalts and rhyolites, with varying depths of wind-blown loess deposits (Wright, 1985). Because of inherent ground and climatic conditions, soils in these areas often exhibit slight water repellency even in the absence of fire. Based on the principles of fire temperature and residency times as described by DeBano (2000), this research project similarly hypothesizes that rangeland soils will exhibit highest incidences of water repellency in areas of moderate burn severity, and lowest occurrences in low severity and unburned areas. Soils in high burn severity areas will display inconsistent and variable rates of water repellency, because of rapid burn times that may not burn vegetation long enough to release water repellent compounds, or because the fire may burn so hot that water repellent compounds break down altogether (DeBano, 2000). In addition to field analysis, this research project involves mapping and classifying burn severity and soil water repellency with hyperspectral images, also known as spectroscopy. Our hypothesis predicts that spectroscopy will discern burn severity and water repellent soils of varying degrees within rangeland wildfire areas. While the spectroscopy of a rangeland fire area is expected to evaluate the burn severity, the most challenging portion of the analysis is the assessment of fire-induced soil water repellency based on the spectral characteristics of the soil. By evaluating the spatial distribution and relationships of soil water-repellency and burn severity with field methods and spectroscopy, this research will provide insight into the dynamics of rangeland wildfire, which are exceedingly unique in comparison to wildland fires of forested ecosystems. The objective of this project is not to craft a comprehensive model of post-fire erosion susceptibility, but to facilitate standardization of methodologies for precisely assessing the input variables of rangeland burn severity and soil water repellency. This methodology will provide a tool for assessing field variables on a landscape scale with remote sensing imagery. By standardizing the classification and assessment of variables, rangeland managers can more effectively evaluate post-fire effects, and input parameters for susceptibility modeling can be more specified.

Study Area

The primary study area for this project is the Clover Fire area (Fig. 1.1), approximately 39 km west of Twin Falls, Idaho, USA. The Clover fire was a lightning-caused rangeland wildfire, ignited on 15 July, 2005 and contained on 20 July, 2005. The fire boundary encloses 192,846 acres (~ 780 km^2), and was the largest wildland fire in Idaho in the 2005 fire season. It extends from Salmon Falls Creek at its eastern boundary, about 8 km west of Castleford, ID, in a northwesterly direction into the Saylor Creek Air Force Range at its western boundary. The elevation of the study area ranges from around 750 m in the northern lowlands, to 1355 m atop Castleford Butte in the southeastern portion of the fire boundary.

The fire boundary is primarily on BLM land, and is adjacent to the Bruneau Desert. Several irrigated farm fields are on the northeast boundary of the area, and the northwest end of the fire boundary is in the Saylor Creek range, a tactical target range utilized by the US Air Force. The topography of the study area is characterized by flat, shallow drainages, bordered by gradually-sloping buttes and ridges.

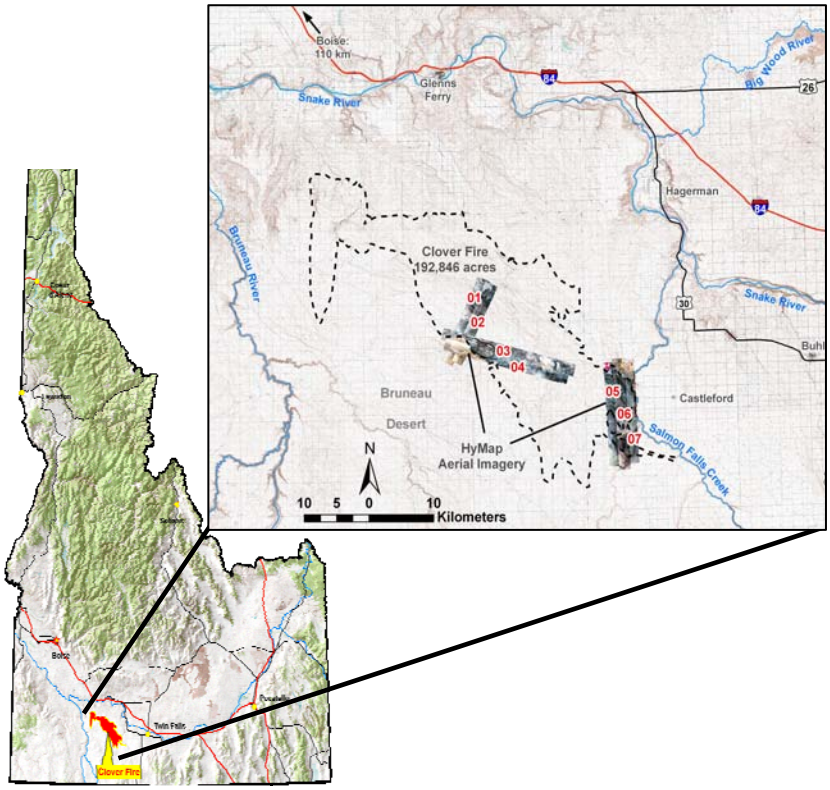

Figure 1.1. Clover fire, Idaho, with hyperspectral flight

Intermittent stream beds lie in steep gullies feeding Salmon Falls Creek and the intermittent Saylor Creek. Pre-fire vegetation within the burn area ranges from seeded areas of crested wheatgrass in the northern end, to dense sagebrush in the southern end. Cheatgrass is abundant throughout the sagebrush areas. Soils range from sandy, gravelly loams in the northern end to silt and loam throughout the middle section. The southern end of the fire boundary is typified by deep silt loam soils. Basaltic rock outcrops are located throughout the study area and along the gullies and stream canyons. The Clover fire area was susceptible to debris flows and excess sedimentation after the fire in the case of heavy rainfall. No significant rain events were observed in the area, however, for at least three months following the fire (Appendix 2).

The field sampling and remote sensing classification took place within 3 sections of designated flight lines inside the study area. HyMap hyperspectral imagery was collected over these sections on August 26, 2005. The 3 sections cover 175 km^2, of which 117 km^2 are inside the burn area, encompassing approximately 15% of the burn area. The slope within the sampling boundaries ranges from 0° to 57°, with the mean slope being 3°. In addition, several canyons and gullies have vertical cliff walls up to 30 m in height.

The study area was chosen based on previously-determined criteria. Personal communications with various experts in the field of wildfire research in Idaho (F.Pierson, USDA Agricultural Research Station; P. Robichaud and C. Luce, USDA-Forest Service Rocky Mountain Research Station), all concur that it is best to assess fire areas for water-repellency as soon after the fire as possible. DeBano (2000) indicates that low severity fires, particularly prescribed burns, exhibit fire-induced water-repellency for less than one year, but water-repellent layers in moderate and high severity wildland fire areas can persist for several years after a fire. Wildland fire areas tend to have excess fuel build-up, in contrast to prescribed burn areas, which cause the fires to burn hotter and with greater volatility. Wildland fires tend to burn during the hottest and driest times of the summer months, and typically burn in steep, often unstable watersheds. In contrast, prescribed fires are typically held in calm weather conditions in the spring or fall season, and the boundaries are controlled so as not to allow the fire to extend uncontrollably into steep, highly erosive basins.

The extent and amelioration of water-repellency is dependent on treatment, including seeding, mulching, mechanical, and chemical treatments, as well as natural responses, particularly meteorological events. Intermountain rangeland environments are known to receive intense thunderstorms during the summer months (Wondzell and King, 2003), that, dependent upon rainfall intensity, can initiate excessive erosion or debris flows and erode water-repellent soil layers (DeBano et al., 1998). Though some rainfall was

recorded in the study area**,** most erosion occurred as a result of severe windstorms between September 1, 2005 and October 30, 2005. The windstorms occurred as a result of Pacific frontal weather systems moving east across the southern Idaho plains, and they developed large dust clouds after encountering the burned area (Fig. 1.2). As a result, scouring and aeolian transport of ash, soils and litter occurred. By late October 2005, the high plateau areas of the study area had experienced at least 4 severe windstorms and all of the topsoil, ash and litter had been removed, leaving only the hard, concrete-like calcic horizon. Because of the variable and unpredictable nature of wildland fire environments, assorted degrees of fire-induced water-repellency were expected at the site, as well as areas of high, moderate and low severity burns. These variable characteristics of the Clover fire provided a reasonable study site for this research project.

Fig. 1.2. A dust storm moves across the Clover fire area, Sept. 16, 2005.

Rangeland Ecosystems

Rangelands have been classified throughout the world, in an agricultural sense, as areas suitable for livestock forage and habitat, yet not agricultural harvest. Covering approximately 50% of the United States, they can vary from forested areas and brushy hillsides to shrubby, near-barren desert land (Holecheck and Pieper, 2001). In the Western USA, rangelands have been typified as primarily public land that is allotted to ranchers for livestock foraging purposes. Public rangelands, however, serve a variety of purposes other than livestock holdings including ecological and wildlife preservation, multi-use recreation, and scientific research.

The vast rangelands of the Intermountain West cover approximately 700,000 km^2 (Knapp, 1995), and are bordered by the Cascade and Sierra Nevada mountain ranges to the West, and the Rocky Mountains to the East. This rangeland area is mostly within the Basin and Range geologic province, a region characterized by numerous fault-block mountain ranges extending in north-south directions, separated by wide flat valleys often wider than 75 km (Knapp, 1995). The physiography of Intermountain West rangelands is exemplified by dry, wind-swept plains, and steep rocky slopes. Precipitation ranges from 25 to 50 cm per year and the climate is typically considered semi-arid above 41° N, due to more frequent Pacific frontal systems, and arid below 41° N. (Knapp, 1995).

The Intermountain Western rangelands are further classified into zones based on vegetation and aridity (Holecheck and Pieper, 2001). The most arid rangeland zones are defined lying southeast and southwest of 41° N in the desert basins of Bonneville, in Central Utah, and Lahontan, in Western Nevada (Knapp,

1995). Vegetation in these areas is typified by shadsscale (*Atriplex confertifolia)* shrubs, horsebrush (*Tetradymia canescens)*, perennial ricegrasses (*Achnatherum hymenoides*) and annual cheatgrass (*Bromus tectorum)*. Primarily south of 41° N is the rangeland zone known as the big sagebrush semi-desert, a sparsely-covered, sagebrush-dominated region with some annual and perennial grasses (Knapp, 1995). North of 41° N is the sagebrush-steppe zone, characterized by semi-arid conditions and higher percentages of vegetation cover. Plant species include big sagebrush (*Artemisia tridentata* Nutt.) shrubs as the dominant overstory, perennial bunchgrasses like crested wheatgrass (*Agropyron cristatum)*, needlegrass (*Achnatherum nelsonii)*, Idaho fescue (*Festuca idahoensis* Elmer), and annuals such as the invasive cheatgrass and medusahead (*Taeniatherum caput-medusae)*. The largest contiguous region of sagebrush-steppe rangeland in the USA is located in eastern Oregon, northern Nevada, southern Idaho, northern Utah, and southwestern Wyoming. Most of the sagebrush vegetation in these locations is found at elevations ranging from 610 to 2135 m (Wright, 1985). Typical soils of sagebrush-steppe zones vary from loamy sand to silty clay, and are a mix of volcanic-derived basalts and rhyolites, as well as windblown loess deposits (Wright, 1985). In areas of higher elevation within the sagebrush-steppe, plant communities may be grass-dominated, often by cheatgrass, and intermixed with pine timber and Western Juniper (*Juniperus occidentalis)* (Knapp, 1995).

Dynamic rangeland environments are exemplified by communities of vegetation that include annual and perennial grass communities and populations of woody shrubs, and by exterior driving factors such as rainfall, fire and grazing by herbivores (Noy-Meir, 1973). The vegetation communities of rangelands are especially susceptible to fire because of drought, high temperatures and steady winds. Due to these factors, single fires within rangelands may easily extend over several thousand hectares when burning a virtually uniform fuel supply. Periodic occurrences of dry lightning storms ignite rangeland fires throughout the Intermountain West. Additionally, humans have utilized fire as a management tool for centuries. Early explorers of the United States West documented native inhabitants setting fire to the plains and forests as a method of enhancing wildlife forage quality by subduing shrubbery, improving access to plant foods, and facilitating travel by clearing underbrush in forests. Across grass and shrub lands, the natives would regularly ignite fires as a means of driving game for harvest. Fire was also an effective tool of communication and battle (Shinn, 1980). While it is well known that native inhabitants of the West definitely utilized fire as a multi-use tool, the extent and frequency with which it was used by the natives is unclear. This is because native populations were sparsely settled in many areas, due to the immense size of the region, and many areas contained meager resources (Shinn, 1980). Thus, certain areas of the Intermountain West likely have experienced more frequent intentional burning than others. Various researchers have attempted to determine the historical frequency of fire across the Intermountain West. Houston (1973) observed scars of tree rings to determine an average historical fire frequency of 32 to 70 years in northern Yellowstone National Park, and smaller plots within that area may have burned every 17 to 41 years. Natural fire-return intervals of lower elevation sagebrush stands may range from 50 years to as low as 100 years. (Whisenant, 1990; Wright, 1985; Young and Evans, 1981). Many plants within semi-arid rangelands have adapted to intermittent fires by developing means of fire resistance, and rangelands continually influenced by fire have become accustomed to lightning-caused and customary burns (Shinn, 1980; Smith, 2000).

After the settlement of western lands by European descendants, the established fire return intervals of the Intermountain West were disrupted due to careless burning by pioneers (Shinn, 1980), and eventual negative attitudes toward uncontrolled fires, leading to strategies of rapid fire suppression. When the federal government established forest reserves in the U.S. in 1891, a policy of total fire exclusion was adopted (Shinn, 1980). Other damaging elements of traditional rangeland fire regimes in the Intermountain West include: the swift introduction of the invasive annual cheatgrass (Whisenant, 1990); the expansion of Western Juniper, which has increased fuel loads and fire dangers in rangelands (Young and Evans, 1981); and disruption of grazing strategies due to the displacement of native herd animals by domestic livestock (Shinn, 1980). It is estimated that the average historic fire return interval of 35 to 100

years on Idaho's Snake River Plain has been reduced to 2 to 4 years due to the increased fine fuel load of cheatgrass populations and the impact of livestock (Whisenant, 1990). This was determined by examining the records of known fire history and regenerative strategies of plant communities on 12 sites in southern Idaho.(Whisenant, 1990).

Rangeland researchers have studied the effects of wildland fires and prescribed burns throughout the past century, particularly focusing on the effects of fire on successional elements of plants and plant communities within rangelands. The predominant and most defining plant species of rangeland environments is big sagebrush (*Artimesia tridentate* Nutt.). Big sagebrush is well-suited to habitation in arid rangeland environments because its deep root system allows the plant to draw water from deep soil layers during the heat of summer. This quality allows the sagebrush to grow throughout the dry season, after all moisture is gone from the upper soil layers. Annual grasses present in rangelands typically grow early in the season because they retain their moisture from the upper soil layers. During growing seasons that are wetter than normal, annual grasses can exploit more water than usual, resulting in an increased, denser stand (Knapp, 1995). These dense stands of annual grasses present a relatively uniform, high fine fuel load, which result in more combustible and severe fires when ignited. A negative impact of increased fuel loads from fine fuels like cheatgrass is that, when burned, the potential for unburned remnant patches of sagebrush and native grasses to remain in the affected area decreases (Whisenant, 1990). When unburned patches remain, sagebrush has been observed to reestablish from seed within 4-6 years, and cover may return to preburn levels within 15 to 25 years of the fire (Bunting, 1985). In completely burned areas, range managers will often reseed big sagebrush because the population cannot reestablish on its own if no unburned areas are available for seed redistribution (Britton and Clark, 1985). Though rabbitbrush shrub populations tend to dominate most soon after fire, if grazing and fire are restricted and controlled, sagebrush will eventually dominate the area. However, if fires return more frequently due to increased fine fuel loads, especially within the first 4-6 years when sagebrush seedlings are establishing, sagebrush stands may be further affected and annual grass stands will continue to dominate (Wright, 1985). When fires occur during late summer or early fall, perennial forbs and grasses appear relatively unaffected, and subsequent productivity may actually be enhanced (Bunting, 1985). While monitoring an 11,000 ha burn site in south central Utah, researchers found cheatgrass cover to be near 100% the year following the burn (West and Hassan, 1985). Two years following the burn, perennial bunchgrass populations appeared to be near preburn conditions. Though native rangeland plant populations can effectively recover from fire, altered conditions such as increased fine fuel load, reduced patchiness and ensuing fires returning much sooner will rapidly break down the ecosystem dynamics by altering plant communities, successional patterns, and fire regimes.

Wildland fires throughout the American West have increased significantly in size, severity, and damage since the early part of the 20th century (Odion et al., 2004). Along with this increase, ensuing research has steadily analyzed fire patterns, behavior, history, and effects. Though a handful of researchers have scrutinized rangeland fires and fire events at lower mountain elevations, particularly in sagebrush-steppe and pinyon-juniper ecosystems (Cannon, 2001; Cannon et al., 2001; Pierson et al., 2001; Pierson et al., 2003), the majority of wildfire-related research has been in forested settings (Odion et al., 2004; Pierce et al., 2004; Robichaud et al., 2003; Wondzell and King, 2003).

Post-fire Sedimentation Processes

The hydrological impacts following rangeland fire can often be severe. Reduction of vegetation, litter, and organic layers on forest and rangeland floors by fire reduces rainfall interception, leading to increased soil erosion and overland flow (Ice et al., 2004). Soil infiltration rates can be decreased by the formation of water-repellent soil layers, and the removal of litter and organic layers (DeBano et al., 1998). These are key factors in the increase of soil erosion in burned areas, and are influenced by fire severity (DeLuis et al., 2002). Post-fire hillslope erosion can also lead to sediment-laden stream flow and debris flows. Debris flows can cover exceedingly large areas, having been known to surpass 10^9 m^3 of volume (Iverson,

1997), and the fluidity of some debris flows can allow for significant runout lengths. Debris flows often occur with little warning, possessing such force that even small flows can transport vast amounts of sediment, inflict damage to infrastructure, and imperil human lives (Cannon, 2001).

Many rangeland environments affected by wildfire are considered susceptible to debris flows because they cover steep topography where vegetation has been removed. Most common to burned watersheds are debris flows that initiate through progressive bulking of sediment within high-order channels and on hillslopes, usually occuring within a short period of the fire (Cannon et al., 2001). The majority of debris flows (93%) on Storm King Mountain, CO noted by Cannon et al. (2001) were traced to zero and first order channels and hollows where noteworthy erosion and runoff was observed. Analysis of a burned rangeland canyon in southeast Idaho identified increased overland flow, resulting from heavy rainfall on hillslopes as the primary initiator of an erosion debris flow that shut down a major transportation corridor (Tucket et al., 2004). Similar debris flow characteristics of progressive bulking sediment flows were identified in Yellowstone National Park after the destructive fires of 1988 (Meyer and Wells, 1997). Cannon (2001) distinguishes two types of fire-related debris flows recognized throughout the Southwest; type 1, a poorly-sorted mixture of boulders and similar-sized material, with significant height, and sharp, distinct margins, having a matrix of fine-grained materials, and type 2 flows, consisting principally of sandy, gravelly materials, with a charcoal and ash-abundant matrix. The sediment-rich type 2 debris flows are differentiated from sediment-laden stream flow because of the lack of hydraulic sorting that would remove the fine material.

Debris flows may also occur as a result of a stable, intact mass of sediment becoming saturated and subsequently moving downhill (Summerfield, 1991). The paths can usually be traced up an easily identifiable channel to a source, known as a soil-slip scar (Cannon et al., 2001) or colluvial failure (Meyer et al., 2001). In previously burned forested areas, soil-slip flows are most often observed five or more years following the fire, because the decaying of tree and shrub roots that anchor colluvium has reduced soil cohesion (Meyer et al., 2001). In contrast, type 1 and 2 debris flows are more likely to occur within a month to a year after the fire event (Cannon et al., 2001; Meyer and Wells, 1997; Tucket et al., 2004).

A detailed analysis of post-fire erosional debris flows involves assessing each of the parameters that affect flow generation. In a relative hazard ranking model, Sprague-Wheeler (2001) attempted to evaluate wildfire areas in Central Idaho based on the parameters of geology, burn severity, slope angle, and aspect. A setback with assigning ordinal rankings to each of the parameters is the preponderance for subjectivity while assessing the variables and it also doesn't effectively represent the physical processes involved. For a susceptibility analysis to be accurate and applicable, the parameter assessment should be standardized prior to input in a comprehensive study. For these particular reasons, this study analyzes two particular variables (burn severity and soil water repellency) that influence debris flow generation. Even though our study area was not at high risk of debris flow generation (primarily because of the lack of precipitation; Appendix 2), by conducting an in-depth analysis of the particular debris flow parameters, future vulnerability studies will be more robust.

In a study of 95 burned basins in the American Southwest, Cannon (2001) identified geology, soil conditions, basin morphology, burn severity, and precipitation as the primary initiating factors of debris flows. Several other conditions that affect slope stability and cause increased sedimentation include decreased soil infiltration rates due to the formation of water-repellent layers and the removal of vegetation, a result of burn severity, which decreases interception and evapotranspiration of water (Cannon et al., 2001). An extensive review of relevant literature has identified fire-induced soil water repellency and wildfire burn severity as two crucial parameters of post-fire debris flow generation that are in need of research in rangeland environments.

Water Repellent Soils

A major dynamic influencing sedimentation events in burned areas is the presence of water repellent soil layers. Soil water repellency is a phenomenon that has been the focus of intense research for over 30 years (DeBano, 1981; DeBano, 2000). These soils are found around the world, in agricultural fields, grasslands, brushlands, and forests (Dekker and Ritsema, 1994). Numerous studies have identified water repellent soils in different plant communities, ranging from soils between grass bunches in Australia, underneath citrus canopies in Florida, around the decaying roots of shrubs in the Sierra Nevada, below aspen stands in Wisconsin, and in Southern California chapparal communities where dense litter layers were present (DeBano, 1981). Johnson and Beschta (1981) noted a seasonal variation in soil water repellency, pointing out that Western Oregon soils exhibited increased repellency during the summer months, due to greater vegetation cover that protected the soil surface, and higher temperatures hardening the soil surface and reducing the viscosity of water. A water repellent soil layer is recognizable because water droplets will ball up and sit on top of the layer, often for longer than five minutes and sometimes over 1 hour (Cannon, 2001; DeBano, 1981; Dekker and Ritsema, 2000), without soaking into the soil.

Rangeland soils sometimes exhibit soil water repellency in the absence of fire because of dry climatic conditions, compaction, unevenly-spaced vegetation, and organic layers that naturally contain hydrophobic compounds (DeBano, 1981). These conditions can lead to water input exceeding soil infiltration rates, resulting in overland flow (Pierson et al., 2001; Wondzell and King, 2003). Water repellent soils may occur for a number of different reasons, but the primary factors affecting it involve organic matter, soil texture (DeBano, 1981), soil water content (DeBano, 2000; Doerr and Thomas, 2000), and plant-soil relationships (DeBano, 2000; DeLuis et al., 2002). Formation of a layer can occur because of the irreversible drying of organic matter, and the leaching of organic substances from litter and mineral particles. Additionally, hydrophobic organic matter can mix with mineral soil particles during heating, creating and/or enhancing water repellency in the soils (DeBano et al., 1998), and at very high temperatures (220°-275°C) (Moody and Smith, 2005), cementation by clay oxide occurs over the soils. Soil water repellency tends to have varying degrees of persistence and intensity, but it is often noted that fire-induced water repellency is more severe in its persistence (DeBano, 1981) and the hydrological effects incurred from it. Water repellent layers in soil are often found at or below the surface, and exhibit variable spatial characteristics. In natural soil conditions, repellency can be present below the surface, but soil remains penetrable because of cracks, root holes, and animal burrow holes that allow preferential flow, and the presence of litter layers above the soil absorbs water, thus, the risk of overland flow is low (Doerr et al., 2006). In burned soils, a subsurface layer can be present at depths of 6 cm or greater, and is much less penetrable, because the litter layer is destroyed, and preferential flow spots are often choked with fine particles from post fire erosion (Doerr et al., 2006).

When a rangeland area is affected by wildfire, organic matter, which often contains hydrophobic compounds, combusts, producing aliphatic hydrocarbons (DeBano et al., 1998; Lewis et al., 2004), that are detectable in the burned soils. The depth and thickness of water repellent soils after fire depends on the severity of the fire. Typically fires with higher burn severity produce a deeper repellent layer, but very hot fires destroy the compounds responsible for the repellency. Laboratory testing by DeBano (2000), observed changes in soil water repellency after heating soils with temperatures similar to those observed in wildland fires. Results indicated that soils exhibited little, if any, change when they were heated no more than 175°C. When soils were heated between 175 and 200°C, water repellency of high intensity was observed, and when soils were heated between 280° and 400°C, water repellency was destroyed. Although it is unclear from the literature which soil types may exhibit higher degrees of repellency, it is stated that the heating of translocated substances within the soil, and not the soil itself, is generally responsible for the presence of water repellency (DeBano, 1981; DeBano, 2000). The texture of soils, however, does play a significant role in the induction of soil water repellency; when organic matter is mixed with coarse-textured soils or sands, and heated, water transport is restricted severely, as opposed to finer soils, in which the organic materials enhance water and air movement (DeBano, 1981). A unique

attribute in the formation of water repellent soils is the tendency of hydrophobic compounds to move downward in dry soils due to temperature gradients in the upper mineral soils (DeBano et al., 1998). After the fire has passed, the heat may continue to move downward, causing more of the hydrophobic substances to volatize, thus thickening the water repellent layer (DeBano, 2000). This characteristic is an important dynamic in the relationship of burn severity and associated burn times to sedimentation events because a water repellent layer deep below the surface that has abundant erosive soil on top of it is capable of producing overland flow following saturation.

Another dynamic relating to the formation of water repellent soils is the cementation of the soil, due to the burning of biomass and the intense heating of the soils chemical properties. While testing the cohesive shear strength of forest soils heated to specific temperatures, Moody et al. (2005), found that the majority of soil water repellency formed because of the heating and volatization of organics occurs at temperatures up to 220° C. At temperatures greater than 220° C, however, the organic repellency is reduced and overtaken by sesquioxide clay cementation, involving the intense heating of aluminum, iron, and titanium oxide clays. This finding is important in relation to post-fire erosion because the sesquioxide clay cementation is responsible for the increase in the size of the eroded soil aggregates after fire. Similar to temperature thresholds for water repellency, Moody et al. (2005) found the critical shear stress of soils to drop abruptly when heated above 275° C, as does the water repellency of soils; and the clay cementation is destroyed, increasing the porosity and erodibility of the soils. The findings of Moody et al. (2005) and DeBano (1981; 2000) indicate that the degree of water repellency can be separated not only between weak, moderate and strong repellency due to the volatization of organics, but also into a category of very strong repellency as a result of sesquioxide clay cementation.

Water repellent soil layers pose serious threats to slope stability after wildfires because of their influence on debris flow generation. When a water repellent layer is present below the surface, there is usually a layer of highly penetrable mineral soil above it. The occurrence of precipitation events over the area can drop heavy amounts of rainfall on the soils, suddenly saturating the soils. Normally, rainfall will infiltrate deep into the soils, but the presence of a water repellent layer presents a barrier to the rainwater. Additionally, the absence of vegetation increases the amount of water falling into the soil, allowing it to erode faster because vegetation does not minimize raindrop impacts through interception. When the upper soil layer reaches saturation, overland flow begins. The increased runoff eventually forms rills, which have a depth to the presence of the water repellent layer. Gradually, the erosive processes within the rills will degrade the water repellent layer, causing it to break down and ultimately become receptive to infiltration (DeBano, 2000). The increased runoff and overland flow, however, can progressively bulk across a watershed and lead to erosional debris flows (Cannon, 2001; Cannon et al., 2001; Meyer and Wells, 1997; Tucket et al., 2004).

Researchers have indicated that water repellent soils can be very difficult to model because of the extreme spatial and temporal variability of the phenomenon (DeBano, 2000; Shakesby and Doerr, 2006). Measurements of fire-induced water repellency in Eucalyptus-dominated catchments in South Africa indicated that vegetation cover was responsible for variations in fire behavior and the variability of water repellency in soils (Scott, 1993). The sparse vegetation that is characteristic of rangelands creates even more variability of water repellency because interspaces between plants are often void of any vegetation, and not directly affected by fire. The areas directly beneath shrubs, known as coppice microsites, are generally the most affected by water repellency during a fire (Pierson et al., 2001). In personal field observations one year after the Red Bull Fire in Spanish Forks Canyon, Utah, water repellent soil layers were observed at very shallow levels (<2 cm) directly below burned shrubs **(Fig. 1.3)**, yet no repellency was observed within 30cm of the burned shrub. In observations at the Clover Fire, soil infiltration was observed to increase with distance from burned vegetation. Fire-induced water repellency is often known to persist near its original intensity to within one year after a fire, but soils generally return to pre-fire conditions within five years of the fire (Pierson et al., 2001).

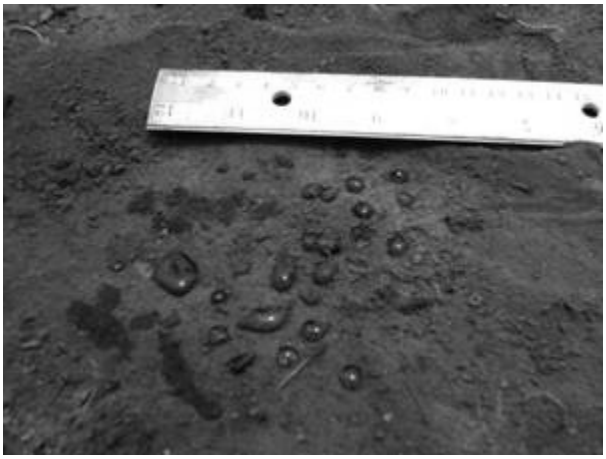

Fig. 1.3. Water repellent soil layers one year after a rangeland wildfire in Uinta NF, Utah.

Remote Sensing

Remote sensing is a science which involves acquiring information about an area on earth, an object, or an occurrence through a device with which it is not in physical contact (Lillesand et al., 2004). In research of natural resources and earth sciences, remote sensing usually involves the acquisition and subsequent processing and analysis of aerial or space-borne imagery covering a portion of the landscape. Remote sensing images hold four forms of resolution: spatial, spectral, temporal, and radiometric. The spatial resolution of an image refers to the smallest quantitative area on the ground that is discernable in the image. Spatial resolution of aerial and space-borne imagery can range from less than one meter (e.g. panchromatic band of Digital Globe, Inc.'s Quickbird imagery), to greater than one kilometer (e.g. NASA's Moderate Resolution Imaging Spectrometer (MODIS)). The spectral resolution of an image describes the range of spectral bands and their associated bandwidths in an image. Traditionally, remote sensing imagery has been panchromatic in nature, capturing brightness values of the ground in a broad band of wavelengths (e.g. from far ultraviolet to near infrared (NIR)) in a grayscale, or multispectral, capturing spectral characteristics of the ground surface through multiple channels of the electromagnetic spectrum. A multispectral image usually contains multiple bands ranging from the visible portion of the spectrum to the NIR, short wave infrared (SWIR) and sometimes thermal infrared (Jensen, 2000). A less traditional and newer sensor type is the hyperspectral sensor, which collects data within hundreds of very narrow, nearly contiguous bands, covering portions of the visible, NIR, and SWIR. Hyperspectral sensors are unique in that the bands are collected adjacent to one another in a near continuous spectrum by oversampling (Lillesand et al., 2004). The bands are typically narrow (e.g. 10 to 15 nm or less), allowing fine absorption features of the earth to be detected. The smaller the spectral window detected in each band, the higher the spectral resolution, (Aspinall et al., 2002). Remote sensing systems have proven valuable in analyzing physical and environmental characteristics of the earth, as well as assessing the effects of natural events and disasters like wildfires, floods, severe storms and earthquakes.

There are a number of challenges related to remote sensing in arid rangelands, foremost being its inherent characteristic of a large soil background that crowds out a low vegetation cover (Okin et al., 2001). The vegetation communities of arid lands often exhibit a reduction of leaf absorption in the visible spectrum, and are intrinsically different in their spectral signature, as compared to humid vegetation (Okin et al., 1999a). These setbacks tend to enhance nonlinear mixing of spectra within pixels and there can be a tendency to misidentify and wrongly estimate the abundance of the materials present within the confines of one pixel. Researchers have utilized hyperspectral image analysis, commonly referred to as spectroscopy, to analyze arid areas in efforts of minimizing the problems associated with spectrally differentiating landscape characteristics.

The science of spectroscopy is unique and beneficial in the fact that the narrow, nearly contiguous wavelengths in spectroscopic images can allow for the spectral signature extraction of specific mineralogical compositions, soil and ground texture, and organic matter. Unlike conventional multispectral remote sensing, spectroscopy requires in-depth analysis of the image spectrum, in order for researchers to understand the contributing composition of materials and their interactions, and to accurately and sufficiently identify the endmember materials in sight. The goal of this project was to identify the unique spectroscopic characteristics of burned rangelands, including burn severity and water repellent soils, and use their spectral signature as training endmembers to determine their distribution across the geographic area of the acquired imagery.

The most important component of spectroscopic imaging is the identification of spectral endmembers to be used for classification of the imagery. Numerous researchers have utilized spectroscopy to identify the unique spectral signatures of materials across an image; most often for mapping soil and mineralogical properties (Chabrillat et al., 2002; Debba et al., 2005; Okin et al., 2001; Palacios-Orueta and Ustin, 1998), and discriminating vegetation types (Bachmann et al., 2002; Glenn et al., 2005; Mundt et al., 2005a; Parker-Williams, 2004). The advantage of mapping mineral distribution, or discriminating vegetation type, is the tendency for individual minerals and plants to exhibit unique and separable spectral signatures. When spectroscopy is utilized over burned rangeland areas, the differentiation of distinct spectral signatures is compounded by the fact that a large soil background is present, and was so before the area was burned, introducing high albedo effects. When a rangeland experiences a wildfire of high severity, the vegetation and fuel is often completely incinerated, leaving much of the area bare of any substantial ground cover, litter, or vegetation, as was the case in much of our study area. Because soils in arid regions tend to be mineralogically similar and bright (Okin et al., 2001), and the burning of vegetated areas leaves little variability across the surface, the distinction and separation of particular soil characteristics in burned areas can be ambiguous. Due to the intricate nature of rangeland wildfire, and its spectral attributes, spectroscopy may have the ability to maximize the obscure differences among them.

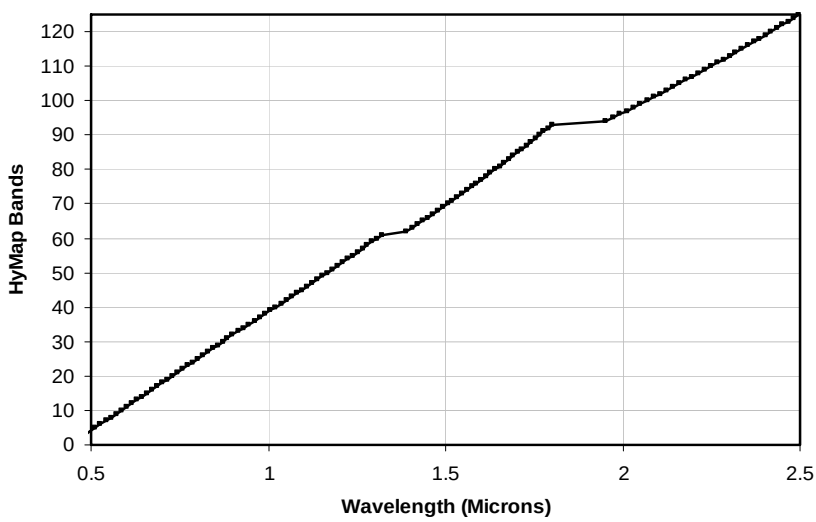

Fig. 1.4. HyMap reflectance

Hyperspectral imagery was used for this study because the seemingly extreme variability often observed with water repellency (Pierson et al., 2001; Shakesby et al., 2003) is undetectable with coarser, traditional sensors. The concurrent collection of full spectral measurements in spectroscopic sensors provides a commanding foundation for the identification of biochemical composition of plants (Ustin et al., 2004), and, when coupled with high spatial resolution, the fine scale, variable absorption features typical of soils can be accurately evaluated (Palacios-Orueta and Ustin, 1998). The HyMap sensor (HyVista Inc., Australia) which was utilized for the current research project, is a hyperspectral sensor capturing 126

spectral bands between 0.45 μm and 2.5 μm, with a spatial resolution of 3 m. The spectral regions covered in HyMap imagery include the visible portion (0.45 μm to 0.7 μm), the NIR (0.7 μm to 1.3 μm), and the SWIR (1.3 μm to 2.5 μm), with the majority of the bands (60-125) lying in the latter (Fig. 1.4). Hyperspectral imagery can be associated with a detailed spectral library, a set of spectral signatures of various materials that can be used for matching a feature to its corresponding wavelength in the image (Lillesand et al., 2004). When a spectroscopy project matches imagery to field-collected spectral libraries, a great advantage is the ability to extend the spectral libraries across wide areas and multiple images to identify target materials (Aspinall et al., 2002). The unique spectral characteristics of hyperspectral images and its processing efficiency are beneficial for evaluating landscape scale disturbances, and can prove useful in developing mitigation response plans after such events.

Previous Studies

Commonly, specific procedures and classification methods are employed when undertaking spectroscopy research and a general flow of processes is followed. Methods developed specifically for spectroscopy involve noise reduction procedures like the Minimum Noise Fraction (MNF), endmember selection like the Pixel Purity Index (PPI) and the n-dimensional visualization of endmembers, and finally, spectral mixture analysis. Because spectroscopy is a relatively new technology, researchers are continuously developing new and improved algorithms, classifications, and methods to compliment the analysis. Palacios-Orueta and Ustin (1998) simulated AVIRIS band reflectance to find the best spectral predictors for classification of soil samples using a series of Principal Component (PC) Analyses. The simulated imagery was conducted on soil samples collected from two adjacent valleys near the Southern California Coast. During the laboratory experiments, the researchers found the albedo of the soil to have the greatest effect on spectral variability, though absorption played a role as well, particularly in samples with high amounts of transparent sand particles. The primary difference in reflectance among the samples was caused by iron content and organic matter (OM) content. After experimenting with PC analyses on the data, the researchers were able to accurately summarize the spectral variability of the soils based on the associated OM and iron content after the second and third PCs (eigenvalues).

In ensuing research, Palacios-Orueta et al. (1999) conducted a landscape-scale classification of the same study area, in an attempt to describe soil properties with AVIRIS. The researchers tested a Hierarchical Foreground and Background Analysis (HFBA), in an effort to discriminate the soils typical of the study site. HFBA is a stepwise series of modified spectral mixture analysis techniques; HFBA develops a sequence of vectors based on foreground and background spectral variation defined by the user. The technique essentially links the spectral variations of the imagery with wave-based multiscale resolution in order to classify spectral endmembers according to the variance of the spatial domain (Pinzon et al., 1998). The hierarchical sequence narrows down the variance of the normalized spectral curves into small reliable ranges of easily detectable variability (Palacios-Orueta et al., 1999). Through the HFBA technique, the researchers were able to detect and classify soils with high OM content and iron content in accordance with their spatial location. A downfall of the HFBA is that its tendency to decrease the variability of the imagery reduces its effectiveness across study areas, without having prior knowledge of endmember characteristics.

Rahman and Gamon (2004) utilized the Water Band Index (WBI) (0.97 μm reflectance/ 0.90 μm reflectance) of temporally spaced hyperspectral reflectance images to accurately and successfully identify fresh biomass (regrowth) and water content in burned and unburned areas at a grassland fire site in Southern California. Their temporal classification study took advantage of the spectral change due to spring regrowth one season after a fire. Statistical procedures tested the performance of a WBI classification in comparison to known indices like the Normalized Difference Vegetation Index (NDVI) and the Photochemical Reflectance Index (PRI), as well as field-gathered data. The WBI correlated

significantly with the NDVI and field-assessed biomass ('r' = 0.67 and 0.79), demonstrating the ability of hyperspectral data to collect biophysical information across the spectrum.

Several studies have demonstrated the power of hyperspectral imagery for the identification and classification of noxious weeds in arid lands. Parker Williams and Hunt (2004) utilized AVIRIS hyperspectral imagery and the reflectance of the noxious weed leafy spurge to determine its occurrence with the Mixture Tuned Matched Filtering (MTMF) spectral mixture analysis procedure at a study site in Northeastern Wyoming. The researchers found differences in their classifications dependent on the preset detection thresholds, which yielded either false positives or false negatives. Out of three land cover types (mixed prairie, riparian, and conifer); leafy spurge was detected best within mixed prairie and riparian areas, with an overall accuracy of 95%.

At a research site in southwest Idaho, Mundt et al. (2005a) used Spectral Angle Mapper (SAM) and MTMF classifications to search for the noxious weed hoary cress with HyMap hyperspectral data. Comparisons of SAM and MTMF classifications found no statistical difference in the two, though visual interpretation indicated that SAM produced a better classification. The researchers found that a multiple endmember SAM classification on MNF transformed data detected hoary cress occurrence with 86% overall accuracy in areas of 30% cover or more. These results are similar to those in Glenn et al. (2005) using HyMap hyperspectral imagery with MTMF to identify low cover infestations of leafy spurge in Swan Valley, Idaho. Spectroscopy is a well-suited method for the detection of noxious weeds in arid lands because of the ability to detect the spectral signatures of the weeds aiding in the identification and treatment of small infestations. Researchers have indicated that hyperspectral imagery is essential for detecting noxious weeds in areas of low percent cover (<30%) within a 3m resolution pixel (Mundt et al., 2005a; Mundt et al., in press) .

In example of the continuing development of new spectroscopic techniques, Mundt et al. (2006) combined the analytical strength of high spatial resolution hyperspectral imagery with Light Detection and Ranging (LiDAR) data to map the distribution and structure of sagebrush stands in the Eastern Snake River Plain, Idaho. The researchers utilized the MTMF classification technique and mean heights of LiDAR pulses to assess the location and heights of sagebrush, increasing the accuracy of sagebrush classifications by 14% to an overall accuracy of 89%. In addition to ordinarily classifying the sagebrush stands, the LiDAR fusion assessments provided information on the stands' health and response to disturbances like wildfires.

While the noticeable spectral characteristics of invasive weeds and other vegetation have allowed scientists to classify them with spectroscopy, the analysis of bare ground and soils in arid lands presents greater challenges because of the subtle spectral distinctions among soils and their inherent high reflectance (Okin et al., 2001). Furthermore, when low cover arid areas are burned in common rangeland fires, the spectral signature of the soil is affected. Burned soils are often blackened, and can be easily detected with remote sensing imagery, but the variation of soil's spectral characteristics in relation to fire-induced effects, like the degree of water repellency, are often ambiguous. In a former study, hyperspectral imagery was collected over the Hayman fire in Colorado, and analyzed for the remote identification of water repellent soils (Lewis et al., 2004). Regions of interest were selected for slight, moderate and high water repellency, based on field examinations, and used as training data for classification. The researchers utilized a PC transform and SAM to detect water repellent soil layers at 80% accuracy, but failed to detect the degree of repellency (Lewis et al., 2004). Researchers in this project used water repellency data collected at 4 m circle plots in the field as regions of interest for detecting strong and moderate and weak water repellency. The majority of the strong and moderate repellency plots were in areas classified as moderate or high burn severity. When the classification was conducted using only the circle plots as training data, the resulting classification accuracy was quite low (17%, 27% and 0% for slight, moderate, and high water repellency). The researchers then increased the

size of the plots with a 3x3 adjacent pixel window for inclusion of the water repellency (WR), and, using 50% of the sample plots for validation (slight WR: n=6; moderate WR: n=11; high WR: n=9), the accuracies increased to 67%, 55%, and 45% for slight, moderate, and high repellency, respectively. Although the repellency degree could not be detected to a finer degree than slight, moderate, or high, the researchers deemed the findings successful because the classification identified regions of water repellency at a landscape scale that could be mitigated for erosion control.

Though the accuracy of the Lewis et al. (2004) classification was strengthened by the inclusion of training plot pixel windows, the pre-fire forest vegetation structure was such that the soil water repellency would likely be more consistent across the forest floor. In a rangeland setting, the spacing of shrubs and other vegetation introduces a unique dynamic that causes fire-induced soil water repellency to be much more variable across the rangeland floor. The buffering of training areas, as done by Lewis et al. (2004) would increase the possibility of false positive classifications with the imagery over our study area.

At the same site, hyperspectral imagery was used to assess burn severity by adapting the Normalized Burn Ratio (NBR; Key and Benson, 2002) and the Normalized Differenced Vegetation Index (NDVI) to Short Wave Infrared (SWIR) hyperspectral bands, and through use of a partial linear unmixing technique (Laes et al., 2004). They found the NBR adaptation to be a fast and effective method of mapping burn severity with minimal fieldwork involved, however, the thresholds and cutoff values for the input bands differed among separate images. Laes et al. (2004) also used field spectrometry information as endmembers to assess the burn severity among the Hayman Fire with partial linear unmixing. Though no validation other than field comparison was presented, the pixel unmixing results were used to represent the abundance of certain materials (ash, scorched vegetation, green vegetation, soil, and rock) across the image in an unconventional burn severity map. In both of the Hayman fire studies the authors indicated that spectral characteristics of soils may be better analyzed for repellency degree if greater soil reflectance was visible, as is the case in a non-forested rangeland area. Our study has taken into account the achievements and pitfalls of previous-related studies, specifically those involving wildland fire and arid environments, to develop methods of reliably evaluating the burn severity and soil water repellency of rangeland wildfire areas with hyperspectral imagery.

MATERIALS AND METHODS

Field sampling at the Clover fire site began in late August 2005, and was completed by the end of October 2005. Following an initial drive-through survey of the burned area, 3 study sections were designated (Fig. 2.1), across which HyMap hyperspectral imagery was collected. Within the 3 sections, we field-assessed burn severity using 9 m x 9 m sample plots across four classes (unburned, low, moderate, and high). Burn severity was assessed using methods of the United States Forest Service (USFS) Burned Area Emergency Response (BAER) teams, as described by Bobbe et al. (2001), which involved ocular ground estimates of vegetation and soil damage, ground cover, and excess sedimentation risk. The burn severity classes were further broken down by the dominant vegetation group (shrub and grass). Additionally, soil water repellency was evaluated at each sample plot using a mini-disc infiltrometer (MDI), and the Water Drop Penetration Time (WDPT) test. A field spectrometer was used to collect supplemental spectral characteristics of endmembers (features to be mapped) within the study area. With the aid of a hand-held global positioning system (GPS) device, these measurements were used as ground control points and spectral reference for the remote sensing classification study. We also conducted a supplemental sampling experiment that analyzed infiltration with the MDI at set-length intervals from burned sagebrush.

Initial Field Survey

We visited the area and conducted a visual survey and assessment of the overall severity and character of the fire and the ecological and geomorphologic characteristics of the landscape. Three regions were designated as the most suitable for acquiring aerial images (flight lines); these regions were selected

based on the range of characteristics among the assessed variables (Fig. 2.1). The easternmost flight line was designated as section A because it was the first section to be sampled. The middle flight line was designated as section B, and the western-most section, which was also the last section to be sampled, was designated as section C. Within each section sample plots were evaluated and assigned burn severity, and 3 points in each plot were tested for soil water repellency.

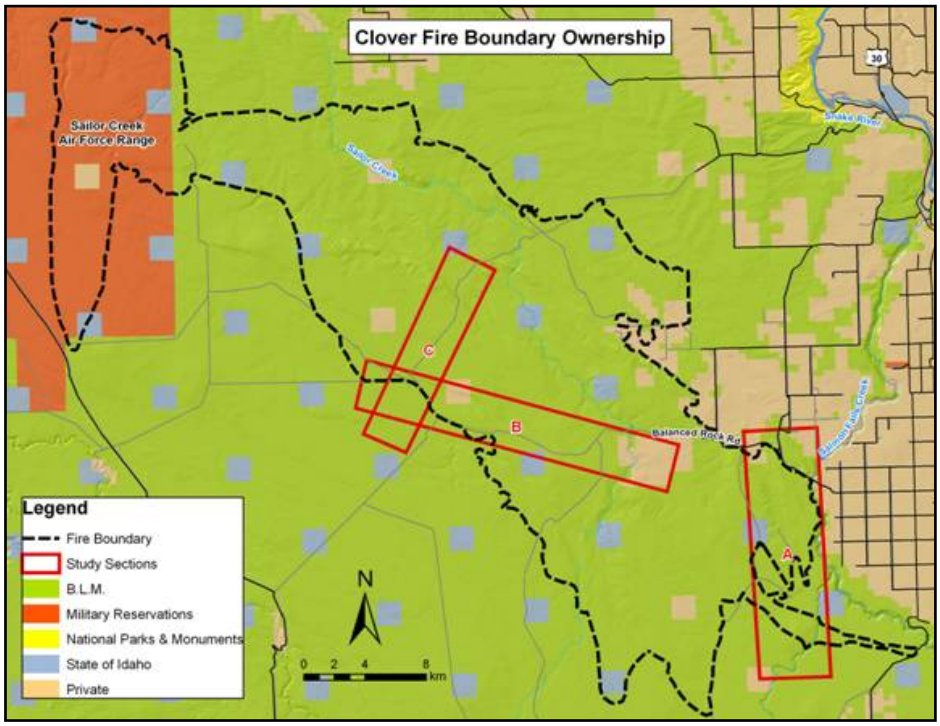

Fig. 2.1. Clover fire boundary and ownership. Field study sections A, B, and C shown in red.

Section A

Sampling of section A began on August 27, 2005, and was completed by September 12, 2005. Within section A burn severity and soil water repellency was assessed at 41 plots. Section A is just west of Salmon Falls Creek and extends from north of the Balanced Rock Road approximately 16.5 km south to the geographic feature known as the Devil Creek Butte. The section is 4.8 km wide, with an area of 482 km^2. The majority of Section A is within BLM boundaries, and is allotted rangeland, while a portion on the eastern side of Salmon Falls Creek, and in the northernmost corner of Section A, is privately owned farmland. The pre-fire vegetation in section A consisted of sagebrush in various stages of growth, perennial bunchgrasses, and stands of annual cheatgrass. Significant amounts of bare ground are present throughout section A. Salmon Falls Creek and Devil Creek are the two drainages within section A, though Salmon Falls Creek is the only perennial stream.

The elevation of Section A ranges from 1038 m, in Salmon Falls Creek Canyon, to 1349 m, atop Devil Creek Butte, with a mean elevation of 1233 m. Section A is relatively flat, with an average slope of about 4°, the drainages of Salmon Falls Creek and Devil Creek canyons are quite steep, however, with slopes near 57°. Salmon Falls Creek also has vertical canyon walls in excess of 30 m in places. Other areas that exhibit relatively steep slopes are the hillsides adjacent to the large grass-covered basin known as the Blue Gulch, slopes around Devil Creek Butte, and several intermittent drainage gullies across the section (Fig. 2.2 A).

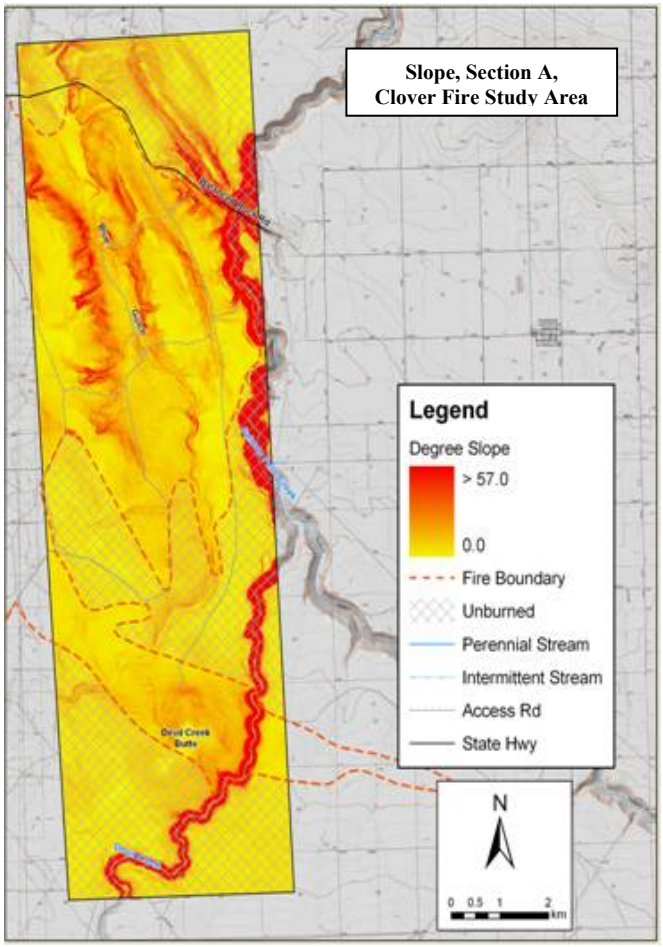

Figure 2.2 A. Slope, section A

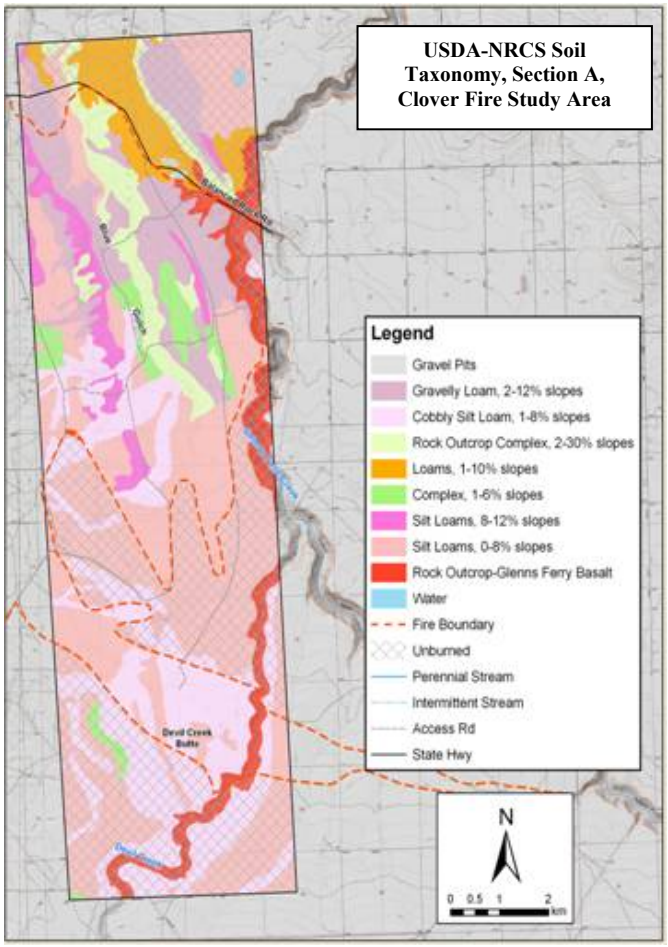

Figure 2.2 B. Soils, section A

The northern portions of section A consist mostly of loam and gravely loam soils, with some areas of silt loam. Rock outcrop complexes are present along the slopes of the Blue Gulch and within the Salmon Falls Creek canyon. The southern portion of Section A is primarily silt loam, with cobbly silt loam present around the Devil Creek Butte. A steep rock outcrop complex (Glenn's Ferry basalt formation) is present within the Devil Creek canyon (Fig. 2.2 B) (USDA-NRCS, 2005).

Approximately 47% of Section A was burned during the Clover fire. Because the fire spread in an easterly direction, section A was one of the last areas to burn. The deep Salmon Falls Creek canyon acted as a natural fire barrier, preventing the flames from crossing it and affecting the agricultural areas to the east. South of the Balanced Rock Road and east of the BLM access road, the fire burned in a large sagebrush stand at moderate severity levels and at high severity levels within the grass covered basin known as the Blue Gulch. The fire continued in an easterly direction, burning very hot in the sagebrush stands to the western edge of Salmon Falls Creek canyon. For approximately 7 km south of the Balanced Rock Road, high severity fire scars were visible in sagebrush stands, and a large area of homogeneous, high burn severity was visible where annual grass stands existed before the fire. About halfway down the section, the fire burned in grassy areas at low severity, and actually stopped burning at this point. The southern half of Section A has a wide swath of unburned sagebrush, punctuated only by south and east-running fingers of burn scars, most likely spot burns across the plain. One more significant fire run is noticeable near the southern edge of the section, where the fire burned severely in sagebrush and grass across the front and on top of the Devil Creek Butte. This last run, approximately 1.5 km wide, and 10 km long, terminates in a flat sagebrush area at the western edge of Salmon Falls Creek canyon (Fig. 2.3).

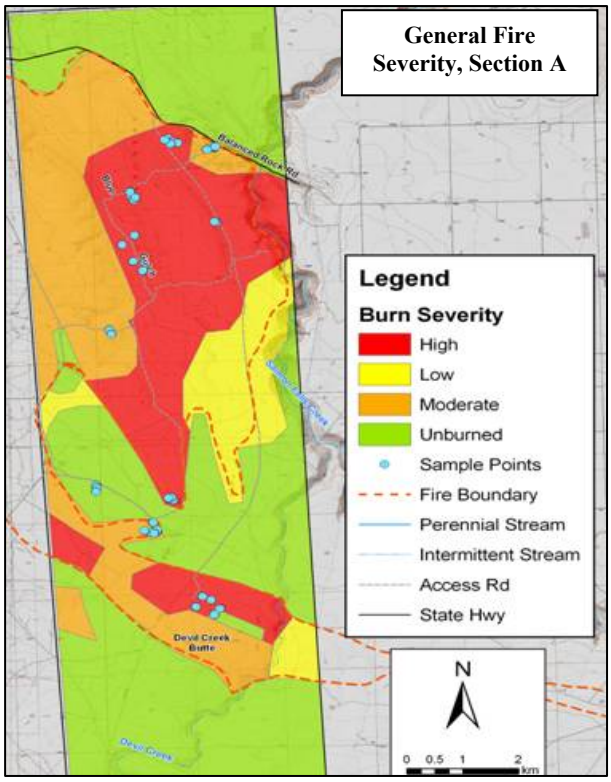

Figure 2.3. General fire severity, section A

Section B

Section B extends approximately 21 km from the southern edge of the geographic feature known as the Big Hill, at the Crows Nest Flat area, in an east-southeast direction, along the Pot Hole Creek drainage, following the Balanced Rock road. The eastern end of the section crosses a portion of the intermittent Sailor Creek drainage. Section B is approximately 3.2 km wide and covers approximately 68 km^2. Field sampling of section B began on September 16, 2005, and ended on October 1, 2005. Within section B, a total of 33 plots were evaluated. About halfway through the sampling period in Section B major dust storms developed (September, 2005), severely altering the soil structure, and removing litter and the top soil layers.

Section B exhibited the most heterogeneity of burn characteristics and vegetation communities within the study area. All of section B is allotted rangeland on BLM property, except for a small area of private property east of Sailor Creek. The western end of section B, which overlaps section C, known as the Crows Nest Flat, is an area of thick sagebrush cover, much of which was unburned during the fire. Further east, up the Pot Hole Creek drainage, a large stand of annual and perennial grass was present prior to the burn. East of the Pot Hole Creek drainage, pre-fire vegetation of Section B consisted of typical rangeland communities, with sagebrush, perennial grasses, and annual grasses. On the west side of the Sailor Creek canyon, a large stand of seeded perennial bunchgrass is present, with intermittent patches of rabbitbrush and sagebrush.

The elevation of Section B varies from 1180 m in the Crows Nest Flat area to 1298 m above the southern edge of the flat, and the Sailor Creek canyon drops to an elevation of 1167 m. The mean elevation of the section is 1224 m asl. The average slope of section B is 2.8^o, although the hillsides along the southern edge of the Big Hill, north of Pot Hole Creek, slope up to 15°, and parts of the Sailor Creek canyon exhibit slopes of 25° (Fig. 2.4A).

The central portion of Section B mostly consists of silt loam soils and stony silt loams, while the eastern portion exhibits complex soil groups. The slopes around the Crows Nest Flat area are stony silt loam and very stony fine sandy loam. The slopes of the Big Hill and within the Sailor Creek canyon are steep rock outcrop complexes (Glenn's Ferry Basalt Formation). West of Sailor Creek canyon, stony silt loams and complex soil groups exist (Fig. 2.4B) (USDA-NRCS, 2005).

Approximately 80% of section B was burned during the Clover Fire (Fig. 2.5). The Crows Nest Flat area is outside of the burn area and heavy sagebrush and grass stands are present. East of the flats, along the Pot Hole Creek drainage, high and moderate severity burns were observed. Above the Pot Hole Creek drainage, a large sagebrush area was moderately burned on the north side of Section B, and high severity burn damage was observed on the south side. Just west of the Sailor Creek canyon, low, moderate, and high severity burns were noticeable, and variable burns were found within the canyon as well. East of the canyon, patchy burn scars were observed, although access to that area was limited because it sits on private property.

Section C

The final section of the study area, section C, is 3 km wide, and extends from the Crows Nest Flat area north approximately 13.4 km, across the Big Hill plateau, along the Crows Nest Road to the Sailor Creek basin, within the BLM Wild Horse and Burro management area. All of section C is on BLM land, and covers nearly 43 km^2. Field sampling of section C began on October 1, 2005, and was completed on October 21, 2005. Only 6 plots were evaluated in Section C because conditions were severely altered by the dust storms; the plateau-like geography of the Big Hill had been raked by strong winds, and the top soil layers were removed. All that was left of the soils on the Big Hill was the hard, concrete-like subsurface calcic horizon layer that was seemingly unaffected by the fire.

The northern end of section C is in a wide basin, which was covered by patchy grass and sagebrush vegetation prior to the burn. On the southern side of this basin, the Big Hill rises abruptly from the valley floor, and gradually slopes southward towards the Crows Nest Flats. Thick sagebrush and rabbitbrush were visible on the northern slope of the Big Hill. Atop the Big Hill and along the plateau, light and moderate sagebrush cover was present prior to the burn, along with perennial bunchgrasses and annual grasses, as well as significant portions of bare ground. The southern end of section C overlaps with section B where the Big Hill loses elevation, sloping into the Crows Nest Flats.

The mean elevation of section C is 1171 m asl. The lowest point is 1000 m, in the northern portion of section C, in the Sailor Creek basin. The elevation on the Big Hill rises to approximately 1230 m, and then drops to near 1180 m in the Crows Nest Flats, before rising abruptly to 1298 m on Crows Nest Butte, at the southern end of section C. While the mean slope of section C is only 2.5^o, the northern edge of the Big Hill has slopes between 20° and 27° (Fig. 2.4A).

The soil groups within the northern portion of section C, in the Sailor Creek basin, are predominantly complex groups, with some areas of sandy loams and stony silt loams, with some rock outcrops. The steep, northern slope of the Big Hill is another band of complex soil groups. Atop the Big Hill, a large area of silt loam exists, and south of that more complex groups are present (Fig. 2.4B) (USDA-NRCS, 2005).

Approximately 70% of section C was burned during the Clover fire. In the northern portion, within the Sailor Creek basin, patchy areas of high, moderate, and low severity burns are present. Along the steep northern slope of the Big Hill, low and moderate burn scars are apparent. Atop the Big Hill, the flat plateau appeared to have burned with high severity to the west, and moderate to low severity to the east. This area was extensively damaged by the windstorms as well. The southern end of section C, the Crows Nest Flat, was not burned (Fig. 2.5).

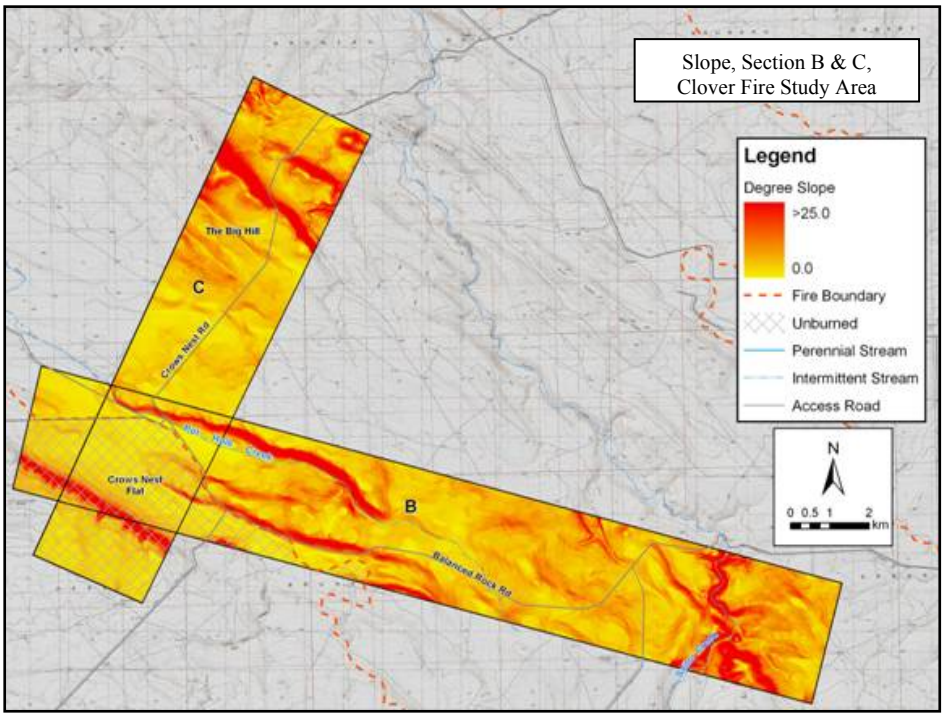

Fig. 2.4A. Slope, section B and C.

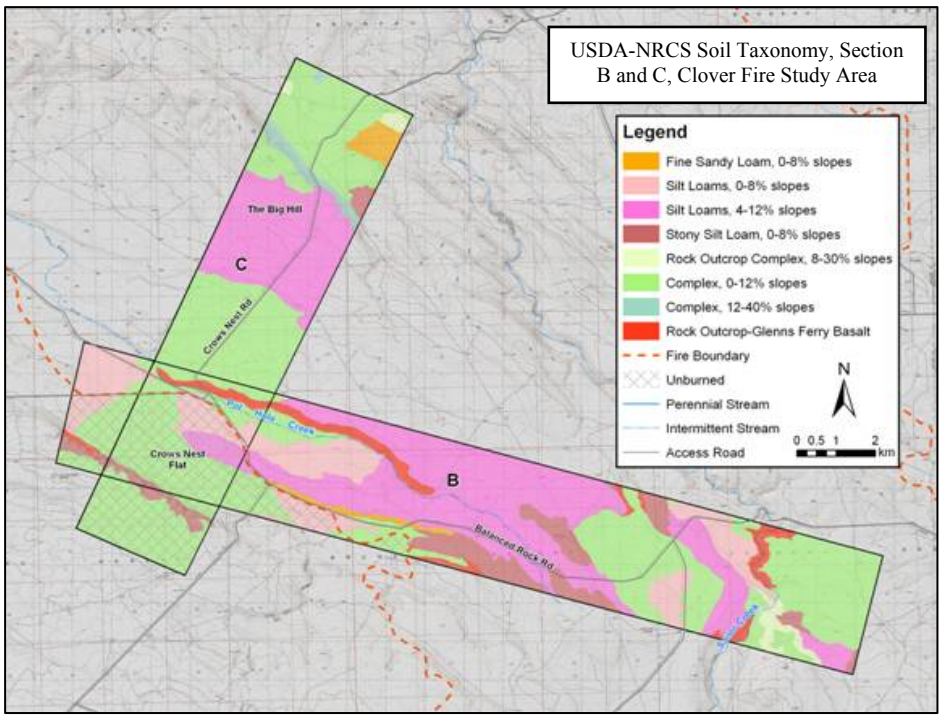

Fig. 2.4B. Soils, section B and C

Field Methods

Sampling Scheme

Prior to conducting field tests, 9 m by 9 m sample plots (Fig. 2.6) were identified and staked out in areas representing the different burn severity categories, which was assessed as described in the following sections. The size of the sample plot was determined based on the accuracy and resolution of the hyperspectral imagery. The HyMap imagery has a pixel resolution of 3 m by 3 m, and thus the field

sample plot encompassed a 9 pixel area. This allowed for errors in georegistration and spectral anomalies within the imagery. The boundary of the plot was recorded with the GPS in a polygon format. Soil conditions and vegetation burn severity most representative of the sample plot were evaluated. Within the 9 m x 9 m sample plot, three sample points were tested for water repellency and infiltration capacity, and the locations recorded with GPS in point format. The water repellency tests were conducted three times within each sample point. Because the accuracy of the Trimble GeoXT hand-held GPS device is no more than 1 meter (Steede-Terry, 2000), water repellency tests (MDI and WDPT) were conducted within 1 meter of the GPS sample point to ensure georegistration of the field-collected data.

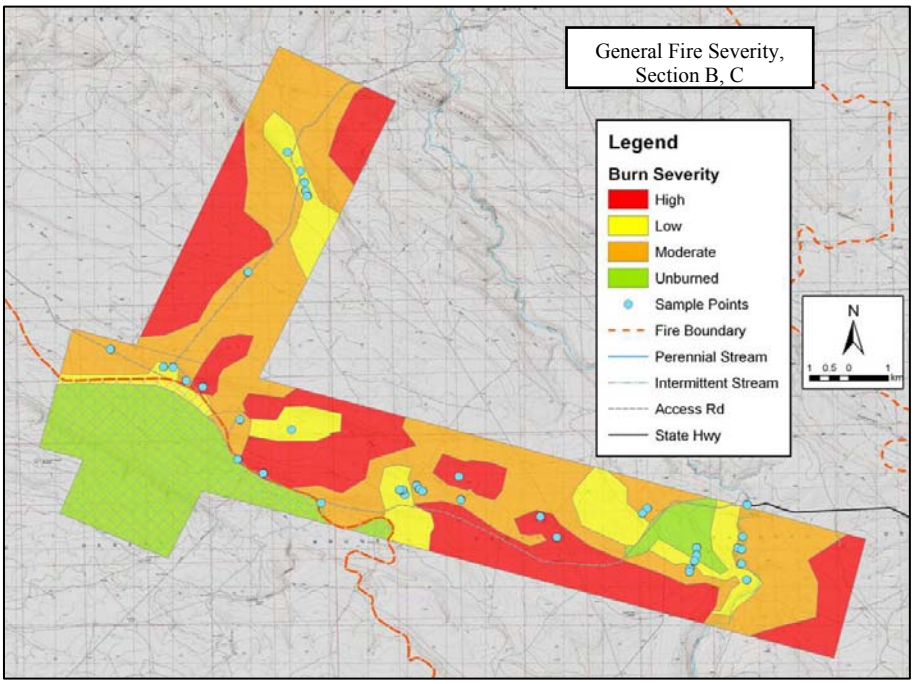

Fig. 2.5. General fire severity, section B and C.

Burn severity

This study assessed the effects of wildfire burn severity on soil properties, particularly the infiltration characteristics of the soil and the formation of water repellent soil layers. Burn severity is the effect the fire has on the soils, vegetation, and all other ecological aspects within the fire area, it is a relative measure of the change endured by the affected ecosystem and is expressed in terms of the share of vegetation killed by the fire as well as that regenerating in the following season (Davis and Holbeck, 2001). Physical and chemical changes of the soils are also taken into account (DeBano et al., 1998), though not comprehensively by most standard methods (Shakesby and Doerr, 2006). A standardized method of assessing burn severity in the field was developed by Key and Benson (2004); this method, however, is primarily meant for analysis of a burned forest ecosystem during the season following the fire, and documents changes in the environment in comparison to pre-burn conditions. The USDA Forest Service (USFS) and National Park Service (NPS) utilize initial and extended burn severity assessments to classify the conditions immediately after a fire (Bobbe et al., 2001; Switky, 2003), often in areas where pre-fire information is unavailable. Areas susceptible to post-fire sedimentation events are most susceptible within the same season as the fire (Cannon, 2001; Cannon et al., 2001; Tucket et al., 2004), thus it was essential for this project that the burn severity assessment take place soon after the fire. Most importantly, burn severity assessment methods like the Normalized Burn Ratio landscape assessment methods (Key and Benson, 2004) are not entirely suited for rangeland ecosystems, and researchers have indicated the need to restructure burn severity classifications relevant to soil changes (Shakesby and Doerr, 2006). The classification of burn severity across our study area, even using the USFS guide,

proved somewhat subjective and ambiguous, based on the pre-fire vegetation load and density, the vegetation group, and the character of the fire. We initally found the separation of unburned, low, and high burn severity to be quite straightforward, while the separation of moderate and high burn severity was at times difficult. Besides the fact that the ground characteristics were altered by wind soon after the fire, areas of high burn severity were often interspersed with less severely burned areas. In addition, the distribution of coppice microsites, or the area directly beneath the shrub canopy, and the interspace microsites between them, caused intermixing of severely burned and lesser burned shrubs and grass in many areas. Even though the separation of burn severity classes was at times subjective, as is the nature of ocular representations, by assessing the effects of the fire on the vegetation in accordance with the soil characteristics, a comprehensive representation of rangeland burn severity was determined.

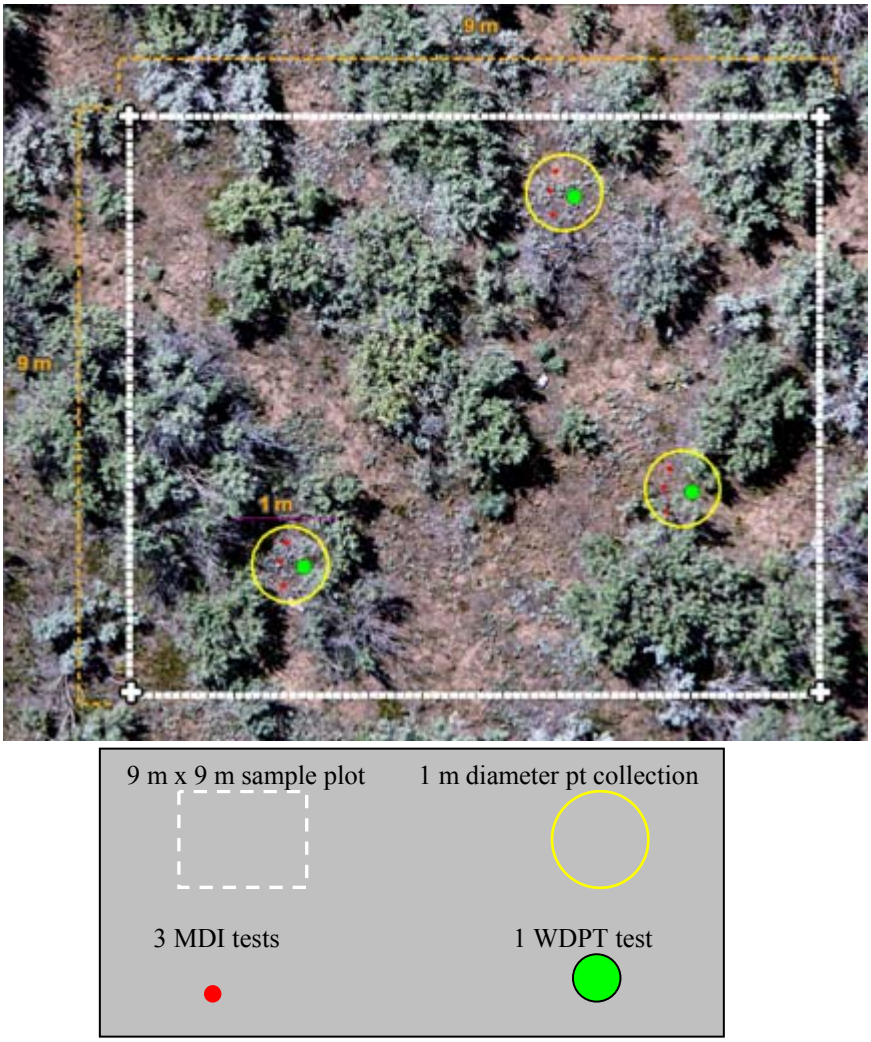

Fig. 2.6. Sampling Scheme

For this project, a burn severity assessment method similar to that used by the USFS BAER teams and the NPS was utilized (Bobbe et al., 2001; Switky, 2003), as the assessment was conducted in the same season as the fire event, and the soil and vegetation had not been assessed prior to the fire. Burn severity was classified into four broad categories: unburned, low, moderate, and high (Table 2.1**)**. The classes were further broken down by the dominant vegetation group of the area, namely grass and shrub, because observations indicated that burn severity and water repellency differed among these two different vegetation groups (Fig. 2.7, A-H).

Table 2.1. Burn severity classifications

Burn Severity	Vegetation	Description
Unburned	**Shrub**	Area not affected by fire
Low	**Shrub**	Foliage singed or consumed, branches still intact, <60% canopy consumed
Moderate	**Shrub**	Foliage, twigs, some branches consumed, branches up to 1cm diam. remain, 40-80% canopy consumed
High	**Shrub**	All shrub parts consumed, only stubs or stumps >1cm diam. remain
Unburned	**Grass**	Area not affected by fire
Low	**Grass**	Stalks & blades may remain slightly blackened, may be burned with at least 5 cm unburned stubble remaining
Moderate	**Grass**	Unburned stubble <5cm tall remains, forb foliage consumed, plant base burned near ground, burns uniform throughout area
High	**Grass**	No unburned grasses visible above root crown, all plant parts of forbs consumed, burns uniform throughout area

Fig. 2.7 A. Low severity shrub

Fig. 2.7 B. Low severity grass

Fig. 2.7 C. Moderate severity shrub.

Fig. 2.7 D. High severity grass

Fig. 2.7 E. High severity shrub

Fig. 2.7 F. High severity shrub

Fig. 2.7 G. High severity grass

Fig. 2.7 H. High severity grass

Assessing Water Repellency

A well-known and commonly used technique for identifying water repellency in soils is the Water Drop Penetration Time (WDPT) test (DeBano, 1981). The WDPT is used extensively because the method is fairly simplistic, enabling users to quickly identify water-repellent soil conditions. This method involves placing a drop of water on to the soil and watching to see if it infiltrates, or balls up and is repelled by the soil. Prior to placing the water drop, the top layer of loose soil, or duff, should be brushed aside because, if not removed, that layer will easily absorb water, and produce misleading results. Researchers have questioned the WDPT, however, because the size and surface tension of the water drop can vary with temperature, and a level of subjectivity is involved in differentiating strongly water-repellent soils (60 s), from extremely water repellent soils (>3600 s) (Dekker and Ritsema, 2000). Numerous variations of the WDPT test have been used. The USDA Forest Service classification standards indicate that if water remains for less than 10 seconds, the water-repellency is considered weak, 10 to 40 seconds indicates a moderate water-repellent layer, and water remaining for longer than 40 seconds is indicative of strong water-repellency (Davis and Holbeck, 2001). Krammes and DeBano (1965) indicated water-repellency if water did not penetrate after 5 seconds, mentioning that most soils repelling water for over 5 seconds generally tended to repel water for several minutes. Cannon (2001) indicated water-repellency if water did not penetrate the surface after 30 seconds, indicating that a 5-second threshold may only reflect the reluctance of water to infiltrate an extremely dry soil. The WDPT is well-suited for identifying the presence of water-repellent soils, but it is ambiguous for analyzing the degree of water-repellency (Dekker and Ritsema, 1994).

The WDPT was conducted at each MDI sample point to validate, correlate values and determine thresholds of the MDI tests. The WDPT involved digging an approximately 10 cm deep, terraced hole and testing the soils at various depths within the hole. Using a dropper or squirt bottle, water was dripped

on the soil at the surface, and depths of 2, 4, 6, and 8 cm. A water repellent layer was apparent if the water beaded up and sat or rolled off of the soil surface.

For this study, water-repellency was indicated in the field if the water drop remained on the soil for longer than thirty seconds (Cannon, 2001). In an effort to classify the degree of water-repellency, and correlate it with the MDI results, the water drop was allowed to remain on the surface for 360 seconds, and drops lasting longer were assigned that threshold value. A WDPT of 30-60 seconds indicated weak water-repellency, 61 to 180 seconds moderate water repellency, and 181 to 360 seconds indicated high water repellency. These values were used in previous studies by Dekker and Ritsema (1994), and Lewis et al. (2006). WDPT values were recorded in correspondence with the infiltration tests at each sample point location.

A newer method for water repellency analysis utilized by researchers at the USDA Forest Service (Lewis et al., 2006) is the Mini-Disc Infiltrometer (Decagon Devices, 1998). The Mini-Disc Infiltrometer (MDI) is a device that measures the infiltration of water into soil (Fig. 2.8). The MDI is a 22.5 cm long, 3 cm diameter hard plastic tube, gradated by milliliters up to 100. A rubber stopper is positioned approximately 5 cm below the top of the tube, creating a separate compartment that controls air suction. A 1 cm-wide steel tube passes from above the stopper to the bottom of the tube, above a stainless-steel porous disk. Another steel tube protrudes from the top, allowing air to escape when the disk is placed on the soil. When the two compartments of the MDI are filled with water, it is under tension, allowing the water to stay in place and not flow out of the disk. When the disk is placed on the soil, the water is pulled through the disk by capillarity, infiltrating the soil (Kirkham, 2005). The inner steel tube allows air to escape from the lower compartment into the upper compartment in a bubble, which then escapes from the top of the MDI by the other steel tube. The time until infiltration and amount of infiltration with the MDI is recorded.

A series of steps was followed for assessing water-repellency with the MDI, and results were correlated with the better-known Water Drop Penetration Time (WDPT) test. With a small shovel, any obstructing debris or rocks were removed to expose the soil surface. Additionally, the loose soil, or duff is cleared to expose the bare mineral soil. The burned areas of the site tended to have little ground cover, other than broken branches or brushes, because it was either consumed by the flames or removed by wind transport after the fire. If the sample site was located on a very steep slope, a small, level shelf was constructed, allowing for an accurate MDI reading without water seeping out of the sides of the disk. When the MDI was set on the top of the soil surface, the water within the tube began to infiltrate the soil through the porous disk and the soil, and a stopwatch was started. The time was recorded as soon as the first bubble entered the infiltrometer, and the MDI was held in place for one minute duration. At the end of the minute, the amount of water, in milliliters, that infiltrated the soil within that time frame was recorded. To compensate for local variability within the soil at the sample site, the MDI test was conducted three times at each sample site, within 50 cm of each other, and the average value of the three measurements was utilized for further analysis. Thus, there were 3 average MDI values within each sample plot. The rate of infiltration measured by the MDI was the primary measurement referred to for water repellency identification.

Daily weather observations at Castleford, ID were obtained for the months of August, September, and October from the National Climatic Data Center (NCDC, 2005) Records indicate that for the three months that sampling took place at the study site, monthly precipitation totals did not exceed 2 mm during August and September, and October received 6.36 mm of precipitation, mostly during the final days of the month, when field sampling was nearly complete (Appendix 2).

Researchers in Portugal found that water repellency in Eucalyptus soils was not present after being thoroughly moistened from wet winter conditions (Doerr and Thomas, 2000). Their study implied a moisture threshold of soils, above which repellency is not a factor, indicating temporal variability with the phenomenon. Because very little rain, which could affect the repellency and infiltration properties of the soil, was recorded during the sampling period, no samples were taken for laboratory analysis of moisture content and water repellency.

Fig. 2.8. The Mini-Disc Infiltrometer by Decagon Devices. Pullman, WA.

A quantitative method of detecting water repellent layers beneath the soil is by digging lateral trenches in the soil after wetting it with a rain simulator (Pierson et al., 2001), or after a rainstorm. By digging a trench and examining the soil layers beneath the surface, subsurface layers can be detected by differentiating the wet soil from the dry soil. Though the trench method gives a greater understanding of the spatial variability of water repellent soil layers and the preferential flow characteristics of rangeland soils, it was impractical in the dry rangeland study area where the amount of water needed for a rain simulator was inaccessible. To reduce the tendency for preferential flow beneath the MDI, the tube was held firmly on the soil surface, so as to keep water from escaping below the side of the porous disk. This, coupled with a multi-depth analysis by the WDPT, provided surficial and subsurface characteristics of soil water repellency in lieu of trenching.

The variability of the soil water repellency in the burned area was analyzed by assessing the infiltration with the MDI at measured intervals away from a burned brush. Pierson et al (2001) observed that soils in the burned rangeland areas tended to exhibit lower water repellency in the spaces between the burned brushes, called interspace microsites, due to the lack of combustible litter and organic material that induce water repellency when burned, within those areas. Additionally, the interspace microsites would not exhibit natural water repellency caused by sagebrush shrubs because they are outside the area of influence. Background repellency levels were measured during this study in unburned areas to obtain infiltration characteristics in an undisturbed setting. This experiment compared MDI measurements at lengths of 25, 50, 75, 100, and 200 cm out from burned sagebrush, to observe the changes in soil water repellency as the proximity to the brush decreases. The transects were sampled in a location and direction where the spacing of adjacent brush was wide enough that collateral effects from the other brush was minimized. This experiment strengthened the understanding of the perceived variability of water repellent soils within a burned rangeland area by demonstrating the spatial characteristics of water repellent soils induced by fire, and affected by vegetation dynamics.

Data Analysis

Following the acquisition of field data, the water repellency values and burn severity classes were statistically analyzed to assess their importance to the research. Initially, descriptive statistics of the MDI values within each burn severity class were calculated. Because the use of the MDI for assessing soil water repellency has only been documented one time (Lewis et al., 2006), the relation of its values (ml/min) were tested with results of the more traditional, and well documented, WDPT test. Due to the more subjective nature of the WDPT, a strong correlation was not expected, primarily due to the threshold of values (360 s) for high water repellency, and the fact that the MDI rate and WDPT essentially measure two different parameters (time of the water drops persistency and amount of infiltration). In addition, the relationship between the WDPT time (s) and the time till infiltration with the MDI (s) was tested, but again, a strong correlation was not expected due to the threshold of the WDPT. In addition, many of the WDPT values were 0, and even in a water repellent soil, the MDI generally began infiltrating quickly.
To help understand the significance of the field data and to test the relationship of the MDI-assessed water repellency with burn severity, a linear mixed model called the Proc Mixed analysis was used in SAS (SAS Institute, 2005). The advantage of the Proc Mixed is that it tests the variance/covariance structure of the field data, while allowing for possible errors created by spatial correlation of the data across the study area (SAS Institute, 2005). The model established the burn severity classes as the subject level, or the lowest information criterion, and the average MDI value at each sample point as the dependent variable.

The first step of the model was to perform a Least Squares adjustment of the mean MDI values of each burn severity class, which chooses a best fit curve of the data based on the least sum of the deviations squared. The model then computed the difference between all pairs of the least squares mean MDI values among the matrix of burn severity/vegetation classes. The resulting t-test levels of significance (p-values) were then adjusted with the Kramer multiple comparison adjustment method for false positives (SAS Institute, 2005). When independent observations (MDI values) are subject to the same criterion (burn severity classes) the chance for false positives increase. The Kramer adjustment is a method of countering the possibility of false positives. If the p-value is less than the alpha value of 0.05, then the null hypothesis that the two variables are the same is rejected, and their relationship is considered significant.

Field Spectrometry

Spectral signatures of endmembers for burn severity and soil water repellency were collected in the field with a handheld spectroradiometer. The purpose of collecting the field spectrometry was to acquire spectral signatures of endmembers within the field for imagery control, and to assess the differences among the endmembers' spectral characteristics. Endmember signatures of bare ground, gravel, basalt rock, unburned grass and shrub, low severity grass and shrub, moderate severity shrub, and high severity grass and shrub were collected.

A FieldSpec Pro spectroradiometer, made by Analytical Spectral Devices Inc. (2004) was used and collects spectrometry information in-situ at a range of 350 to 2500 nm (Fig. 2.9). The device has a 25° field of view (bare fiber) with a sampling interval of 100 milliseconds (Analytical Spectral Devices, 2004); when held waist high, the sensor acquires a spectral signature of approximately 1 m^2 on the ground. A fiber optic sensor relays the data to a notebook computer where the input spectral data is saved. After collecting the field spectrometry, the spectra (reflectance versus wavelength) were imported into ENVI, where the values were plotted in the spectral library viewer. The values were then resampled to match the spectral scale of the HyMap hyperspectral imagery, in micrometers (μm).

Before collecting the field spectrometry, the device was calibrated with a white spectralon plate to calibrate and normalize the data collection for reflectance. Optimally, field spectrometry should be collected on the same day as the aerial imagery if it is to be used for endmember control when classifying

hyperspectral imagery. The lack of instrument availability and logistics prevented same day data collection; however, the field spectrometry was collected within two weeks of the aerial imagery, and it was collected on a cloudless day, near solar noon, so as to limit atmospheric dust, water vapor, and shadows.

Fig. 2.9. The FieldSpec Pro by Analytical Spectral Devices.

GPS Data Collection and Processing

This research project relied heavily on Geographic Information Systems (GIS) as a data collection, analysis, and organization tool. GIS utilizes digital spatial information with relational attributes to efficiently manage multiple layers of data in similar map projections. While conducting field sampling, a hand held Trimble GeoXT (Trimble Navigation, 2005) global positioning system (GPS) device recorded the boundary of the sampling plots as polygon shapefiles, along with the points at which the soil water repellency tests were conducted in the form of point shapefiles. The data were collected in Universal Transverse Mercator (UTM) Projection; zone 11 north, with the North American Datum of 1983. The GPS records of each sample point and plot were used as ground-truth verification for the remote sensing analysis.

A total of eighty sample plots were evaluated and their position recorded with the GPS, and the three sample point locations within each plot were also recorded, totaling 235 (several plots contained less than 3 points because the GPS did not receive an ample signal to record their locations). After collecting the field data with GPS, the information was downloaded onto a workstation, post-processed, and differentially corrected for inherent geometric error using Trimble Pathfinder (Trimble Navigation, 2005) software. The data was then input into ArcGIS (ESRI, 2005), where the records were assessed, edited, and additional fields were added. Finally, the GIS shapefiles were imported into a geodatabase, which is a centralized collection of relevant geospatial data. The geodatabase included the field-collected sample point and polygon shapefiles and point locations at which the ASD spectradiometer data was collected, along with their attribute tables, and ground control points (GCP's). Other data included in the geodatabase were the fire boundary, local soil classifications, roads, elevation, slope, and generalized burn severity. The attributes included with the point and polygon field-collected data are listed in Table 2.2.

Table 2.2. GIS attribute table of field-collected data

Sample point attributes	
1	Point number
2	Burn Severity
3	Ground Cover at point
4	Dominant Vegetation (in plot)
5	MDI time till infiltration (seconds)
6	MDI rate of infiltration (ml/min)
7	WDPT value (2, 4, 6, 8 cm)
8	Water repellent layer present (yes/no)
9	Depth of water repellent layer
10	Sample Date
11	Average MDI value
12	WDPT repellency rating
13	UTM X coordinates
14	UTM Y coordinates
15	NRCS soil classification
Sample plot attributes	
1	Plot number
2	Burn Severity
3	% ground cover across plot (ocular estimate)
4	Dominant vegetation
5	Comments
6	Sample Date

Transect Repellency Experiment

In order to strengthen the understanding of water repellency in a rangeland wildfire setting, we conducted a supplemental experiment that examined the infiltration capacity of soils at predetermined distances from a burned shrub. The experiment was designed to show that the infiltration of soil increases, or the water repellency decreases, as the distance from the brush increases. Soil infiltration was tested with the MDI. The experiment was conducted on various-sized shrubs, with canopy edge ranging from 25-100 cm from the center of the shrub.

To conduct the experiment, a burned shrub was identified, and flags staked at lengths of 25 cm, 50 cm, 75 cm, 100 cm, and 200 cm from the shrub (Fig. 2.10). At each flag location, the MDI test was conducted three times, within 20 cm perpendicular to the measured transect. The three measurements at each increment were averaged and input into a table (Table 2.2**)**. The tests were conducted on October 15 and October 21, 2005. On October 21, the ASD FieldSpec Pro spectroradiometer was used to collect field spectra at the transect sites. Spectra were collected at 25 cm, 50 cm and 100 cm. Because of weather conditions (cloudy sky), the FieldSpec Pro could not be used on October 15.

Spectroscopy Methods

Hyperspectral data was acquired over the study area with the HyMap sensor, by HyVista, Inc. A total of seven flight lines were flown over the three study sections (Fig. 2.11). The flight lines are approximately 10-15 km long and 1-2 km wide. The HyMap imagery consists of 125 bands, with a contiguous spectral range from 0.45 to 2.5 μm. Bandwidths range from 0.015 μm in the visible and NIR to 0.020 μm in the SWIR, and the imagery has a pixel size of 3 m. The data were collected on August 26, 2005, between 12:00 noon MST and 12:33 MST. The geographic locations of study sections and flight lines were chosen based on the variability of fire effects and local geography observed within the areas.

Hyperspectral Processing Flow

Spectroscopic research generally follows a standard processing sequence (Fig. 2.12). After selecting a study area and acquiring hyperspectral imagery, an initial assessment of the imagery is conducted. This is done by visually assessing individual bands within the imagery, examining various color composites, and evaluating individual band statistics to assess the signal-to-noise ratio, to determine if any areas of the data contain null data values or are missing lines, and to evaluate the geometry of the imagery for any visual flaws (Jensen, 2005). After an initial assessment of the imagery, radiometric and geometric correction of the imagery is carried out (in this case by the vendor, HyVista).

Fig. 2.10. Sagebrush transect

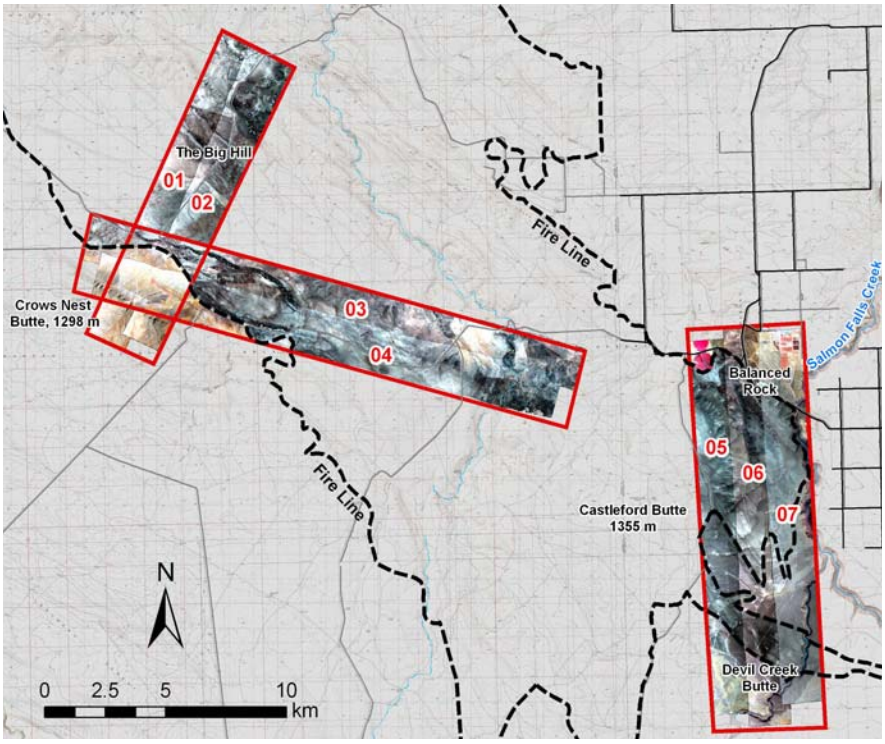

Fig. 2.11. HyMap flight lines (01-07) collected over the study area.

Following radiometric and geometric correction of the imagery, the dimensionality of the data is reduced to find relative bandwidths for analysis. Hyperspectral datasets are very rich in information, due to the large amount of spectral bands, or data dimensionality (Jensen, 2005) within them. Because all of the bands may not be pertinent for a specific analysis, standardized methods have been developed to reduce the dimensionality of hyperspectral imagery. This is completed through the use of statistical methods that delete and transform bands with redundant and unnecessary information. A statistical algorithm for reducing hyperspectral data dimensionality is the Minimum Noise Fraction (MNF) transform, which is a two-phase principal components analysis performed on the data to reduce noise and determine the useful, coherent bands to be used (Jensen, 2005). The MNF output results in a 125 band transformed data set with the noise as the unit variance and no wavelength correlation. The resulting 125 band images are eigenvalues and are sequentially reorganized according to data coherency. After examining the eigenvalue plots and images, the 125 images can be separated between coherent and noise-dominated bands.

Following data reduction, the pixels of the imagery are analyzed and reduced to subsets of only pure pixels, or those pixels containing only one material, also known as extreme pixels. In a 3 m x 3 m pixel, for example, the area on the ground a pixel covers may contain a certain percentage of litter, vegetation, rock and bare ground. In this case, the pixel would not be considered pure, because of the existence of multiple endmembers or materials within its geographic confines. If another pixel contained the spectral signature of 100% bare ground, or 100% rock, or 100% litter, then that pixel would be considered pure, as it contains only one material. Pure pixels are important for identifying endmembers present in the imagery and are later used as training data to find similar pixels through the use of the n-Dimensional Visualizer (n-DV), and classification techniques like the Spectral Angle Mapper. Identification of pure pixels is first implemented using Pixel Purity Indexing (PPI) in ENVI. The PPI repeatedly projects scatter plots of image spectra onto random unit vectors in n-dimensions (n=number of bands) for a set number of iterations (10,000 or more), and records the outliers as extreme, or pure pixels. A user-defined threshold sets the range of pixel digital number (DN) values that will be grouped with the identified extreme pixels for each projection of vectors. The more iterations completed during the PPI, the greater the likelihood one will find all of the most extreme pixels in the image. At the end of the iterations, the pixels that have been marked extreme the highest number of times are considered pure. After the pure pixels are identified, those that are most extreme (representing the highest portions of the accumulated distribution percentage), are assessed to determine what portion of the spectrum, and which endmembers, they represent. The spectral qualities of the extreme pixels are analyzed with the n-DV.

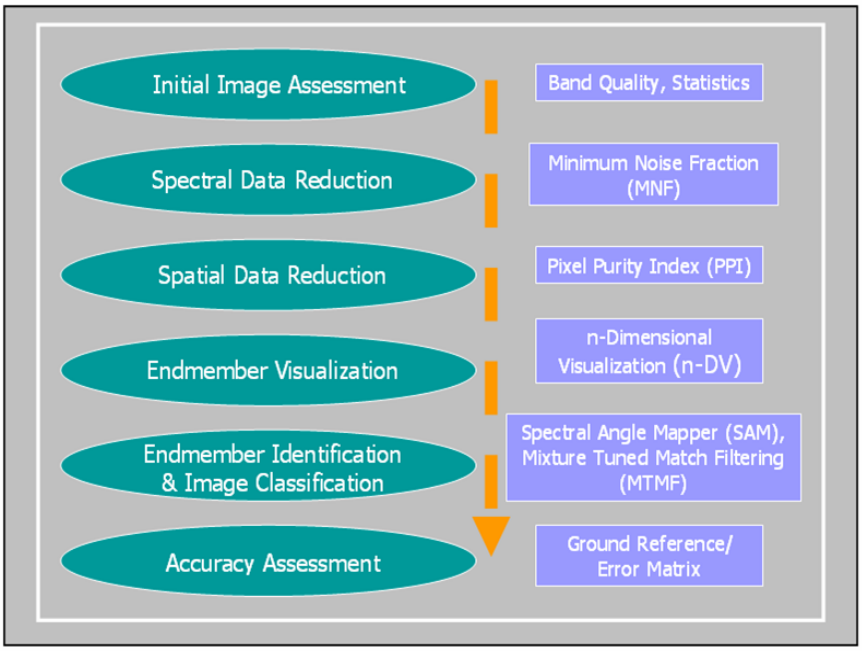

Fig. 2.12. The hyperspectral processing flow (adapted from Jensen, 2005).

After identifying the extreme pixels in an image with the PPI process, the pixels' spectra can be multi-dimensionally visualized in the n-DV. Through the use of the n-DV in ENVI, a collection of spectra can be plotted and visualized in a point cloud of n dimensions. By rotating the point cloud in accordance with the selected band axes, spectra of specific endmembers will appear in clumps within the point cloud (Jensen, 2005). According to the total number of endmembers, those that are pure will fall at vertex points. For example, with two endmembers, the pure spectra will appear at two ends of a line, and the mixed spectra in the middle. Likewise, with three endmembers, mixed pixels will appear inside of a triangle, with the pure spectra at the triangle points, and so on. Because the mixed pixels appear inside the endmember vertices and the extreme pixels as outliers, the pure pixels are readily identified (Kruse et al., 1997). After the purest pixels are located, ground collected spectral information, spectral libraries, and/or ground-based user knowledge are employed to determine what each pure pixel represents. After identifying the endmembers within the imagery, classification techniques are applied to map the material they represent across the remainder of the image. This can range from endmember classification within a single pixel, or sub-pixel, to the application of specific classification techniques developed for spectroscopy. One such classification method often utilized in spectroscopy is the Spectral Angle Mapper (SAM). SAM allows efficient classification based on the similarity of image spectra to a spectral reference (Kruse et al., 1993). When the SAM is computed, vectors of reference spectra are projected in n-dimensional space (n = number of bands), and a specified angle is set for which pixels falling within that angle are placed within the category of that certain reference spectra. Depending on the size of the reference angle, the classification can be generalized when large reference angles are used, or specialized when a small angle is used. The smaller the angle, however, the more likely it will be that portions of the image will be unclassified. One advantage SAM has over other classifiers is that only the length of the reference (and unknown) vectors and not the angles of the vectors are affected by the albedo within the imagery. This means that changes in albedo across an image (e.g. from topography or sun angles) will not affect the classification of a target material.

While SAM is a presence/absence classifier, examples of methods of detecting sub-pixel abundance include Linear Spectral Unmixing (LSU) and Mixture Tuned Match Filtering (MTMF). LSU is an automated attempt to unmix single pixels that have various materials and spectral properties within them (Kruse et al., 1997). MTMF is a more advanced form of spectral unmixing, in that it does not require knowledge of all the endmember signatures to map the sub-abundance of a pixel (Aspinall et al., 2002). The MTMF results in a matched filter (MF) score (a linear measure of abundance) and an infeasibility value (indication of false positives). Between the MF and infeasibility value, there is potential to identify subpixel abundances. To locate the endmembers being mapped by the MTMF, the MF and infeasibility values are simultaneously analyzed in a 2-dimensional scatter plot. The analyst can interactively select and/or threshold pixels in the scatter plot representing the desired target. After mapping and classification of the imagery, an accuracy assessment is normally carried out to statistically quantify and analyze the integrity of the results.

The most typical accuracy assessment conducted on remote sensing classifications is the confusion matrix, or error matrix (Jensen, 2005). The confusion matrix is a method of categorically assessing the accuracy of a remote sensing-derived classification map by comparing it with ground truth information. The matrix outputs a square matrix indicating which classes on the map fall within the ground truth reference classes. The overall accuracy of the map is computed, as well as producer's and user accuracies, the kappa coefficient, and errors of commission and omission. Producer's and users accuracies refer to how well individual categories have been mapped; the producer's accuracy indicates the probability, as percentage, that a pixel of a certain classification actually falls where the ground truth area of that same class is, and is determined by dividing the total number of correctly classified pixels in each category by the total number of training set pixels used for that particular category (Lillesand et al., 2004). The users accuracy is computed by dividing the total number of correctly classified pixels in each class by the total number of pixels placed in that category (row total). The users accuracy indicates the

probability that a particular classified pixel on the map is actually represented by the same class on the ground (Lillesand et al., 2004). Errors of commission and omission indicate the percentage of a class that is wrongly included in a class (commission error) and the percentage of a class that is wrongly excluded from its category (omission error) (Congalton and Green, 1999). The Kappa coefficient of agreement (K_{hat}), is a multivariate accuracy assessment technique (Jensen, 2005) that indicates the measure of agreement between the actual agreement of the classified map (indicated by the error matrix) and the chance agreement of the reference data (the row and column totals). A Kappa value greater than 0.80 indicates strong agreement, 0.40-0.80 represents moderate agreement, and values less than 0.40 indicate poor agreement) (Congalton and Green, 1999).

The processing and classification of the imagery for this study followed the described hyperspectral processing flow. The objective of processing the imagery was to classify the burn severity of the study sections in accordance with the burn severity assessment made in the field. After accurately classifying the burn severity, endmembers representing high water repellency were identified and a separate set of classifications was conducted to map areas of high water repellency, and thus, likely at risk of elevated erosion levels. A total of 7 images were collected over the three sections of the Clover fire study area. The image that had been most thoroughly field sampled within its boundaries was image 6, of section A. The proceeding section describes the processing and classifications of image 6.

Processing, Image 6

Initial Image Assessment

Preliminary image processing was conducted by the vendor and included geometric and radiometric (atmospheric) correction. The HYCORR algorithm was used to atmospherically correct the imagery, and the images were refined with the Empirical Flat Field Optimal Reflectance Transformation (EFFORT), an algorithm commonly used after the initial atmospheric correction of the imagery. The EFFORT spectral polishing technique further improves the data accuracy and accounts for errors within the HyCorr algorithm, due to anomalies and accuracy limits (Jensen, 2005), by applying a linear correction to each individual band in the scene. The imagery was converted from radiance values to reflectance values, and spatially projected to the UTM Projection, zone 11, with the WGS 84 datum. A preliminary evaluation of all the bands indicated them to be spectrally correct. After acquiring the HyMap data, all image analysis was conducted with ENVI software (RSI, 2005).

Minimum Noise Fraction

To reduce the dimensionality of the dataset, a minimum noise fraction (MNF) transform was computed. The result of the MNF is a transformed data set with noise as the unit variance, and eigenvalue images arranged according to noise correlation. The most optimal image processing is made possible by using the bands that display the most dominant and coherent variance. Although all the transformed bands in a MNF may have some useful information, it is more feasible and practical to subset the images to those bands containing the high amounts of variance. Additionally, at least two of the image bands were almost completely noise-dominated (bands 62 and 63). By examining the output eigenvalue plots of individual band variance in comparison with the cumulative MNF band variance, the percentage of band variance to be utilized for further processing can be determined (Fig. 2.13). Typically, the decision of which bands to utilize is made by determining where the eigenvalue plot flattens out and coherent data is lost, and choosing the corresponding variance and band threshold (Mundt et al., 2005a). To begin, a subset of 30 MNF bands was used, corresponding to a threshold of 77% cumulative variance (Fig. 2.13). The subsequent PPI failed to identify all extreme pixels, however, so it was decided to utilize the full 125 band MNF for processing. Despite the fact that several of the bands were noise-dominated, they were still included in the MNF because of the possibility that those bands may have viable data identified by the MNF.

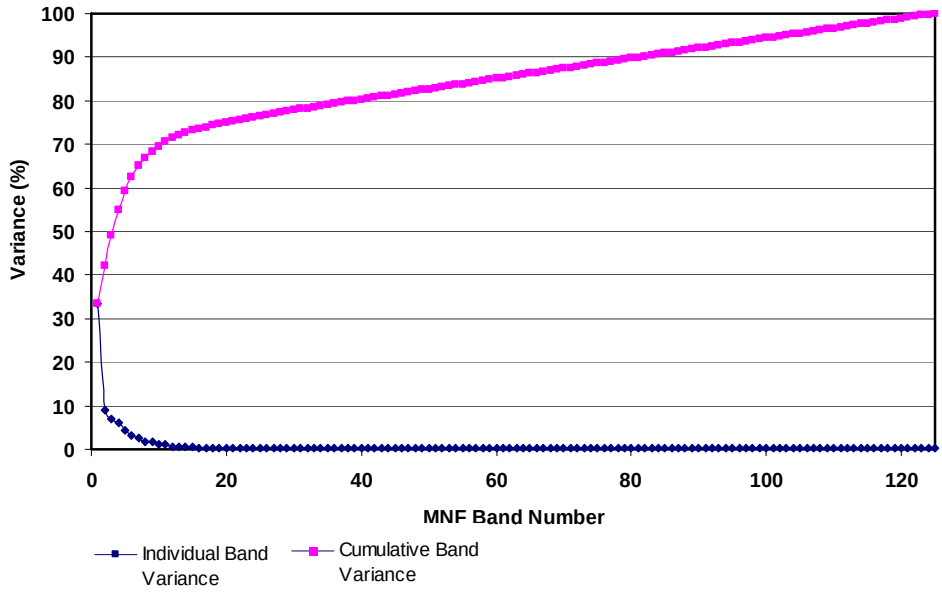

Fig. 2.13. Individual vs. cumulative band variance, MNF-transform. 30 bands = 77% cumulative variance.

Image Masking

Because the study aimed to classify only the burned areas, the unburned areas of the image were isolated from the burned areas, and a mask was applied over them for further analysis. Using band 1 of the MNF image, the burned area was easily isolated from the unburned areas using an interactive image histogram stretching technique (Fig. 2.14 A-C). The histogram of brightness values for band 1 of the MNF has two peaks and a trough in the middle between the positive values of the burned area, and the negative values of the unburned areas. By stretching the histogram to encompass only the positive brightness values, the unburned area is blacked out. The values below 0 were then thresholded to a region of interest (ROI) and subsequently used as a mask. By applying the mask to the MNF image, a new image was created with brightness values for the burned area only, and all unburned areas that previously had negative brightness were set to 0. Setting the unburned areas brightness values to 0 removed them from analysis, and allowed subsequent image processing to be performed on only the burned area.

Pixel Purity Indexing (PPI)

The purpose of the Pixel Purity Index is to identify the extreme, or pure, pixels within the MNF-transformed image. As mentioned, the PPI was originally computed on the subset, 30 band MNF image (considered the most coherent). After masking out the unburned areas of the image, the first PPI was run with 10,000 iterations, with a pixel threshold of 3.

When completed, the PPI routine results in a plot illustrating the total extreme pixels selected in relation to the total iterations (**Fig. 2.15**). A typical PPI curve should rise sharply and then flatten out near the end of the iterations after all of the extreme pixels have been found. As Fig. 2.15 demonstrates, the plot of iterations versus extreme pixels did not flatten out, even though 65,000 pixels were identified as extreme. The primary reason is likely due to the homogeneity of the burned area brightness values across the image. For example, a histogram of MNF band 1 (**Fig. 2.16**) shows the DN brightness values of the image ranging from -25.00 to 22.00. In comparison, the DN values of band 1 of the original reflectance image range from 0 to 1600. After experimenting with a range of iterations and various threshold values and obtaining similar results, it was presumed that the homogeneous, spectral similarity of the target materials within the burned area increased the difficulty for the PPI to distinguish pure pixels among the image

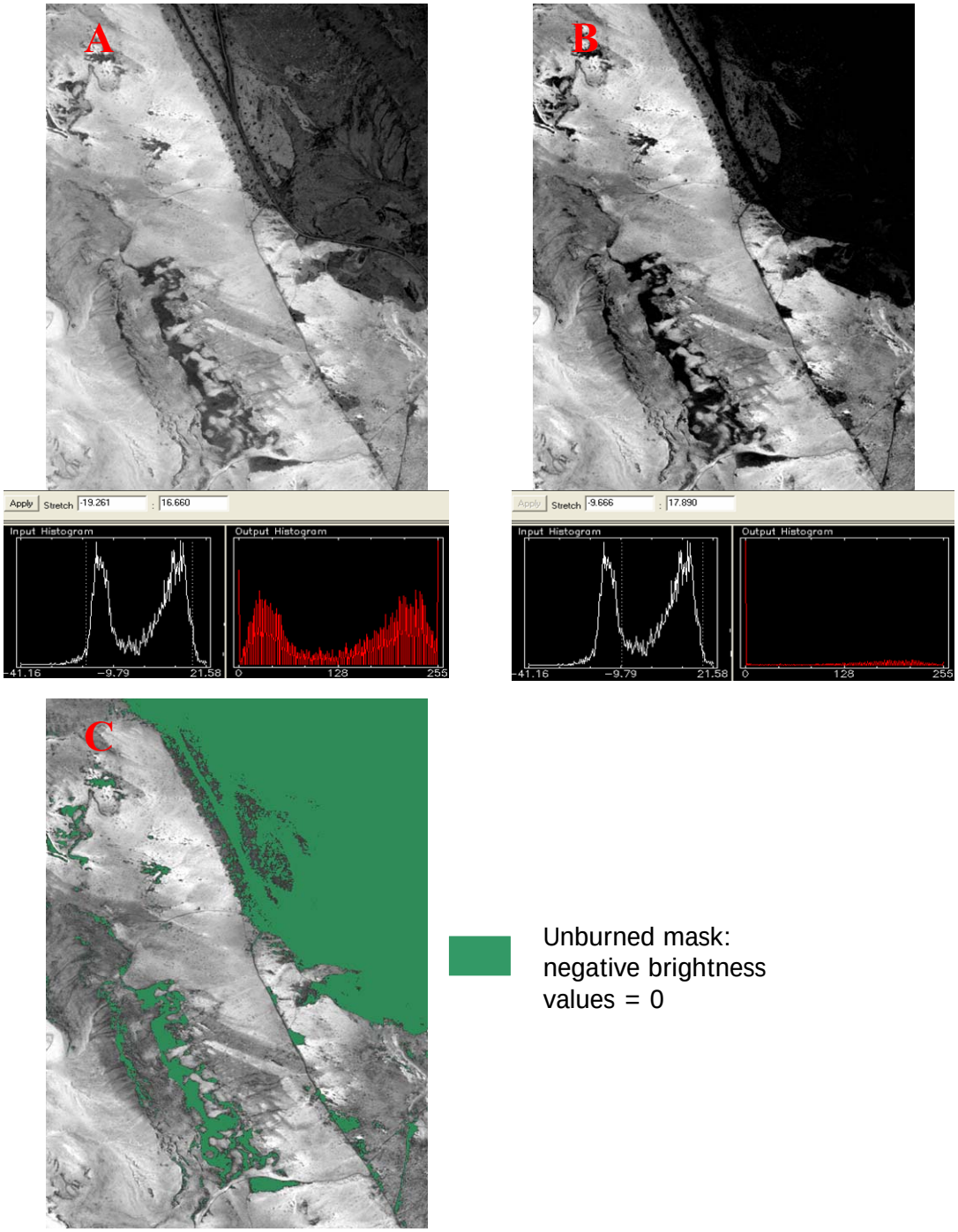

Fig. 2.14. Isolating the burned area with Band 1 of the MNF. A: Unadjusted histogram; B: Stretched histogram; C: Mask applied over unburned area after thresholding negative values and setting them to 0.

The utilization of the 125 band MNF compensated for the difficulty of identifying extreme pixels, by allowing the maximum variance of pixel and data coherency to be considered for extreme pixel detection. This second PPI with the 125 MNF bands was run at 30,000 iterations, with a threshold of 2.5 pixels (**Fig. 2.17**). Though this resulted in an acceptable PPI, it was very heavy on resources, taking approximately 24 hours to compute and maximizing the computer-allocated memory in excess of 1400 MB. Due to the

large allocation of memory and time needed for this computation, this was the only image in which a PPI was computed using all 125 bands. The other flight lines on which PPI's were computed used the first 50 MNF bands (~85% variance) (**Appendix 3**). The tradeoff of discarding the top 15% of data variance for performance was worthwhile because it was determined that the use of the remaining variance would not considerably increase the results of extreme pixel identification. The primary factor in identifying the extreme pixels was the amount of iterations (30,000) conducted with the PPI, as subsequent PPIs on other images with 50 MNF bands would demonstrate.

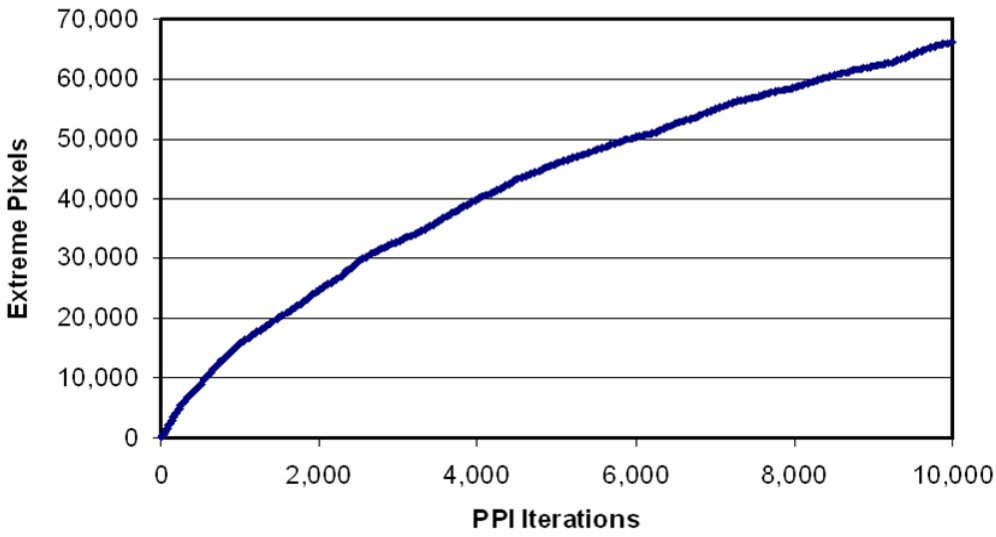

Fig. 2.15. PPI plot of 30 band MNF, 10,000 iterations, threshold 3.

The 125 band PPI identified 1,517,669 pixels out of 2,182,656 total pixels (**Fig. 2.17**). Of those total pixels, 1,365,902 were discarded, because they constituted the lower 90% of the accumulated percentage of extreme pixels found. This was done because the most extreme (pure) pixels are likely to be in the upper portions of the accumulated percentage of pixel distribution. After discarding the lower 90%, approximately 152,000 pixels remained to be analyzed for endmember identification. To identify the extreme pixels of the image, the PPI band values were thresholded to DN values between 73 and 10,879 (highest), corresponding to the top 152,000 extreme pixels. This resulted in a threshold of 151,386 pixels in the upper cumulative 10% of the frequency distribution (**Fig. 2.17**).

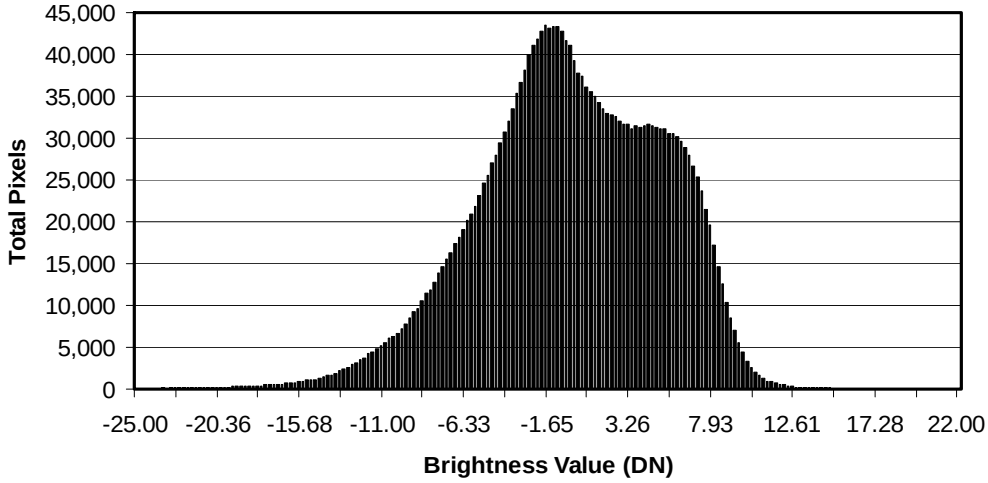

Fig. 2.16. MNF band 1 (masked) brightness value histogram.

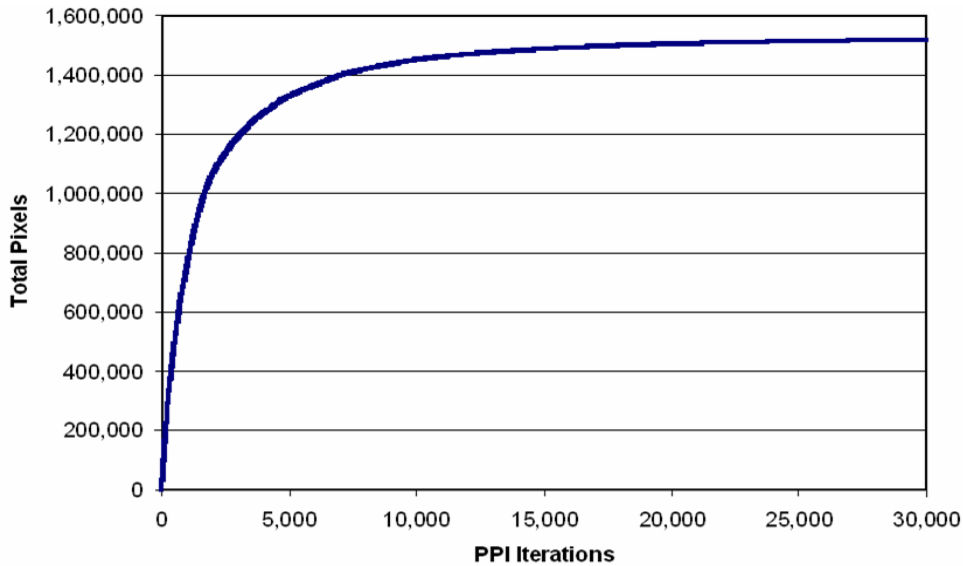

Fig. 2.17. PPI plot of 125 MNF, 30,000 iterations, threshold 2.5.

n-Dimensional Visualization

After discarding the lower 90% of cumulative pure pixels, the 152,000 remaining pixels were analyzed with the n-DV to identify extreme pixels. The number of pixel spectra projected in the n-DV should not be so high that the visualizer is overcrowded and its capability reduced. Because 152,000 pixels were too many for projecting at one time, they were viewed in increments of about 25,000 pixels (Table 2.3), between the DN values of 73 and 10,879 (Fig. 2.18 A-G).

Table 2.3. Pixel increments for n-Dimensional Visualization

Pixel increment	DN value range	Total pixels
1	73-80	24,416
2	81-91	25,526
3	92-107	25,801
4	108-133	25,218
5	134-191	25,011
6	192-10,879	25,413

After viewing each pixel increment in the n-DV at dimensions up to n=125, it was evident that extreme pixels could not be distinguished until the highest value increments were visualized. Using the autocluster option, ENVI selected 46 classes of extreme pixels in the n-DV from the spectral cloud of DN 134 – 10,879, the two highest pixel increments. After the 46 extreme pixel classes were detected the remaining pixel spectra were manually examined, and 6 additional classes were selected. The 52 extreme pixel classes identified in the n-DV were then exported back to the image as regions of interest (ROI's), and a geographic projection was applied to them, so that they could be identified and related to ground truth information.

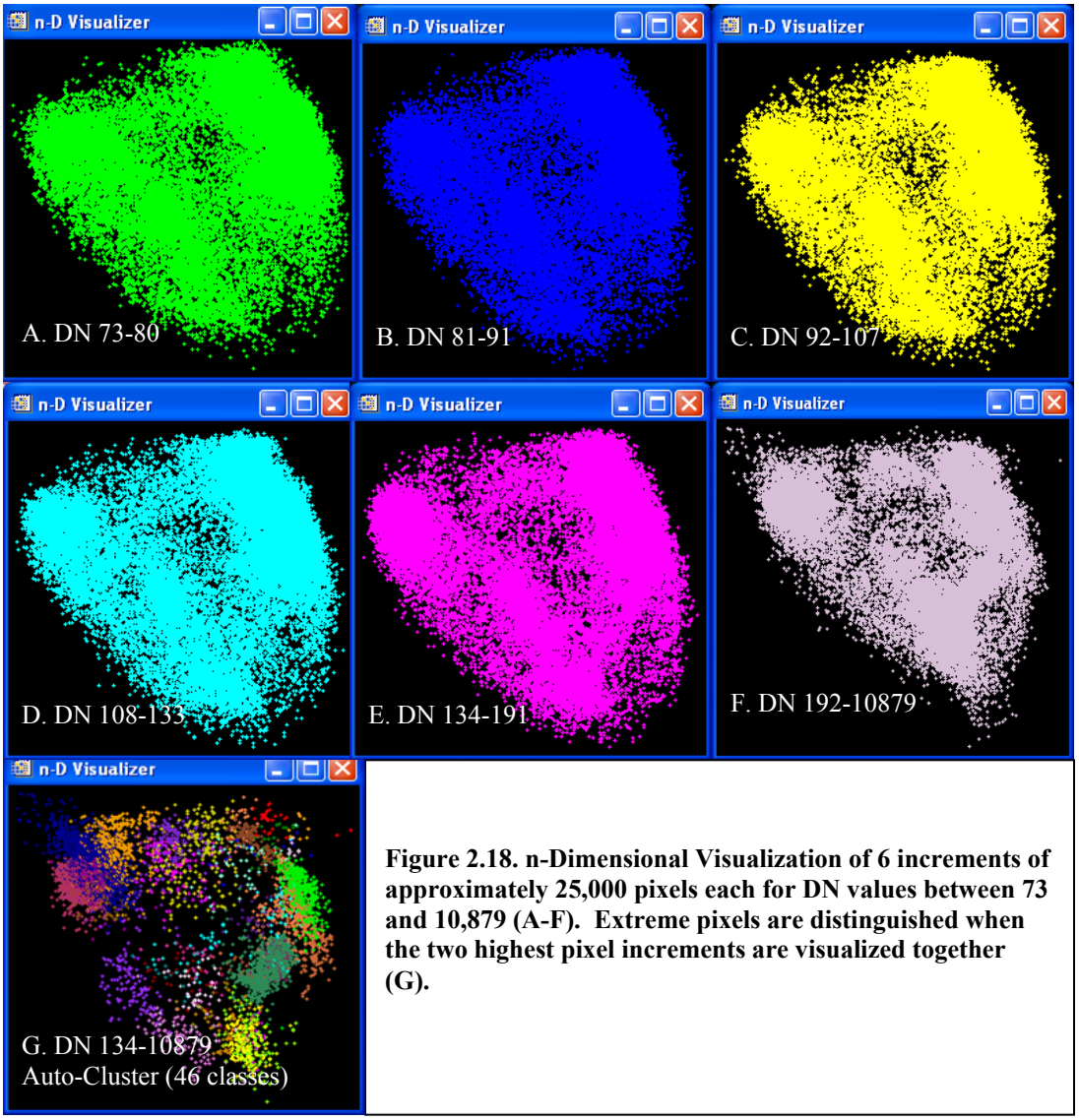

Figure 2.18. n-Dimensional Visualization of 6 increments of approximately 25,000 pixels each for DN values between 73 and 10,879 (A-F). Extreme pixels are distinguished when the two highest pixel increments are visualized together (G).

Identifying Burn Severity Endmembers

The most difficult and time-consuming portion of spectroscopy is the identification of endmembers. This study utilized the functionality of ArcMap GIS to interactively view the extreme pixels identified in the HyMap image in the same geographic projection as the field-collected ground truth data, as well as other geospatial data, to identify the extreme pixels that could be used as endmembers. After the extreme pixels were selected in ENVI, they were converted to a class image, and then to a vector dataset, and saved as a shapefile. The shapefiles, which represented the 52 categories of extreme pixels found in the n-DV, were overlaid with the ground truth information collected in the field, as well as 2004 National Agriculture Imagery Program (NAIP) ortho-rectified digital color aerial photos (USDA-FSA, 2005). A supervised classification portraying the dominant pre-fire vegetation groups of shrub or grass was created from the aerial photos and supplementally used as a guide for identifying the dominant vegetation group of the extreme pixels pre-fire vegetation group (Appendix 4). The NAIP ortho imagery is representative of the study area approximately one year before the fire, and its true color, high resolution (1 m) allows for accurate visual detection of vegetated areas, bare ground, roads, and other man-made features. Prior to analysis, the geo-registration of the HyMap imagery was assessed in comparison with the ortho-rectified NAIP ortho imagery, and found to have a mean error of 6.4 m (Appendix 1). The average shift difference between the Hymap and NAIP imagery was an acceptable difference for the purpose of identifying burn

severity endmembers, particularly since many of the burned areas tended to cover large, homogeneous areas.

The extreme pixel classes were assigned their respective burn severity endmember (e.g. unburned, low, moderate, high) by assessing the geographic location of the extreme pixels with respect to other ground truth information. When pixels were found near a sample plot (10-20 m), the underlying vegetation classification was consulted to verify the dominant vegetation group (e.g. shrub, grass), and the pixels were assigned the vegetation group and burn severity of that plot. Extreme pixels were also spectrally matched to endmembers by examining the average spectral profile of the pixels in comparison to the spectra of the sample plots. Some burn severity classes exhibited unique spectral signatures (e.g. low severity grass) that extreme pixels could easily be matched to, while others displayed signatures that were virtually indistinguishable from the typical spectra of the image (e.g. moderate and high severity shrub). This introduced a certain level of subjectivity to the assignment of moderate and high burn severity training endmembers that likely evoked error in the classifications. Extreme pixels that could not be identified based on their spatial association to other GIS layers or their spectral association with training plots were discarded for further use. Of the 52 extreme pixel classes analyzed in ArcGIS, 10 were discarded because their material could not be confidently identified, resulting in 42 extreme pixel classes, of which the similar classes were merged together for input into the classification algorithms.

Identifying Water Repellent Soil Endmembers

A considerable portion of the remote sensing analysis for this project involved analyzing the spectral characteristics of the soils across the burned area; within various burn severity zones, at points designated as having high water repellency and no repellency, and across areas of different pre-fire vegetation characteristics. The predominant spectral characteristic across the entire burned area is the high reflectance within the short wave infrared (SWIR; 1.5-2.5 μm). A typical spectral profile from the hyperspectral imagery of burned soil at the study area (Fig. 2.19) exhibits reflectance between 5% and 10% at the beginning of the visible spectrum (0.5 μm), and rises steadily to about 35% reflectance around 1.75 μm in the SWIR, where it flattens out; the curve then demonstrates a rise up to about 40% reflectance around the clay absorption band at 2.3 μm (which demonstrates a dip in the signature due to the water retention capabilities of clay minerals) (Chabrillat et al., 2002), and then levels off around 37% reflectance (the absorption near 1.4 μm and 1.9 μm are due to atmospheric water absorption and noise). The majority of the spectral signatures across the burned area, and particularly in the moderate and high severity shrub areas, display a similar curve, with most of the variation in the SWIR. To depict the locations of water repellent soils in the image, the spectral profile had to be defined and used as training endmembers. None of the extreme pixels overlapped the water repellent sample plots, indicating that water repellent soils did not demonstrate a pure spectral signature, as identified by the PPI, which could be used as a training endmember. To define spectral signatures for the soils, the ground-collected data was overlaid on the projected HyMap reflectance data in ENVI, and spectral profiles of sites representing high water repellency were recorded. Initially, the average spectral signature of each sample plot containing water repellent soils was recorded. After analyzing the average spectra of the sample plots, it was apparent that plots having weak to moderate repellency or high repellency only at points, did not always demonstrate a clear spectral difference from plots without repellency. These plots did have slightly lower reflectance (~5%) in the SWIR portion of the spectrum, however. It was clear, however, that plots with very strong water repellency throughout (e.g. average MDI rate of all 3 points were MDI = 0-3 ml/min) exhibited a noticeable decrease of 5% - 10% less reflectance in the SWIR portion of the spectrum than those with weak or moderate water repellency, and up to 15% lower SWIR reflectance than sites with no repellency (Fig. 2.20).

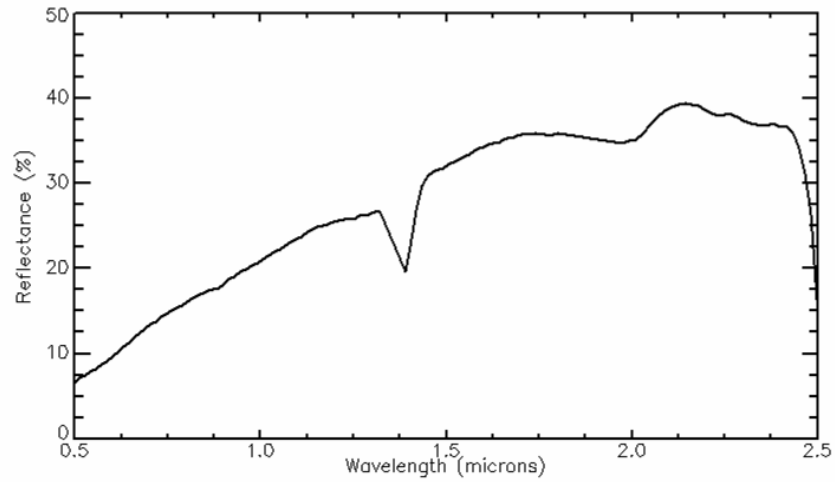

Fig. 2.19. Typical spectral profile of soil in burned area

An ideal goal of the spectroscopic analysis was to identify features of the reflectance spectrum that were unique to fire-induced water repellent soils. Two features of fire-induced water repellency that may introduce a unique spectral characteristic are aliphatic hydrocarbons, which are created through the combustion of organic matter (DeBano, 1998), and the reduction of the clay absorption layer at 2.3 µm, due to the cementation of clay oxides in the soil after a fire burns at very hot temperatures (220°-275°) (Moody et al., 2005). An indication of aliphatic hydrocarbons would likely be noticeable in the spectral regions typical of absorption by organic compounds. These regions include the NIR and SWIR region of the spectrum between 1.4 µm and 2.1 µm (Hummel et al., 2001; Lewis et al., 2004). Fire-induced soil cementation due to intense heating of clay oxides (AlOH, FeOH) would be indicated by absorption in the clay absorption band at 2.3 µm (Fig. 2.20). The reflectance spectrum of the soils was carefully analyzed at these wavelengths, and no noticeable difference of absorption within the NIR and SWIR (other than a general decrease in reflectance) was observed that would indicate a change in the organic chemistry of the soil. It is most probable that any change in reflectance or absorption due to organic compound alterations in this region of the spectrum was blocked by the presence of charred soils and ash on the surface. No difference in absorption caused by intense heating of the soils was detected at the clay absorption band (2.3 µm) other than the decreased reflectance among the moderate and high water repellent soil sites.

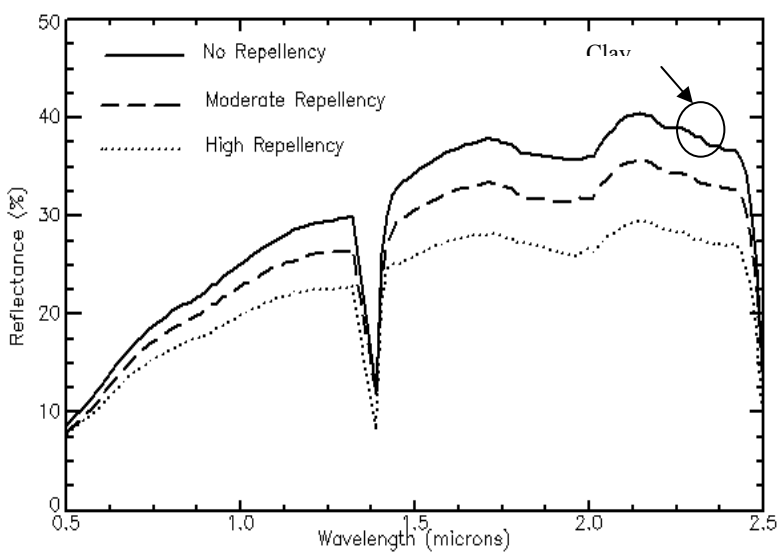

Fig. 2.20. Spectral signatures of non water repellent, moderately water repellent, and highly water repellent soils within the burned area.

A field-collected spectral signature of highly water repellent soils (Fig. 2.21) was used as a guide for the identification of those materials on the image, and sample plots that were assessed as highly water repellent were compared to it. The field-collected spectral signature of the water repellent soil is unique in that its peak reflectance at the clay absorption band (2.3 μm) is only 25%, and the SWIR portion of the curve displays minimum variation save for the slight bump in reflectance at about 2.0 μm. The overall low reflectance of the entire spectral curve is not surprising because the field spectrometry was acquired only 1 m above the burned, blackened soil, and thus it was not as affected by atmospheric noise or the albedo of the surrounding brighter, less severely burned soils. Though the field collected spectra of water repellent soil demonstrated lower average reflectance than other highly repellent sites assessed in the imagery, its general shape and reflectance values served as a guide for the detection of strongly water repellent soil spectra in the imagery. After detecting and recording the spectral profiles of the water repellent sample sites, their spectral signatures were saved in a spectral library in order to be used as endmembers for classification.

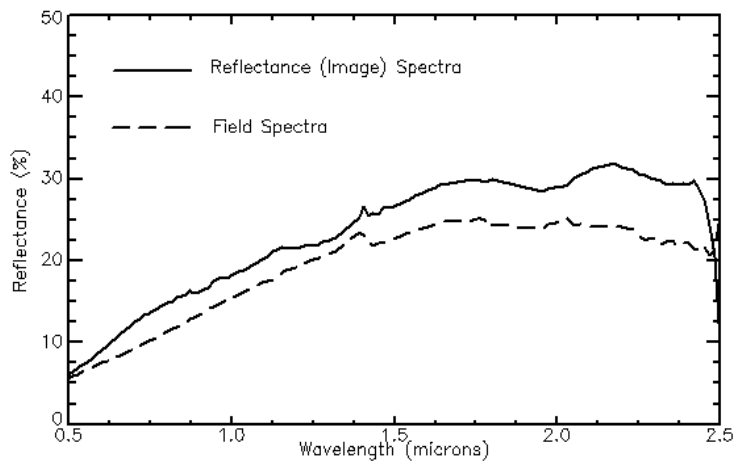

Figure 2.21. Field-collected spectra of water repellent soil (dashed), and HyMap reflectance spectra from the same location (solid).

Unsupervised Classification

As a first cut classification of the imagery, the Iterative Self-Organizing Data Analysis Technique (ISODATA) unsupervised classification was performed on the masked MNF image. After the desired number of classes is established by the user, the ISODATA classification calculates the mean class values within a dataset, and classifies all the remaining pixels with a minimum distance technique (RSI, 2005). Five classes were established for the ISODATA classification to compute, in order to separate the burn severity classes of low severity grass and shrub, moderate severity shrub, high severity grass and shrub, and bare ground. The user does not determine endmembers or training classes for an unsupervised classification. This has some advantages in heterogeneous systems (e.g. rangelands) because the data is statistically categorized without user bias. However, because the ISODATA classification is unsupervised, it is unclear what endmembers the resulting classes represent. The primary reason for conducting the unsupervised classification was to determine the separability of the burned areas brightness values prior to more rigorous classification procedures.

Burn Severity Classifications

The Spectral Angle Mapper (SAM) and Mixture Tuned Match Filtering (MTMF) classification methods were conducted to independently classify burn severity and areas of high water repellency. The spectra of the identified extreme pixels were used as input endmembers (reference spectra) for a SAM classification of burn severity and included the following: bare ground, rock, low, moderate, and high severity grass, and low, moderate, and high severity shrub. The bare ground endmember was included because patches of bare ground, which portrayed high reflectance and albedo, were naturally present across the area, even

though they were minimally affected by the fire (due to the lack of vegetation present on them). It is noted that unburned areas were not included as endmembers in the classification because those areas had been masked out for further analysis. In addition, bands of basalt (rock) were visually identified among the extreme pixels, but no ground truth information was available to verify their presence. The SAM classification was conducted using a maximum angle of 1 radian for all of the endmember classes. The single angle value was used because of the high number of reference classes input for the classification, and it was not yet known which classes would over- or under-classify. After the SAM classification was computed, similar endmember classes were combined, and a confusion matrix was conducted to assess the accuracy of the classification image.

A separate classification for each burn severity class (unburned, low, moderate, high shrub and grass) was then conducted on the image using the MTMF technique, and the extreme pixels as endmembers. The MTMF outputs 2 images for each endmember; a matched filter score image and an infeasibility score image. The results are interpreted by plotting the MF score versus the infeasibility values in a 2-dimensional scatter plot. The MF scores of the MTMF typically have a mean value around 0, which indicates no match of spectra was detected in the pixel. Pixels with a MF score of 1.0 are considered a perfect match, containing 100% pixel abundance, pixels scored greater than 1.0 have been overestimated or misinterpreted due to noise, however they are still considered to have 100% abundance (MF scores of 0-1 represent linear abundance of 0 - 100%), and MF scores of 0 or less are background and not considered target components (Mundt et al, 2006; In Press). The values of the infeasibility image, which can range from 0 to the 100's, are output in noise sigma units, and indicate the feasibility that the MF scored pixel is indeed of its expressed value (RSI, 2005). The infeasibility values of the MTMF are advantageous to the accuracy of the classification because high values (>2) indicate the possibility of pixels being false positives and not matching the target, although their MF score is high (RSI, 2005). The most accurately mapped pixels of a MTMF classification will have a MF score near 1, and a low infeasibility value. After assessing the pixel distribution in the 2-D scatter plot, the user determines a threshold for infeasibility and the acceptable MF score (pixel abundance) that can be considered as presence of the target material.

After computing the MTMF for each burn severity endmember and assessing the 2-D scatter plot, the best thresholds for each endmember were established (Fig. 2.22 A, B, Table 2.4), and subsequently converted to vector files in ENVI. All of the severity classes were included in the MTMF except for moderate severity grass, which was determined to be too spectrally dissimilar from low severity grass, and therefore not classifiable. The vectors of the thresholded pixels were then exported to ArcGIS as shapefiles, where an accuracy assessment was conducted on them. Because the most important function of the MTMF is to map the abundance of an endmember in a particular pixel, a traditional classification map portraying the algorithmic spatial detection of all the endmembers (as with the SAM) would fall short of portraying its unique and prevailing quality. This is because the MF scores of the pixels are scaled according to the amount of a particular endmember's spectra within each pixel (Fig. 2.22C). In addition, since many pixels in an image are a mixture of multiple endmember spectra, mapping multiple endmember MF scores would result in overlapping of MF scores on pixels, and an incorrect portrayal of the classification.

Although the MF score results can be related to a measure of subpixel abundance of an endmember, the proportion of an endmember within a pixel is difficult to quantify and verify without a large number of extremely precise field measurements. For the purpose of identifying areas of soil water repellency, we did not attempt to quantify the subpixel abundance of their quantity, but instead utilized the MTMF to predict their presence. The best way to interpret and validate a target material's presence with the MTMF is by thresholding the output band to the desired spectral quantity within the pixel, and performing an accuracy test that verifies a presence or absence of the endmember within the thresholded pixel.

Table 2.4. MF score and Infeasibility thresholds for the MTMF burn severity classification, Image 6

Endmember Class	MF Score Threshold	Infeasibility Threshold
High Severity Shrub	0.65 - 2.00	> 20
Moderate Severity Shrub	0.85 - 2.00	> 20
Low Severity Shrub	0.50 – 1.50	> 20
High Severity Grass	0.50 – 2.00	> 20
Low Severity Grass	0.50 – 1.50	> 15
Bare Ground	0.40 - 2.00	> 20

Performing a presence/absence error assessment involves overlaying the thresholded pixels in projected space with the ground truth reference polygons or points (collected with GPS) of the corresponding classes to indicate presence of the target material, as well as ground truth polygons or points representing a separate class to indicate absence of the endmember. A matrix is established, in which one of the following is denoted: True positive, when a reference polygon is inside of the classification, indicating the classification to be correct in that area; false positive, when an absence polygon falls inside the classification, indicating the classification to be incorrect in that area; false negative, when an reference polygon falls outside of the classification, indicating an incorrect classification in that area; and true negative, when an absence polygon falls outside of the classification, indicating a correct classification (or absence of) in that area.

Water Repellency Classifications

A separate set of classifications was conducted to identify the presence of water repellent soils in the imagery. The average spectra of the moderate and highly water repellent training sites (Fig. 2.20) were used as training endmembers for the SAM and MTMF classification of water repellent soils. The training spectra for the moderate and high water repellent soils did not indicate any unique change in spectral composition from the surrounding areas, but they were separable due to their decreased reflectance in the SWIR portion of the spectrum. The highly water repellent soils were expected to be detected more accurately because their SWIR reflectance was 10%-15% lower in reflectance than the non-water repellent areas. The moderately repellent soils, however, only exhibited 5%-10% less reflectance in the SWIR than non-repellent soils, and their classification was not expected to be as accurate, because of their spectral similarity to non-repellent soils.

Since the spectral analysis of the water repellent endmembers indicated most of the variability of the data to be in the SWIR region, the original reflectance image was subset to the SWIR wavelengths of 1.43 μm – 2.5 μm (bands 65-125) for the classifications. The remaining 61 bands were MNF-transformed and masked, as described in section 3.3.2, and the supervised classifications were conducted on them. Following the classifications of water repellency, a confusion matrix and a presence/absence error matrix was performed to test the accuracy of the classifications.

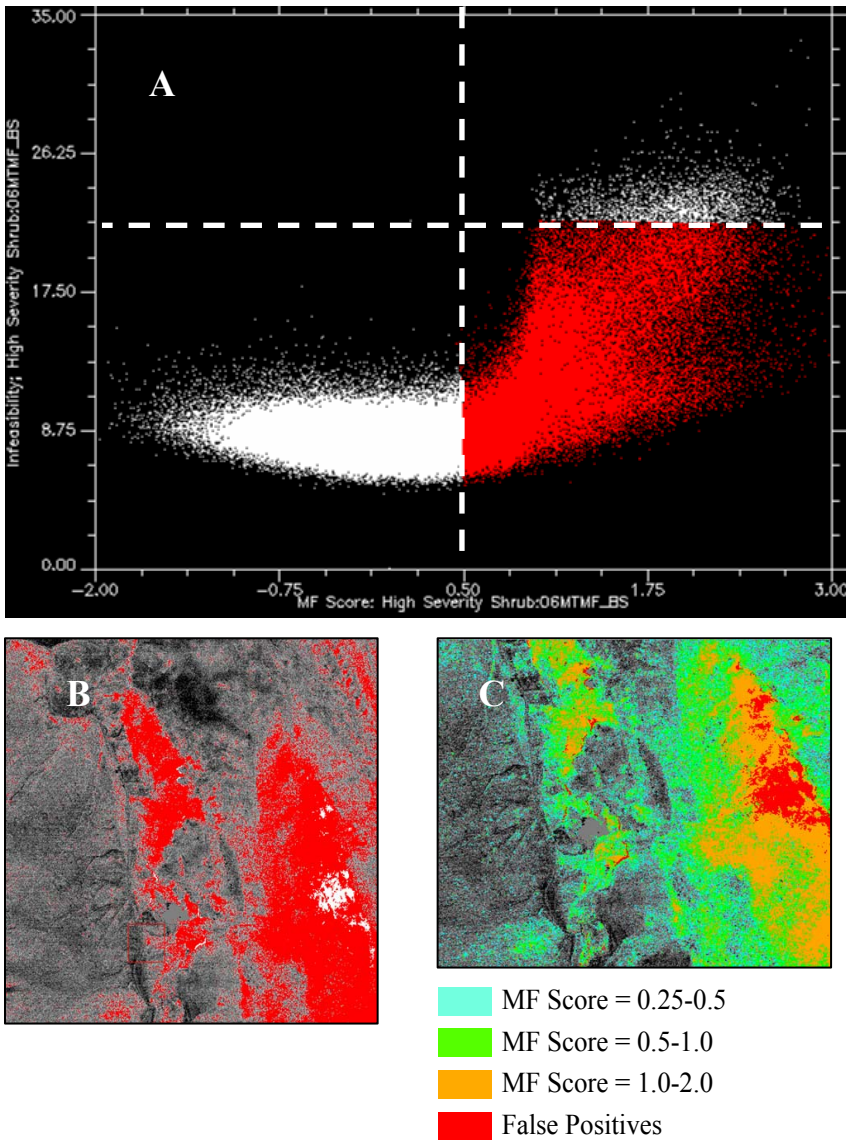

Figure 2.22 A, B, C. 2-D scatter plot of MF score vs. Infeasibility value (high severity shrub). Red indicates pixels most likely to be high severity shrub (A). Corresponding pixel selection of 2-D scatter plot in a portion of image 6 (B). Thresholded MTMF pixel abundance values (MF Scores), in a high severity shrub area of image 6 (C).

RESULTS

Field Data Results

Across the 3 sections of the study area, 235 total points were assessed for water repellency within 80 sample plots. The water repellency was assessed at three points within the sample plots with the Mini-Disc Infiltrometer (MDI) and the Water Drop Penetration Test (WDPT). Of the 235 points, 61 were located in high burn severity, 81 in moderate severity, 69 in low severity, and 24 in unburned. Initial data review indicated that infiltration differed within similar burn severity classes of different vegetation groups, therefore the classes were further broken down by the dominant vegetation group, namely grass and shrub, of the area being sampled. According to the burn severity classes broken down by vegetation, 12 points were recorded in unburned shrub, 51 in low burn severity shrub, 63 in moderate severity shrub, and 41 in high severity shrub. Within the grass vegetation groups, 12 points were in unburned grass, 18

in low severity grass, 18 in moderate severity grass, and 20 in high severity grass (Table 3.1). Most of the water repellent soils were found in the top 2 cm of the soil layers. Mean values and standard deviations of the MDI values were computed for each burn severity class (Table 3.1). In addition, the descriptive statistics of the MDI sample points were listed in accordance with the corresponding WDPT rating at the sample point location (Table 3.2). The WDPT ratings assisted in designating the class ranges of the MDI values. Soils with a WDPT value of 30s-60s were classified as having weak water repellency. Soils with a WDPT value of 61s-180s were classified as moderately water repellent, and soils with a WDPT greater than 180s were strongly water repellent (Dekker and Ritsema, 1994; Lewis et al., 2006).

Table 3.1. Descriptive statistics and standard deviation (SD) of MDI measurements (ml/min), describing infiltration characteristics (as measured by MDI) in each burn severity class.

Burn Severity Class	Count	Min MDI	Max MDI	Mean MDI	SD MDI
Unburned Shrub	12	4.00	16.67	9.89	3.38
Low Severity Shrub	51	3.00	12.67	6.57	2.12
Moderate Severity Shrub	63	1.00	8.33	4.47	1.95
High Severity Shrub	41	1.33	15.00	5.81	2.73
Unburned Grass	12	2.67	12.00	5.31	2.65
Low Severity Grass	18	2.33	8.00	5.22	1.56
Moderate Severity Grass	18	0.00	8.00	4.31	2.33
High Severity Grass	20	2.33	13.00	7.32	2.66
All Data	**235**	**0.00**	**16.67**	**5.78**	**2.70**

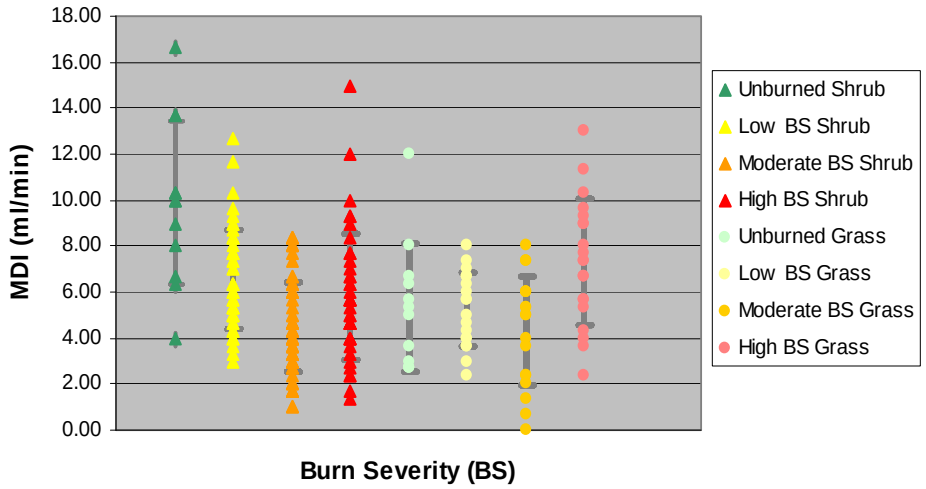

Fig. 3.1. Soil water repellency distribution of MDI values (ml/min) among burn severity (BS) classes

The MDI measures the amount of water infiltrating the soil per 1 minute (ml/min). The highest MDI value (16.67 ml/min) was recorded in an unburned shrub section, and the lowest value (0 ml/min) was recorded in a moderately burned grass area. Mean MDI values were consistently lower in the moderately burned shrub (4.47 ml/min) and grass areas (4.31 ml/min), and highest in unburned shrub areas (9.89 ml/min). Areas of high severity shrub, low severity grass, and unburned grass all had similar MDI values between 5 and 6 ml/min, and areas of low severity shrub and high severity grass had moderate MDI values of 6.57 ml/min and 7.32 ml/min (Fig. 3.1). Because the use of the MDI for assessing soil water repellency has only been documented by one other study (Lewis et al., 2006), its values were correlated with the results of the more traditional, and well documented, WDPT test. Due to the subjective nature of

the WDPT, a strong relationship was not expected, primarily due to the threshold of values (360 s) for high water repellency. Soils that were highly water repellent often had WDPT values greater than 360 s, but were assigned a value of 360 s. In addition, there were numerous data points that exhibited WDPT values of 0. Although there was a broader range of WDPT values between 0 s and 125 s, most points either exhibited no water repellency (0 s) or water repellency lasting longer than 360 s. A comparison of the MDI repellency range with respect to WDPT time values at the 103 points in the burned portion of section A (Fig. 3.2) indicates a moderate inverse trend ($r^2 = 0.50$) between the two. Because the WDPT values of 360 s are thresholded values and are not considered real values, a separate analysis was conducted without the 360s values. The resulting fit was no better than that indicated in Fig. 3.2 and is not shown.

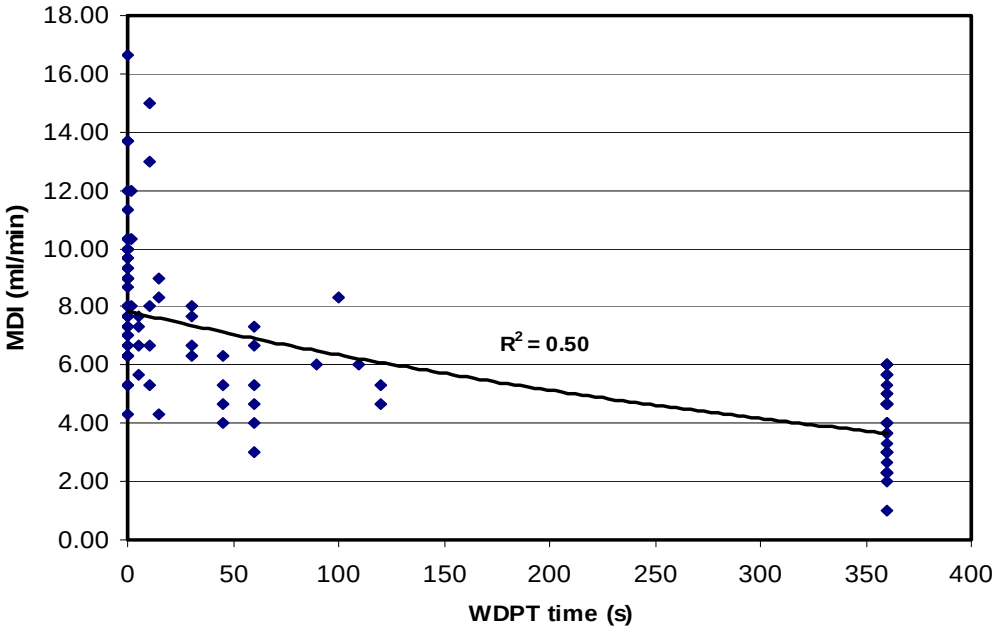

Fig. 3.2. Comparison of MDI repellency values with respect to WDPT time values at sample points in Section A. WDPT times lasting longer than 6 minutes were assigned a value of 360 s. The R^2 value of 0.50 indicates a slight inverse trend between the variables.

The MDI time till infiltration was also tested against the time of the WDPT (Fig. 3.3) and included the bias due to the 0 and 360 values of the WDPT. Soils with no water repellency would be expected to infiltrate right away with the MDI, while soils with high water repellency often take time to allow water to infiltrate. A slight trend was detected with this comparison as well, indicating that highly water repellent soils are resistant to infiltration. Even though a slight relationship was detected, the capillarity of the soils often allowed infiltration to begin faster with the MDI test, even on soils that repelled a water drop. Extremely high water repellent soils (WDPT >360 s) that were tested, however, had high MDI time values as well, indicative of the relationship between the two testing methods. The WDPT measures the persistence (in seconds) of a water drop on the soil surface, and is a reliable indicator of the presence of a water repellent layer. Of the 13 points assessed in unburned shrub areas, only 1 point exhibited weak water repellency (WDPT 30s-60s). Of the 51 points assessed in low burn severity shrub areas, 1 point exhibited weak water repellency, and 3 points exhibited strong water repellency (WDPT >181s). Of the 63 points assessed in moderate severity shrub areas, 9 points exhibited

weak water repellency, 16 points exhibited moderate water repellency (WDPT 61s-180s), and 29 points exhibited strong water repellency. Of the 41 points assessed in high severity shrub areas, 6 points exhibited weak water repellency, 5 points exhibited moderate water repellency, and 15 points exhibited strong water repellency. None of the 12 points assessed in unburned grass exhibited water repellency with the WDPT. Within low burn severity grass areas, 1 of the 18 points assessed exhibited weak water repellency, and 1 exhibited strong water repellency. Within the moderate severity grass areas, 5 of the 18 points assessed exhibited moderate repellency by the WDPT, and 11 points exhibited strong repellency. Of the 20 points assessed within the high severity grass areas, 4 exhibited weak repellency, 2 exhibited moderate repellency, and 3 exhibited strong repellency (Table 3.2). Though the high severity grass areas did not exhibit strong water repellency when tested at the surface with the MDI, the WDPT test indicated repellency in the soils at depths of 2 cm or deeper, below a layer of highly penetrable, loose soil (Appendix 6). The subsurface layers of soil was likely a result of the downward transfer of heat during the fire (DeBano et al, 1998), causing hydrophobic substances to volatize below the burned organic matter, and create a water repellent layer. The WDPT measurements proved useful for identifying subsurface water repellent layers within the study area that were unrecognized by the MDI measurements; they also supplemented the MDI measurements when ranges were established indicating the soils' strength of repellency.

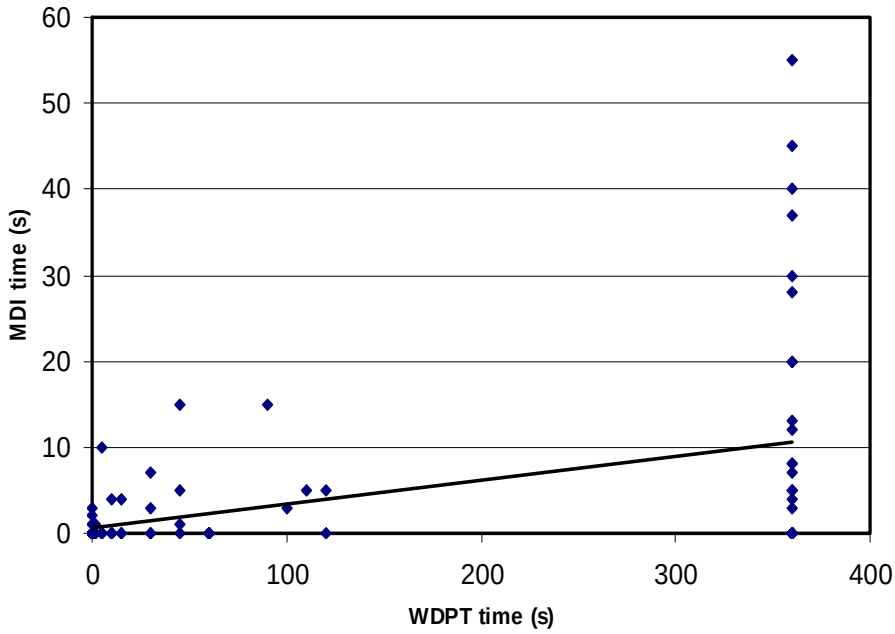

Figure 3.3. Comparison of MDI time till infiltration with WDPT time values in Section A

A mixed model analysis was computed in SAS to assess the relationship of the MDI-assessed water repellency with burn severity. The first step of the model was to perform a Least Squares adjustment of the mean MDI values of each burn severity class (Fig. 3.4, Table 3.3). The model then computed the difference between all pairs of the least squares mean MDI values among the matrix of burn severity/vegetation classes (Column A/B - Column C/D; Table 3.4). The resulting t-test p-values (unadjusted p-value) were adjusted with the Kramer multiple comparison adjustment method (adjusted p-value) to reduce the chance of false positives among independent observations. For those comparisons with p-values below the alpha level of 0.05, the null hypothesis of the two variables being the same was rejected, indicating the difference between those classes to be significant (SAS Institute, 2005) (Table 3.4). In the mixed model, the denominator degrees of freedom were equal to the number of samples (n=79) minus the rank (XZ) matrix, where XZ = burn severity (4 classes) x vegetation (2 classes), and is established by the software to be the same for all comparisons throughout each iteration of the model (SAS Institute, 2005).

Table 3.2. MDI values (ml/min) and WDPT repellency ratings among burn severity classes

Water Repellency (WR) rating	Count	Min MDI (ml/min)	Max MDI (ml/min)	Mean MDI (ml/min)	SD MDI (ml/min)
Unburned Shrub					
No WR	12	4	16.67	10.18	3.55
Weak WR	1			6.67	
Moderate WR					
Strong WR					
Low Severity Shrub					
No WR	47	3	12.67	6.61	2.2
Weak WR	1			7.67	
Moderate WR					
Strong WR	3	4.67	7	5.67	1.2
Moderate Severity Shrub					
No WR	9	3	8.33	5.07	1.68
Weak WR	9	2	8.33	4.63	1.83
Moderate WR	16	1	8.33	5.06	2.13
Strong WR	29	1	8	3.91	1.92
High Severity Shrub					
No WR	15	4	15	7.62	3.01
Weak WR	6	2.67	9.33	6.28	2.34
Moderate WR	5	4	8.33	5.67	1.65
Strong WR	15	1.33	6.67	3.85	1.51
Unburned Grass					
No WR	12	2.67	12	5.31	2.76
Weak WR					
Moderate WR					
Strong WR					
Low Severity grass					
No WR	16	2.33	8	5.25	1.64
Weak WR	1			6.33	
Moderate WR					
Strong WR	1			3.67	
Moderate Severity Grass					
No WR	2	5.33	8	6.67	1.89
Weak WR					
Moderate WR	5	0	7.33	4.93	2.85
Strong WR	11	0.67	7.33	3.61	2.08
High Severity Grass - Includes subsurface values at ~ 2 cm.					
No WR	11	6.67	11.33	8.7	1.43
Weak WR	4	3.67	13	6.25	4.51
Moderate WR	2	5.33	6.67	6	0.95
Strong WR	3	2.33	5.67	4.56	1.93

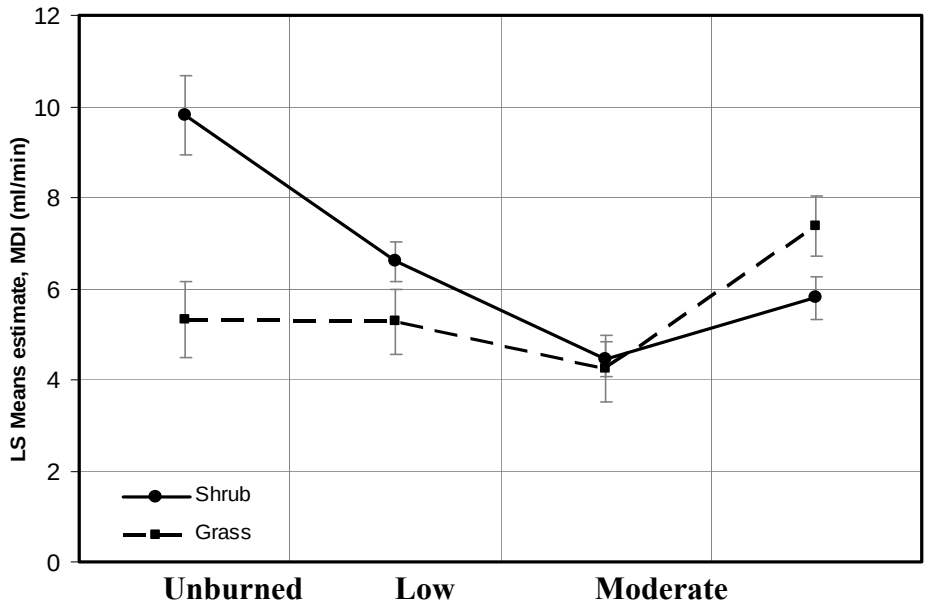

Fig. 3.4. Least squares adjusted means of MDI values (ml/min) among burn severity classes.

Burn severity classes exhibiting significant differences of repellency between each other are unburned grass and unburned shrub (p=0.0098), unburned shrub and low severity grass (p=0.0036), unburned shrub and low severity shrub (p=0.0296), unburned shrub and moderate severity grass (p=0.0001), unburned shrub and moderate severity shrub (p<0.0001), unburned shrub and high severity shrub (p=0.0032), low severity shrub and moderate severity shrub (p=0.0073), moderate severity grass and high severity grass (p=0.0414), and moderate severity shrub and high severity grass (p=0.0062). Aside from the clear significant differences between the unburned shrub and all other classes, the mixed model demonstrated the tendency for repellency to increase significantly with respect to burn severity within shrub areas; while grass areas did not exhibit significant changes in repellency until those areas experienced high severity burns, at which point the repellency significantly decreased.

Table 3.3. Least squares adjusted means of MDI values

Burn Severity	Vegetation	Least Squares Means Estimate (ml/min)	Standard Error
Unburned	Grass	5.3306	0.8433
Unburned	Shrub	9.8134	0.8744
Low	Grass	5.28	0.7185
Low	Shrub	6.5938	0.4221
Moderate	Grass	4.2496	0.7206
Moderate	Shrub	4.4456	0.3794
High	Grass	7.3788	0.6636
High	Shrub	5.8021	0.471

The decrease in initial repellency in the high severity grass areas, as measured by the MDI, is slightly misrepresented, however, because subsurface repellency was found at several points in high severity grass areas at or below a depth of 2 cm (Fig. 3.4). The subsurface repellency within the high severity grass areas was found near a depth of 2 cm with the WDPT.

Table 3.4. Results of Proc Mixed Analysis Difference of Least Square Means calculation. Adjusted P-values less than α = 0.05 in bold indicate significant class differences.

A. Burn Severity	B. Vegetation	C. Burn Severity	D. Vegetation	Estimate	Standard Error	Degrees Freedom	t-Value	Unadjusted P-value	Adjusted P
Unburned	**Grass**	**Unburned**	**Shrub**	**-4.4827**	**1.2148**	**71**	**-3.69**	**0.0004**	**0.0098**
Unburned	Grass	Low	Grass	0.05067	1.1079	71	0.05	0.9636	1
Unburned	Grass	Low	Shrub	-1.2632	0.943	71	-1.34	0.1847	0.8804
Unburned	Grass	Moderate	Grass	1.081	1.1092	71	0.97	0.3331	0.9766
Unburned	Grass	Moderate	Shrub	0.8851	0.9247	71	0.96	0.3417	0.9789
Unburned	Grass	High	Grass	-2.0482	1.0731	71	-1.91	0.0603	0.5497
Unburned	Grass	High	Shrub	-0.4715	0.9659	71	-0.49	0.627	0.9997
Unburned	**Shrub**	**Low**	**Grass**	**4.5334**	**1.1318**	**71**	**4.01**	**0.0002**	**0.0036**
Unburned	**Shrub**	**Low**	**Shrub**	**3.2195**	**0.9709**	**71**	**3.32**	**0.0014**	**0.0296**
Unburned	**Shrub**	**Moderate**	**Grass**	**5.5637**	**1.1331**	**71**	**4.91**	**<.0001**	**0.0001**
Unburned	**Shrub**	**Moderate**	**Shrub**	**5.3678**	**0.9532**	**71**	**5.63**	**<.0001**	**<.0001**
Unburned	Shrub	High	Grass	2.4345	1.0977	71	2.22	0.0298	0.3539
Unburned	**Shrub**	**High**	**Shrub**	**4.0113**	**0.9932**	**71**	**4.04**	**0.0001**	**0.0032**
Low	Grass	Low	Shrub	-1.3139	0.8334	71	-1.58	0.1193	0.7624
Low	Grass	Moderate	Grass	1.0303	1.0176	71	1.01	0.3148	0.9711
Low	Grass	Moderate	Shrub	0.8344	0.8126	71	1.03	0.308	0.9687
Low	Grass	High	Grass	-2.0989	0.9781	71	-2.15	0.0353	0.3966
Low	Grass	High	Shrub	-0.5222	0.8591	71	-0.61	0.5453	0.9987
Low	Shrub	Moderate	Grass	2.3442	0.8352	71	2.81	0.0065	0.1096
Low	**Shrub**	**Moderate**	**Shrub**	**2.1483**	**0.5676**	**71**	**3.79**	**0.0003**	**0.0073**
Low	Shrub	High	Grass	-0.785	0.7865	71	-1	0.3216	0.9733
Low	Shrub	High	Shrub	0.7917	0.6325	71	1.25	0.2147	0.913
Moderate	Grass	Moderate	Shrub	-0.1959	0.8144	71	-0.24	0.8106	1
Moderate	**Grass**	**High**	**Grass**	**-3.1292**	**0.9796**	**71**	**-3.19**	**0.0021**	**0.0414**
Moderate	Grass	High	Shrub	-1.5525	0.8609	71	-1.8	0.0756	0.6199
Moderate	**Shrub**	**High**	**Grass**	**-2.9333**	**0.7644**	**71**	**-3.84**	**0.0003**	**0.0062**
Moderate	Shrub	High	Shrub	-1.3566	0.6048	71	-2.24	0.028	0.3396
High	Grass	High	Shrub	1.5767	0.8138	71	1.94	0.0567	0.5305

Transect Repellency Experiment

The transect repellency experiment analyzed the infiltration of the soil at set lengths away from a burned brush. The values of the MDI (ml/min) at the lengths of 25, 50, 75, 100 and 200 cm are listed in Table 3.5. All the transects except transect 1 on October 15, demonstrated a general increase in infiltration as distance from the burned shrub increased (Fig. 3.5A). In the case of transect 1 on October 15, the soil was apparently disturbed at 25 cm, presumably from animals, allowing infiltration at that location. The transect exhibited little variation in infiltration, ranging from 3.7 ml/min to 5.0 ml/min. The values of transects 2, 3, and 4 on Oct. 15 had similar values of infiltration at 25 cm, ranging from 1.0 ml/min to 1.7 ml/min. Infiltration in transect 2 rose sharply to 4.0 ml/min at 50 cm, then to 6.0 ml/min at 100 cm, before dropping down to 4.0 cm at 200 cm. Transect 3 demonstrated a general increase in infiltration from 25 cm to 200 cm, with the values steadily climbing from 1.3 ml/min to 4.0 ml/min. Transect 4 rose sharply between 25 cm and 75 cm, from 1.0 ml/min to 4.7 ml/min, then dropped back down to 3.3 ml/min at 100 cm, where the infiltration was constant to 200 cm.

The transect values from October 21 (Fig. 3.5B) demonstrated analogous increases in infiltration with distance. All of the transects behaved similarly when they were within the coppice area (soils that had were beneath the canopy of the brush prior to the fire). Typically, the soil was blackened beneath the canopy of the shrub, due to the heat and flames enveloping it. Outside of this area, soil qualities were likely not as affected from the heat of the flames. For example, in the case of transect 3, the edge of canopy was at 25 cm, and the remaining infiltration measurements were within 2 ml/min. This

experiment demonstrated that water repellency in rangeland areas can be assessed based on the distance between shrubs, or the size of the interspaces.

The October 21 transect measurements were supplemented with measurements of field spectrometry at distances of 25 cm, 50 cm and 100 cm, radially from the burned brush (Fig. 3.6A-C). For all three transects, the 25 cm location exhibited the lowest reflectance, beginning near 5% in the visible portion of the spectrum, and consistently staying below the other reflectance values into the NIR spectrum portion. The anomalies in reflectance near 1.4 and 2.7 µm are due to atmospheric water absorption.

Table 3.5. MDI values (ml/min) at set transect lengths, Oct. 15 and Oct. 21 plots.

	15-Oct				21-Oct		
	Plot 1	Plot 2	Plot 3	Plot 4	Plot 1	Plot 2	Plot 3
25 cm	4	2	2	2	1	2	2
25 cm	7	1	1	1	1	5	3
25 cm	4	2	1	0	3	4	5
Average	**5.0**	**1.7**	**1.3**	**1.0**	**1.7**	**3.7**	**3.3**
50 cm	4	5	1	2	4	5	5
50 cm	4	3	0	2	4	4	5
50 cm	4	4	3	3	4	5	3
Average	**4.0**	**4.0**	**1.3**	**2.3**	**4.0**	**4.7**	**4.3**
75 cm	3	5	3	5	5	7	4
75 cm	4	4	1	5	4	4	4
75 cm	4	4	1	4	3	5	4
Average	**3.7**	**4.3**	**1.7**	**4.7**	**4.0**	**5.3**	**4.0**
100 cm	5	7	3	4	6	5	5
100 cm	6	6	2	3	6	5	5
100 cm	4	5	3	2	6	5	5
Average	**5.0**	**6.0**	**2.7**	**3.0**	**6.0**	**5.0**	**5.0**
200 cm	4	3	4	2	5	8	5
200 cm	6	5	3	4	6	8	4
200 cm	4	4	5	4	6	10	3
Average	**4.7**	**4.0**	**4.0**	**3.3**	**5.7**	**8.7**	**4.0**
Canopy Edge	**50**	**50**	**75**	**50**	**100**	**50**	**25**

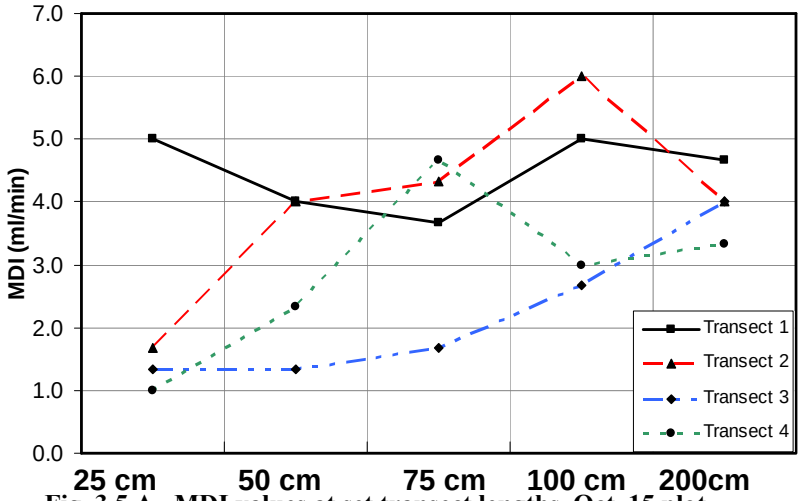

Fig. 3.5 A. MDI values at set transect lengths, Oct. 15 plot

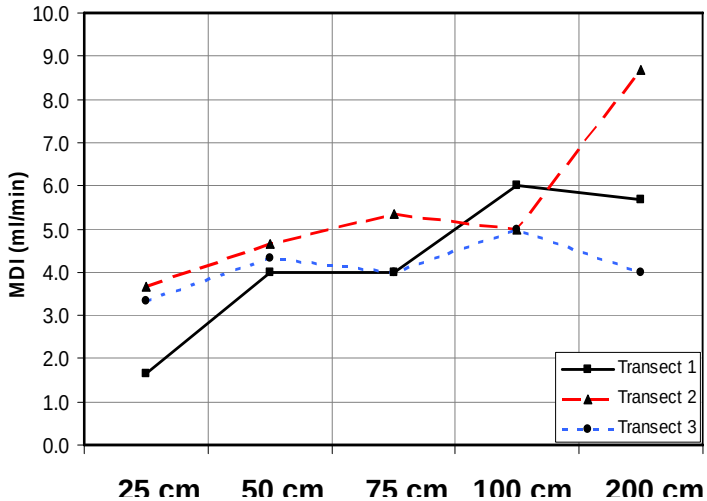

Fig. 3.5 B. MDI values at set transect lengths, Oct. 21 plot

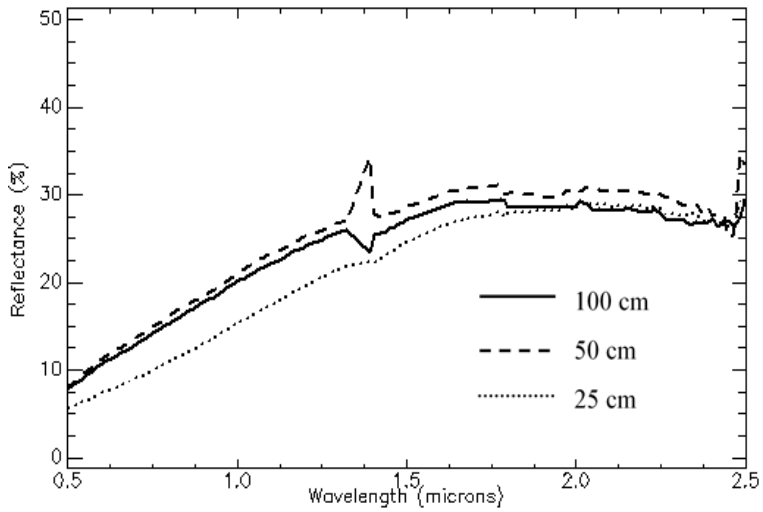

Fig. 3.6 A. Transect 1, spectral signatures at sampled intervals

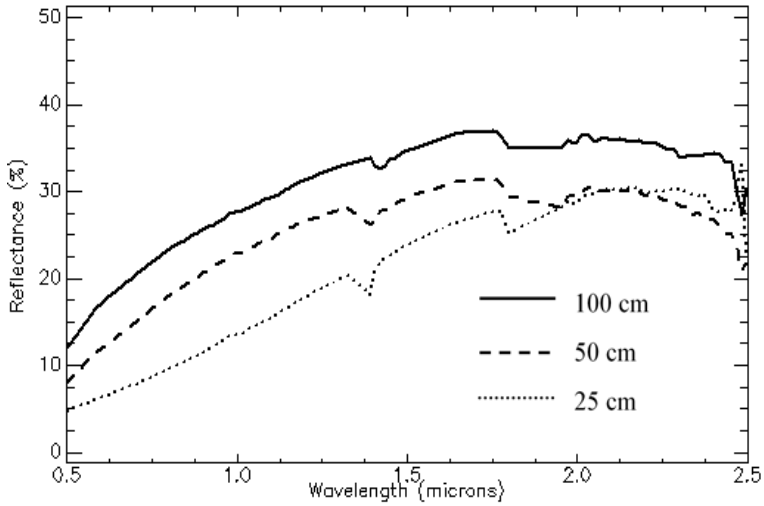

Fig. 3.6 B. Transect 2, spectral signatures at sampled intervals

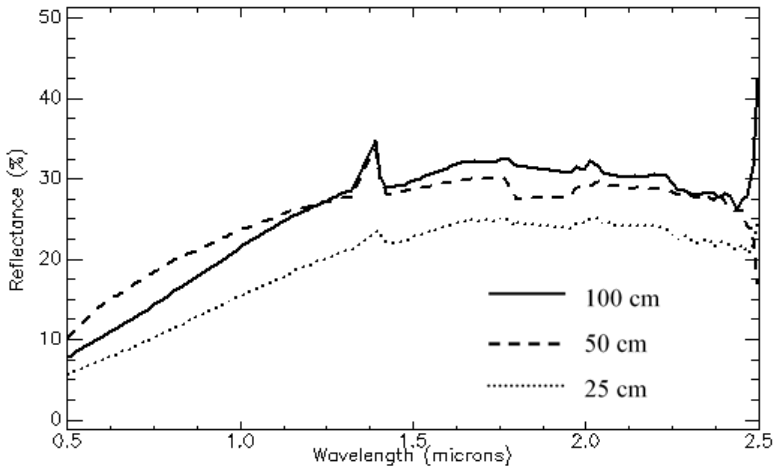

Fig. 3.6 C. Transect 3, spectral signatures at sampled intervals

Field Spectroscopy

Endmember signatures collected with the field spectrometer included unburned grass and shrubs (sagebrush), low severity grass and shrubs (sagebrush), moderate severity shrubs (sagebrush), high severity grass and shrubs (sagebrush), gravel, basalt rock, and bare ground (Fig. 3.7A, B). Bare ground areas included patches of soil exhibiting high reflectance, with no vegetation, and little to no litter cover. The endmembers portraying the highest reflectance were the grassy areas (Fig. 3.7A), including the unburned grass, which had the highest reflectance in the NIR, and the low and high severity grass. Other endmembers exhibiting high reflectance were the bare ground, rock and gravel areas. The signatures that exhibited the least reflectance were the unburned and burned sagebrush (Fig. 3.7B) because of the reduced reflectance among the leaves of the unburned shrubs, and the blackened soil from the burned shrubs, respectively. All signatures exhibit spikes in reflectance near 1.4, 1.9, and 2.7 µm because of the atmospheric noise and water absorption at those wavelengths. The signature of bare ground (not pictured) displayed excess noise across the entire signature, due to the extremely high albedo, or increased reflectance among the entire spectrum of the bright, bare ground.

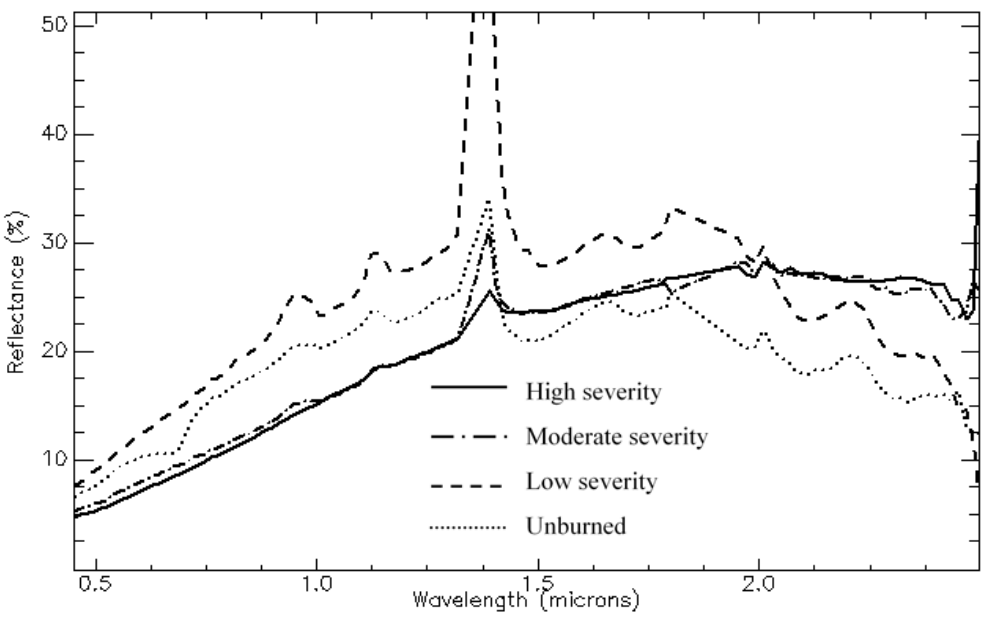

Figure 3.7A. Field collected spectral signatures of high severity shrub burn (solid line), moderate severity shrub burn (dash-dot line), low severity shrub burn (dashed line), unburned shrub (dotted line).

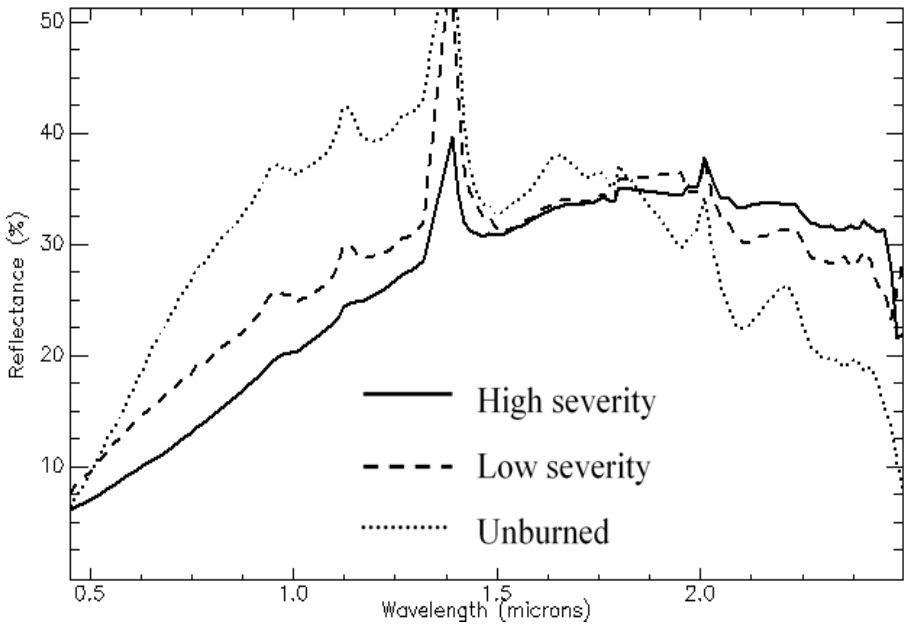

Fig. 3.7B. Field collected spectral signatures of high severity grass burn (solid line), low severity grass burn (dashed line), unburned grass (dotted

Spectroscopy Results

Unsupervised Classification of Burn Severity

The ISODATA unsupervised classification was performed on the masked MNF-transformed image 6. The unsupervised classification method detected 7 mean classes among the image, given a user specified input range of 5-10 classes. After the image was classified, a projection was applied to it, and the ground truth training plots were overlaid to match the classes (Fig. 3.8). The visual assessment of the classification with the ground truth plots indicated that the unsupervised classification separated the classes primarily among high severity shrub and moderate severity shrub, and high severity grass and low severity grass/shrub. The burn severity that was best separated among the image was high severity grass. Moderate severity shrub areas were confused and classified with areas of high severity shrub. The classifier also mixed areas of low severity grass with low severity shrub. A confusion matrix error assessment was not conducted on the class image because the ground truth regions of interest (ROI's) were used to identify the classes and it was evident that the accuracy would be low within each class because more than one burn severity ground truth endmember was present. As a first look at the image, the unsupervised classification demonstrated that the image could be generally classified among high and low burn severity areas based on the separability of the MNF-transformed spectra.

Supervised Classification of Burn Severity

The Spectral Angle Mapper (SAM) and mixture tuned matched filtering (MTMF) algorithms were conducted on the image to classify the burn severity of the study area. The results of the two classification techniques were displayed and compared to determine the most suitable method, and confusion matrices were computed to assess their accuracy. The SAM confusion matrices, computed in ENVI, calculated the total pixels within the ground truth reference plots that fell within each burn severity class. The error matrices computed for the MTMF were conducted manually, and indicated the presence or absence of classified pixels within a sample plot. Therefore, the cell totals of the MTMF error matrix were much lower, because they only equaled the number of sample plots input for the matrix, and not the total pixels within the plots.

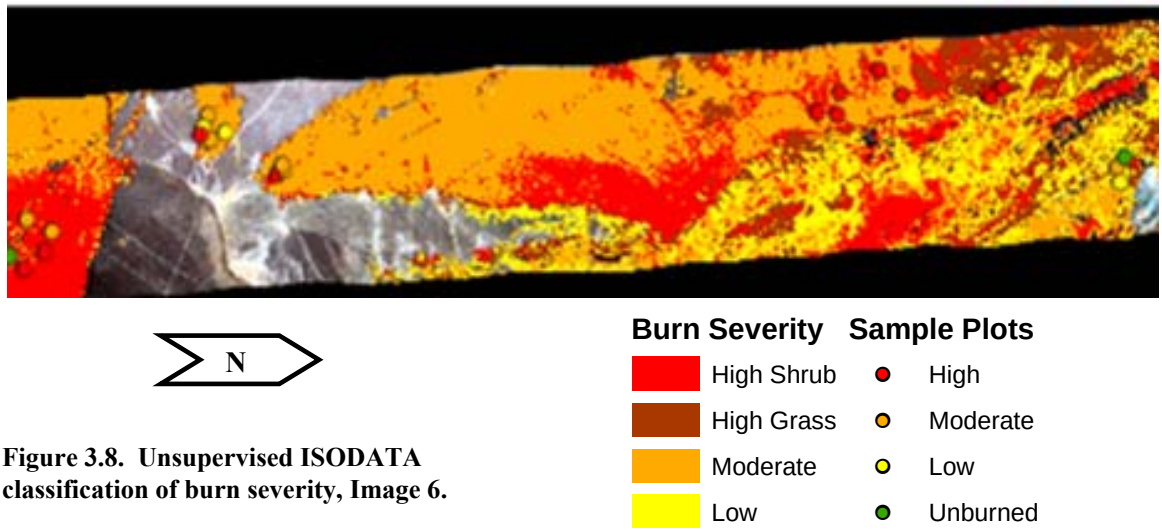

Figure 3.8. Unsupervised ISODATA classification of burn severity, Image 6.

Spectral Angle Mapper (SAM) Classification

The first burn severity classification utilized the SAM algorithm (Fig. 3.9A); the SAM designates spectral classes within the image based on a user-specified angle set around a reference spectra in n-dimensional space. The reference endmembers used in the SAM classification were the extreme pixels found and designated to a burn severity class through n-dimensional visualization. A maximum spectral angle of 1 radian was set for each endmember as designation of that burn severity class. After the algorithm was computed and the extreme pixel endmember classes representing the same severity classes were combined, a confusion matrix was conducted (Tables 3.6 A, B). The confusion matrix was built using the field-assessed sample plots (Fig. 3.9B) with their assigned burn severity as ground truth. The confusion matrix calculated an overall accuracy of 72%. A kappa coefficient of 0.65 indicated a moderate agreement that the classification was better than a classification resulting strictly from chance agreement.

The producer's and users accuracies indicate acceptable values for all of the classes, except for the high (39% and, 66%, respectively) and moderate (54% and 39%, respectively) severity shrub classes. It is important to examine the producer's and users accuracies in an error matrix report, because examining the overall accuracy alone can be misleading. Although the overall accuracy of the error matrix is quite high, the low producer's and users accuracies for high and moderate severity shrub areas indicate that the SAM had trouble differentiating moderate severity shrub areas from high severity shrub areas, and is supported by the spectral signatures obtained with the field spectrometry which recorded nearly identical signatures for the high and moderate shrub areas (Fig. 3.7B). Low severity grass areas were also confused with bare ground areas, because of the high reflectance in both areas. No moderate severity grass areas were detected with the SAM. For the purpose of classifying soil reflectance exhibiting water repellency, it was acceptable for high and moderate shrub areas to be confused in the classification, because field data statistics indicated no significant difference in repellency values between moderate severity shrub areas (mean MDI = 4.45 ml/min) and high severity shrub areas (mean MDI = 5.8 ml/min). The moderate and high severity areas that were confused were combined for a second accuracy assessment, and the overall accuracy increased to 78%, and producer's and users accuracies for the merged high and moderate severity shrub area increased to 81% and 87%, respectively, and the Kappa value increased to 0.72 (Table 3.7).

Table 3.6A. SAM burn severity classification error matrix and results

Class (pixels)	Ground Truth (pixels)						
	Bare Ground	**High Severity Shrub**	**High Severity Grass**	**Low Severity Shrub**	**Low Severity Grass**	**Moderate Severity Shrub**	**Total**
Unclassified	24	6	8	4	130	19	191
Bare Ground	**271**	6	1	0	0	1	279
High Severity Shrub	0	**52**	0	8	0	19	79
High Severity Grass	0	0	**107**	0	0	2	109
Low Severity Shrub	12	6	0	**123**	0	3	144
Low Severity Grass	56	0	0	0	**406**	0	462
Moderate Severity Shrub	3	63	0	16	0	**52**	134
Total	366	133	116	151	536	96	**1398**
Overall Accuracy = 72% (1011/1398)							
Kappa Coefficient = 0.65							

Table 3.6B. SAM burn severity classification producer's and users accuracy

Class	Commission (%)	Omission (%)	Producer's Accuracy (%)	Users Accuracy (%)
Bare Ground	2.87	25.96	74.04	97.13
Low Severity Grass	12.12	24.25	75.75	87.88
High Severity Grass	1.83	7.76	92.24	98.17
High Severity Shrub	34.18	60.9	39.1	65.82
Low Severity Shrub	14.58	18.54	81.46	85.42
Moderate Severity Shrub	61.19	45.83	54.17	38.81

Table 3.7. Producer's and users accuracies after merging the SAM classes of moderate and high burn severity, overall accuracy 78%, K = 0.72

Class	Commission (%)	Omission (%)	Producer's Accuracy (%)	Users Accuracy (%)
Bare Ground	2.87	25.96	74.04	97.13
Low Severity Grass	12.12	24.25	75.75	87.88
High Severity Grass	1.83	7.76	92.24	98.17
High/Moderate Severity Shrub	12.68	18.78	81.22	87.32
Low Severity Shrub	14.58	18.54	81.46	85.42

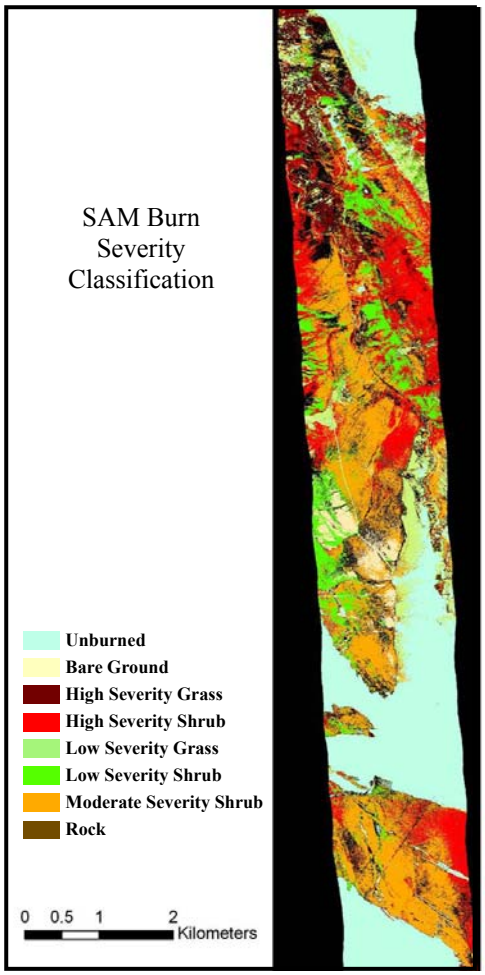

Fig 3.9A. SAM burn severity classification

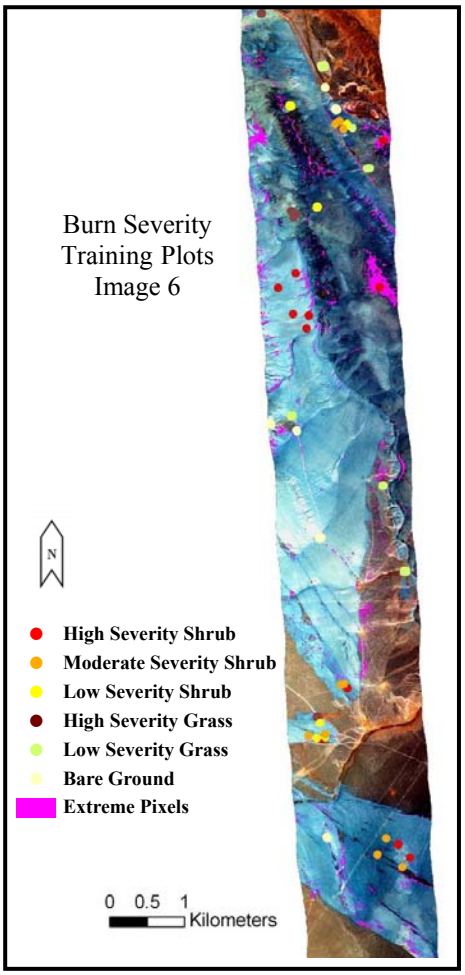

Figure 3.9B. Burn severity training plots overlaid on false color composite of image 6

Mixture Tuned Matched Filtering (MTMF) classification

The next burn severity classification used the MTMF method. MTMF classifications of burn severity were computed on image 6, using input spectra from the extreme pixels representing all of the burn severity categories, and bare ground. The MF scores were plotted in the 2-D scatter plot (as described above and in Fig. 2.22A-C) and after interactively assessing the locations of pixels within the scatter plot, band thresholds were determined for each endmember class in the MTMF (Table 3.8). Ideally, the lower value of the MF thresholds represent the percent abundance of a pixel that is designated to represent the endmember being mapped, and the infeasibility threshold represents the values of the output infeasibility image above which the classified pixels are considered false positives. Figure 3.10 (A-G) illustrates the MTMF image for each burn severity class, and the determined MF score and infeasibility value threshold, as listed in Table 3.8. After the MF Score and infeasibility values were thresholded for each burn severity class, a presence/absence error matrix was calculated (Table 3.9A-D). Because the MTMF classification technique is basically an identifier of one specific endmember class with respect to every other material in the image, the most suitable method of assessing the accuracy of the classification is by assessing the presence or absence of the endmember material being mapped with respect to a ground truth reference location.

Table 3.8. MF Score and infeasibility thresholds for the MTMF burn severity classification, Image 6

Endmember Class	MF Score Threshold	Infeasibility Threshold
High Severity Shrub	0.65 - 2.00	> 20
Moderate Severity Shrub	0.85 - 2.00	> 20
Low Severity Shrub	0.50 – 1.50	> 20
High Severity Grass	0.50 – 2.00	> 20
Low Severity Grass	0.50 – 1.50	> 15
Bare Ground	0.40 - 2.00	> 20

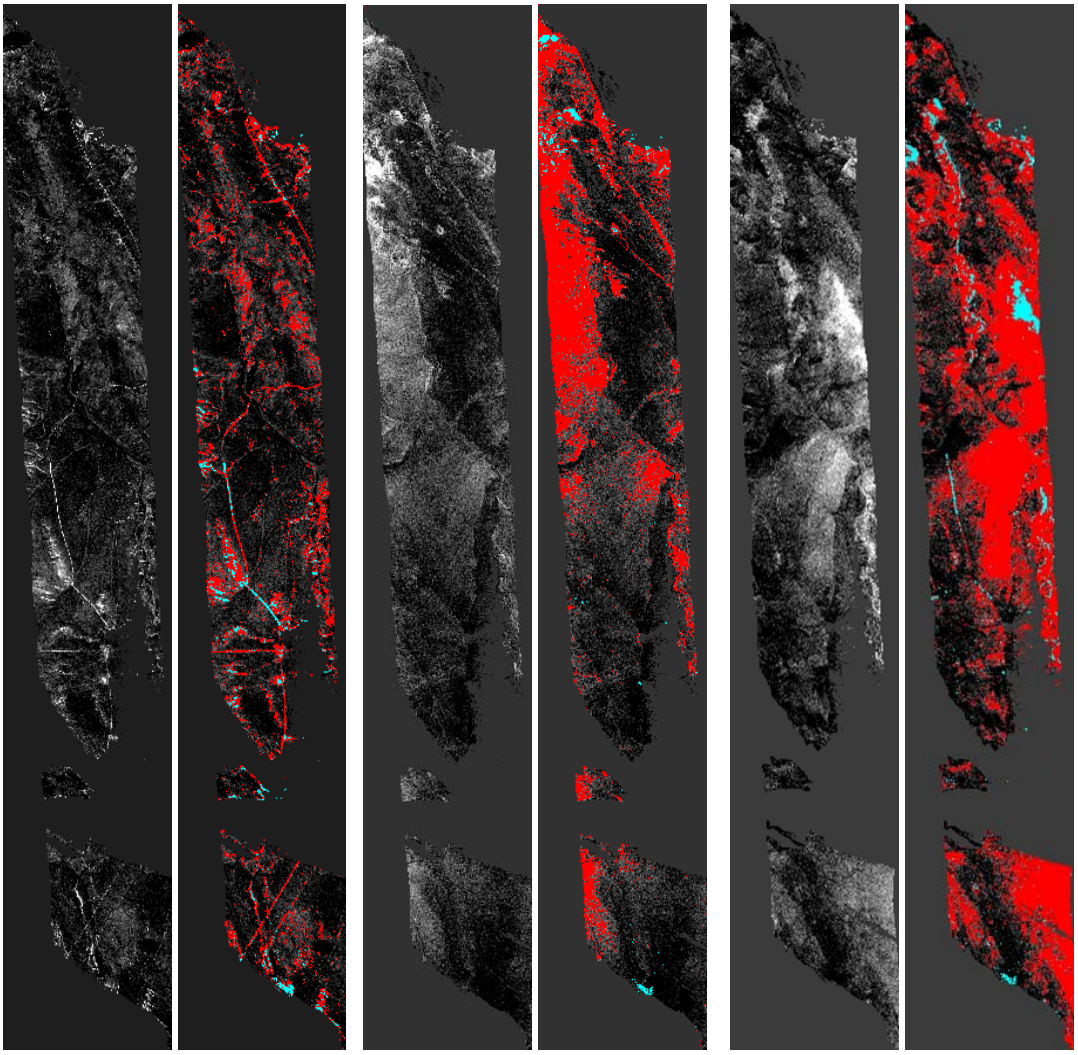

A. Bare Ground **B.** High Severity Grass **C.** High Severity Shrub

Figure 3.10, A-C (above) & D-F (next page). MTMF burn severity classification output images (left image) and thresholded MF Scores in red and infeasibility scores in cyan (right image).

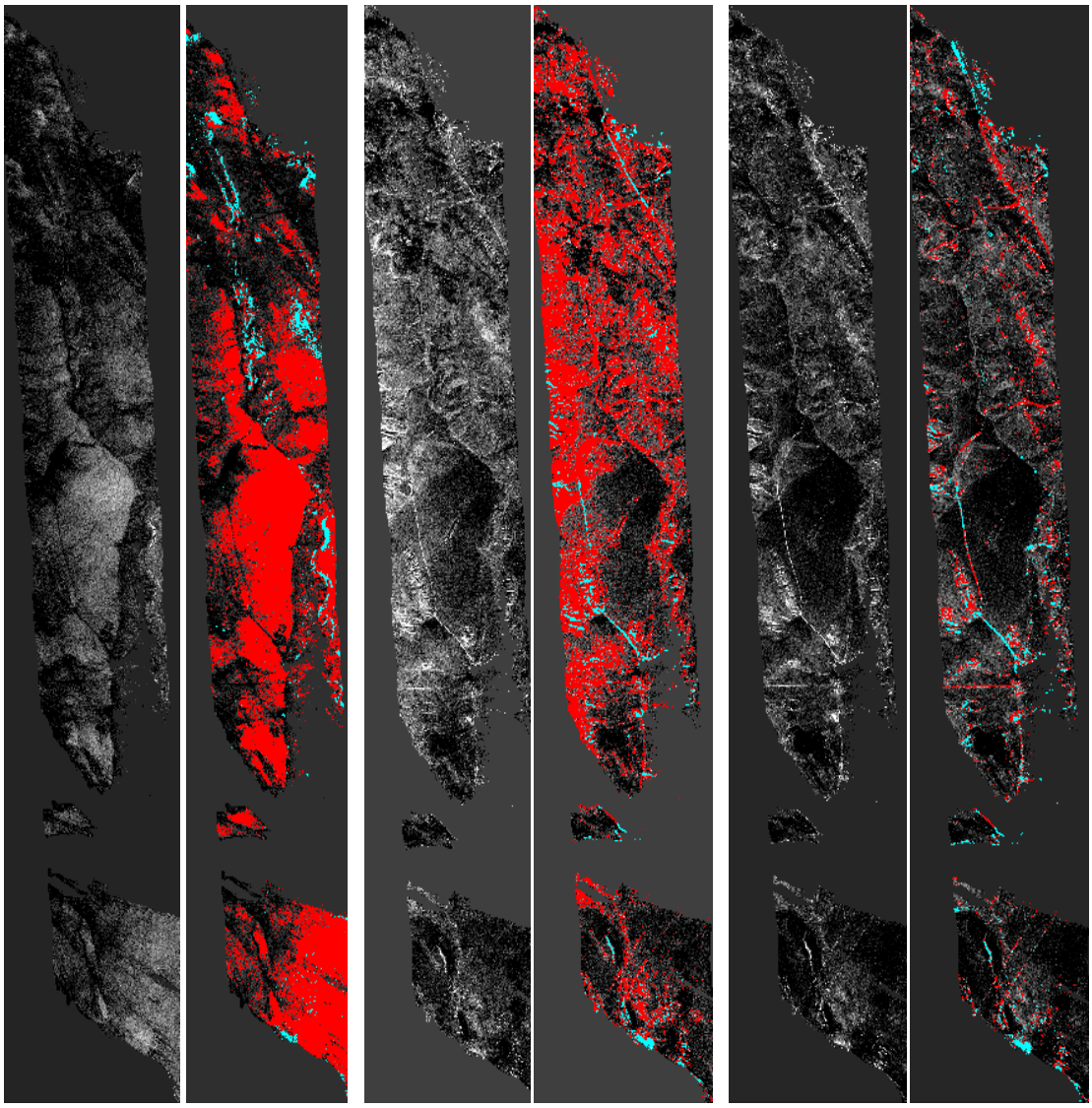

D. Moderate Severity Shrub **E.** Low Severity Shrub **F.** Low Severity Grass

Table 3.9 A-D. Presence/Absence matrices for MTMF classification of burn severity (indicating plots within or outside of classified areas).

A. Class 1: High Severity Shrub			
MTMF Class	**Reference Positive**	**Reference Negative**	**Users Accuracy**
Classified Positive	**6**	4	60%
Classified Negative	3	**5**	62.50%
Producer's Accuracy	66%	55%	**61%**

B. Class 2: Moderate Severity Shrub			
MTMF Class	**Reference Positive**	**Reference Negative**	**Users Accuracy**
Classified Positive	**5**	4	55%
Classified Negative	5	**4**	44%
Producer's Accuracy	50%	50%	**50%**

C. Class 3: Low Severity Shrub			
MTMF Class	**Reference Positive**	**Reference Negative**	**Users Accuracy**
Classified Positive	**2**	4	33%
Classified Negative	2	**4**	33%
Producer's Accuracy	50%	50%	**50%**

D. Class 4: High Severity Grass			
MTMF Class	**Reference Positive**	**Reference Negative**	**Users Accuracy**
Classified Positive	**4**	3	57%
Classified Negative	0	**5**	100%
Producer's Accuracy	100%	63%	**75%**

The MTMF display and accuracy is dependent on thresholding; while smaller MF score thresholds increase the accuracy of endmember presence in a pixel, the displayed abundance of the endmember is increased, resulting in overlapping of classes. The overall accuracies of the MTMF classes (bottom right values in Table 3.9 A-D) are a quotient of the correctly classified reference plots with respect to the total reference plots.

The cell totals of the presence/absence accuracy assessment demonstrate low values in comparison to the cell totals of the traditional confusion matrix performed on the SAM, because the cell values here represent the number of ground-assessed reference plots present or absent in the classification, while the values of the SAM error assessment represent total pixels present within an endmember class. Plot totals were used in the presence/absence error matrices, instead of pixel totals, because the presence/absence error matrix was conducted manually (by the user), while the SAM error matrix was conducted in ENVI, allowing the software to accurately total the number of pixels present in a class. An error matrix was not conducted for the class of low severity grass because there were too few ground truth training sites for input, and the classified area was minimal (Fig. 3.10F), as the endmember was mainly detected around the fringes of the burn area, and moderate severity grass was not classified. The error matrices for the MTMF-classified burn severity classes demonstrate the accuracy of the classification based on the presence or absence of ground-referenced plots within or outside of the classified area.

Supervised Classifications of Water Repellency

After identifying soils in the field that exhibited the presence of soil water repellency, their spectral signatures were used as training endmembers to classify soil water repellency with the SAM and MTMF

classification algorithms. The spectral endmembers used as training in the classifications represented strong and moderate fire-induced water repellency, and were located in moderate and high burn severity areas. The average spectra were obtained from two plots each of strong and moderate soil water repellency that had been identified in the field, and had consistent levels of repellency throughout the plots. The results of the two classification techniques were displayed and compared to determine the most suitable method, and accuracy assessments were conducted on them.

Table 3.10A. Confusion matrix of SAM water repellency classification, Image 6 (pixels)
Overall Accuracy = 51% Kappa = 0.31

Class (pixels)	Strong Repellency	Moderate Repellency	Total
Unclassified	40	0	40
Strong Repellency	15	0	15
Moderate Repellency	23	51	74
Total	78	51	129

Spectral Angle Mapper (SAM) Classification

The first SAM classification was conducted with a maximum spectral angle of 0.65 radian for accepting spectra of that endmember class, and was applied to both endmembers (strong and moderate repellency). The initial classification result failed to classify at least 50% of the image, and the overall accuracy was below 25%. To increase the amount of area being classified, as well as the accuracy, the SAM classification was conducted again with a maximum angle of 0.75 radian for each endmember. The results categorized 52% of the burned area as having moderate water repellent soils, 23% as having strong water repellent soils, and 25% of the image was unclassified (Fig. 3.11). A confusion matrix was calculated on the SAM using the ground locations of 8 moderate water repellent sample plots and 9 strongly water repellent sample plots (not including those input for training data), and the resulting overall accuracy was 51% (Table 3.10A, B). The low overall accuracy and the Kappa value of 0.31 suggest the SAM may not be the best method for classifying soil water repellency.

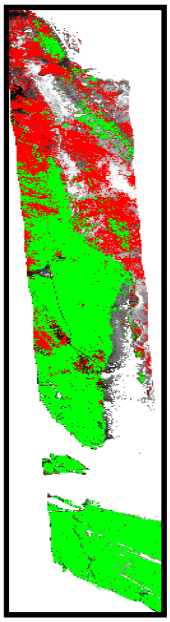

Figure 3.11. SAM classification of strong (red) and moderate (green) water repellent soils, Image 6.

Table 3.10B. Commission and omission errors and producer's and users accuracies for SAM water repellency classification, Image 6

Class	Commission Error (%)	Omission Error (%)	Producer's Accuracy (%)	Users Accuracy (%)
Strong Repellency	0	80.77	19.23	100
Moderate Repellency	31.08	0	100	68.92

MTMF Classification of Water Repellency

The MTMF algorithm was conducted on the imagery to classify moderate and high water repellent soils. The same training spectra were used for the MTMF classification as was used in the SAM classification. The MF scores and infeasibility values of each mapped endmember were plotted in a 2-D scatter plot (Fig. 3.12) to determine the thresholds of the pixels' endmember abundance and false positive values that would be displayed. After examining the 2-D scatter plot, a MF score threshold of 1-2 was chosen for display the pixels with 100% abundance of the soil water repellency endmember (Fig. 3.12, in red). For the strong water repellency classification, pixels with infeasibility scores greater than 16 were determined to be areas most likely to have false positives, most of which were high reflectance bare ground areas.

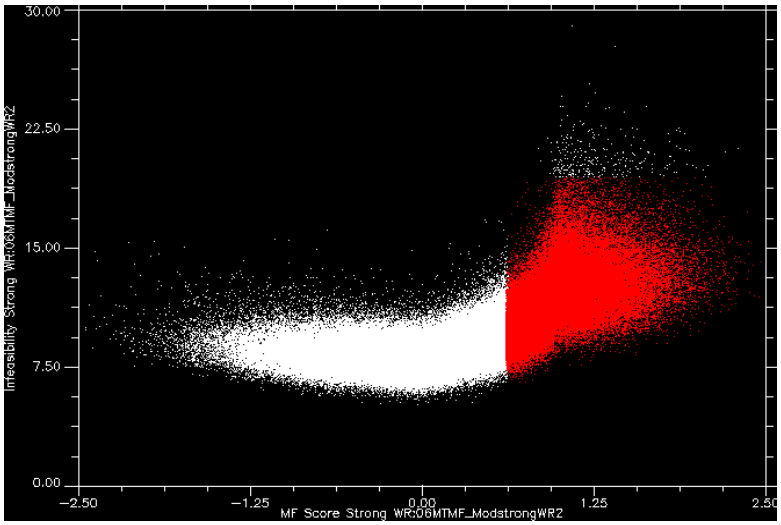

Figure 3.12. 2-D scatter plot of strong water repellency MF scores (x-axis) vs. Infeasibility scores (y-axis). Red area depicts thresholded pixels with MF score (pixel abundance) of 0.5-2.0, and infeasibility scores less than 20, indicating values above 20 to be false positives.

After the pixel thresholds were determined and displayed as ROI's, the ground truth sample plots were overlaid on the image in order to determine the accuracy of the classification. A presence/absence matrix was conducted using 9 sample plots that displayed high water repellency (presence endmembers), and 8 sample plots that displayed moderate water repellency (absence endmembers). The error matrices were conducted for the moderate and high water repellency at MF score thresholds of 0.3-2.0, 0.5-2.0, and 1.0-2.0 (Table 3.11A-C; Table 3.12A-C, respectively), representing endmember abundance within a pixel of 30%, 50%, and 100%, respectively.

For the described image, MF Score thresholds (subpixel abundance of endmembers) of 100% abundance, 50% abundance, and 30% abundance all indicated an overall accuracy of 65% (Table 3.11A-C). Within the threshold ranges of 100%

and 50% abundance, the producer's accuracy of reference positives, or training sites present in the positive classification area was 55%, while the accuracy of negative reference sites not being present was higher, at 75%. When the threshold was increased to include 30% pixel abundance, the positive reference accuracies increased to 78%, while the accuracies of negative reference sites decreased to 50%. The change in producer's accuracy indicates that with the increase in subpixel abundance (or a lower MF score threshold), there is a higher likelihood that pixels classified as strong water repellency will be overlaid by ground truth plots representing strong water repellency as well.

Table 3.11A-C. Presence/absence matrices for MTMF classification of strong water repellency (indicating plots within or outside of classified areas).

A. MF score threshold = 1.0-2.0 (88,321 pixels classified at this threshold)			
MTMF Class	**Reference Positive**	**Reference Negative**	**Users Accuracy**
Classified Positive	5	2	71%
Classified Negative	4	6	60%
Producer's Accuracy	55%	75%	**65%**

B**. MF score threshold = 0.5-2.0 (191,399 pixels classified at this threshold)**			
MTMF Class	**Reference Positive**	**Reference Negative**	**Users Accuracy**
Classified Positive	5	2	71%
Classified Negative	4	6	60%
Producer's Accuracy	55%	75%	**65%**

C**. MF score threshold = 0.3-2.0 (542,403 pixels classified at this threshold)**			
MTMF Class	**Reference Positive**	**Reference Negative**	**Users Accuracy**
Classified Positive	7	4	64%
Classified Negative	2	4	67%
Producer's Accuracy	78%	50%	**65%**

For the MTMF classification of moderate water repellency, 8 positive references and 9 negative references were input for validation of the high repellency classification, and MF Score thresholds of 100% abundance, 50% abundance, and 30% abundance indicated overall accuracies of 65%, 35% and 35%, respectively. The overall accuracy was higher for the original MF Score threshold of 1.0 – 2.0 primarily because no negative references were among the 5,942 pixels in that threshold. When the MF score threshold was reduced to 0.5 or 0.3 (50% or 30% abundance), the overall accuracies decreased; this was because the total number of thresholded pixels substantially increased, presenting negative reference points among them. Although the MTMF classifications of water repellency did not have strong accuracies for verification, it's output is an accurate representation of water repellency across the study area because it demonstrates the discontinuous nature of soil water repellency in burned rangeland areas.

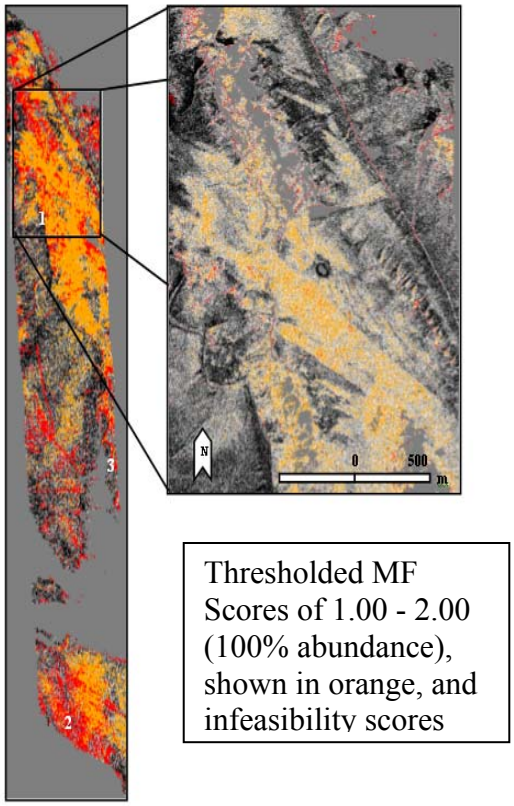

Figure 3.13. MTMF classification of high water repellency, Image 6

Table 3.12 A-C. Presence/Absence matrices for MTMF classification of moderate water repellency

A. MF score threshold = 1.0-2.0 (5942 pixels)			
MTMF Class	**Reference Positive**	**Reference Negative**	**Users Accuracy**
Classified Positive	2	0	100%
Classified Negative	6	9	60%
Producer's Accuracy	25%	100%	**65%**

B. MF score threshold = 0.5-2.0 (169,910 pixels)			
MTMF Class	**Reference Positive**	**Reference Negative**	**Users Accuracy**
Classified Positive	3	6	33%
Classified Negative	5	3	38%
Producer's Accuracy	38%	33%	**35%**

C. MF score threshold = 0.3-2.0 (393,151 pixels)			
MTMF Class	**Reference Positive**	**Reference Negative**	**Users Accuracy**
Classified Positive	3	6	33%
Classified Negative	5	3	38%
Producer's Accuracy	38%	33%	**35%**

DISCUSSION AND CONCLUSIONS

This study presents a technique for mapping burn severity and fire-induced soil water repellency in a burned rangeland area of the Intermountain West. The utilization of high spatial and spectral resolution imagery proved crucial for this project due to the lack of spectral separability across the burned portion of the study area. The SAM burn severity classification detected classes of low, moderate and high severity shrub areas, and low and high severity grass with an overall accuracy of 72%; the MTMF algorithm detected water repellent soils in over 30% of the burned area with an overall accuracy of 65%. Additionally, the field evaluations demonstrated pertinent methods for assessing burn severity and water repellency in burned rangelands, and analytical results provide valuable insight to the dynamics of rangeland fire related to pre-fire vegetation cover and vegetation type. The image-wide classification of burn severity and detection of water repellent soils is useful for locating areas susceptible to increased sedimentation, and in need of treatment or preventative measures.

The primary difficulty of assessing burn severity in rangelands is the apparent homogeneity throughout many areas of the burn. Despite the fact that native rangeland vegetation often exhibits ample spacing of bare ground interspaces among shrubs and native bunch grasses, annual grasses like the invasive cheatgrass often grow within them. The presence of annual grass among interspaces serves as a bridge in the case of fire, allowing it to burn rapidly through the interspaces, reaching other coppice microsites more readily. This dynamic of rangelands often results in very uniform burns throughout large areas, of which a severity description is ambiguous. In the case of rangelands that have been previously burned, the uniformity of successive burns is much more pronounced, as annual grasses have become more prevalent and shrubs are often immature, and the low fuel load is wholly incinerated.

In this study, the time lag between the fire and the image acquisition and field study was approximately one month, and may have attributed to errors in the field assessment and remote sensing classification of burn severity. A more accurate assessment of burn severity might have been possible had the sampling begun closer to the fire date. Local weather records indicated only 1.2 mm rainfall during the month of August (NCDC, 2005). Disturbance by wind and aeolian transport was more likely than precipitation, however, but not quantifiable.

The important contributions of the field analyses were the indications of water repellency variability among various burn severity classes. The significant differences of repellency values between all the burn severity classes of shrub, as well as unburned shrub, indicate a general increase in water repellency among shrub areas as burn severity increases and a drop in repellency after being burned at high severity. This indicates that water repellency is likely to reduce in a high severity burn due to the destruction of aliphatic hydrocarbons by excess heat. The repellency observed in grass areas was consistently strong in unburned, low and moderate severity areas, but decreased significantly in high severity areas, and is indicative of natural water repellency in grass areas, often noted even in the absence of fire (Pierson et al., 2001). When grass is burned at high severity, however, the organic matter inducing the natural water repellency is seemingly incinerated along the surface, resulting in non-water repellent soil. Several of the high severity grass areas exhibited subsurface water repellency, however, at a depth of 2 cm indicative of a downward heat gradient, often noticed in high temperature fires. The presence of subsurface water

repellent layers, as well as the behavior or water repellency in respect to changes in fire severity is supportive of DeBano's (2000) findings. Because grass areas have considerably less vegetation prior to fire, fire-induced water repellency within those areas is not expected to be as high as in shrub areas. This is contradicted, however, by the observation of the lowest mean MDI being in moderately burned grass (MDI = 4.31 ml/min). This value is not an anomaly, however, and is probably due to the fact that, as stated, the grass areas demonstrate natural repellency in the absence of fire. The fact that the mean MDI value of the moderate severity grass is not significantly different from low severity or unburned grass areas also indicates that the soil is not greatly affected by moderate burn severity. Conversely, the mean MDI value of moderate severity shrub areas (MDI = 4.47 ml/min), which is nearly identical to that of moderate severity grass, is more indicative of fire-induced water repellency, because of its significant difference from other unburned, low, and high severity shrub areas. The statistical analysis of the field data was beneficial for this study because it indicated relationships between burn severity and water repellency that proved useful in the subsequent remote sensing analysis classification, and also provided insight to the dynamics of rangeland wildfire effects.

The use of the MDI for assessing water repellency is valuable because it indicates the degree of repellency among a soil in a less subjective manner than the WDPT. In the case of subsurface soil water repellency, however, the MDI results may be misleading if the above layer of penetrable soil is not removed. The WDPT values served to indicate which MDI values represented very strong repellency. Even though the correlation of the MDI with the WDPT times was not strong, a slight inverse relationship was present between the two. Observations of the WDPT indicated that the water drop usually soaked in immediately, or was present for longer than 360 s. Even though the threshold of the WDPT at 360 s seemed to censor its correlation with the MDI by clustering the highly repellent measurements at that time value, a slight trend was discovered when the two methods were tested against each other. Even after removing the values at 360 s, however, the methods' relationship did not improve, suggesting that the perceived censoring of the threshold values did not have as great an effect on the validity of the WDPT results. Longer observations of the WDPT would have resulted in a more normal distribution of the time values, and likely a greater correlation. Other methods have been used for assessing fire-induced water repellency that account for preferential flow within the soil. The use of rain-simulators and trench analysis (Pierson et al., 2003) assesses sub-surface water repellency, and provides an indication of its spatial variability across an area, as opposed to the point scale measurement by the MDI. The dry conditions of the study area and logistical incompatibility deemed the use of rain simulators infeasible for this project. A comparison of the rain simulator and trench analysis with MDI measurements would be an important contribution to water repellency research.

The inception of soil water repellency across burned rangelands is largely dependent on the pre-fire vegetation. In the discontinuous vegetation distribution of rangelands, the interspaces are not nearly as affected by fire and water repellency as the areas where shrubs are rooted. The variability among interspace microsites is also confounded, however, by the amount and density of pre-fire vegetation, which affects the severity and temperature of the fire, and in turn the formation of water repellent soil layers. The presence and amount of biomass differed across our study area, which in turn affected the distribution and inception of soil water repellency, resulting in its sporadic, discontinuous distribution. Because of the discontinuous nature of vegetation communities across the study area, it was presumed prior to field analysis that the spatial distribution and presence of soil water repellency would vary considerably. In areas of more mature pre-fire vegetation, where the interspersion of coppice and interspace microsites was prevalent, 1-2 m wide black spots were noticeable across the high severity burn areas. These spots represented sites where shrubs had been incinerated, and typically demonstrated higher repellency than the lighter reflectance areas around it. The transect repellency experiment conducted around burned sagebrush proved that soil water repellency is not spatially homogenous by indicating that repellency of the soil decreased as distance from a burned shrub increased. The results of the experiment suggested that soil water repellency was most influenced by the burned shrub when under

its canopy edge, which was evident by the blackening of the soil. When the soil was out of the canopy influence (which was usually between 50 and 100 cm) the repellency of the soil tended to decrease. The final measurements at 200 cm were incomparable among transects because at that distance various other unknown factors were influencing the soil, other than the burned brush. The findings of the transect repellency experiment suggest that water repellency distribution, pre- or post-fire, can be depicted based on the distribution and spacing of shrubs.

The classification of burn severity with the hyperspectral data was compounded by the fact that the extreme pixels of the image (used as classification endmembers) were primarily in areas of extremely high and low reflectance. Their spatial examinations showed few of them actually overlying any of the study plots, and most were further away from the study plots than the imagery's georegistration difference would displace them. Though the extreme pixel classes were assigned their respective burn severity based on their spatial association with the ground truth plots as well as the spectral association among them, a certain level of subjectivity was involved in the assignments. While the assignments were more confident among spectrally unique classes, like low and high severity grass, and low severity shrub, the differentiation of moderate and high severity shrub and moderate severity grass areas was much less distinct. The spectral signatures of moderate and high severity shrub areas are virtually analogous in most cases, and it is difficult for the untrained eye to differentiate the classes in the field. The low users and producer's accuracies of the moderate and high burn severity SAM classifications exhibit this. No moderate severity grass areas were detected in the burn severity classification, in part because few extreme pixels were matched to the moderate grass areas. Additionally, the spectral characteristics of moderately classified grass areas are quite similar to low severity grass areas, due to the lack of charring among the soil, the presence of root crowns, and the high reflectance among the areas. The increased accuracy that was achieved after combining the moderate and high severity shrub areas demonstrates that the SAM classification technique is best for differentiating areas of low severity from moderate or high severity (of which the spectral signatures are very similar).
The results of the field spectrometry provided supplemental understanding of the burn severity classifications by indicating the spectral separability among the classes. The unburned and low severity grass areas were separable from other classes because the senesced (unburned) grass in those areas presented higher reflectance in the NIR than other areas. Their high soil background portrayed higher reflectance in the SWIR as well, and was not reduced due to excess charring. Classes that low severity grasses were most confused with included moderate severity grass and bare ground, both of which had high reflectance in the NIR and SWIR as well. The high severity grass areas still demonstrated higher reflectance than burned shrub areas because the soils were not as damaged and charred as soils within shrub areas. The field spectrometry also indicated very similar reflectance in the high and moderate shrub areas, as was demonstrated in the classifications. The signatures acquired with the field spectrometer were sometimes dissimilar from signatures of the same material acquired from the imagery because the field spectrometer's small field of view (25°) acquired an approximate reflectance area of 1 m^2 data. This presents discrepancies with image reflectance, especially in unburned or low severity areas, because, while the field spectrometry predominantly acquires the material in target (dependent upon height of acqusition), the image pixel acquires the target along with background material(s).

Aside from the confusion of moderate and high severity shrub areas, the SAM algorithm was a better method of assessing burn severity using extreme pixels as endmembers, due to its ability to detect continuous zones of burn severity across the landscape. Results of an MTMF classification of burn severity indicated a low overall accuracy of 50% for all classes except high severity grass. One reason for the low accuracies among the MTMF is because the user-determined pixel thresholds indicate the abundance of an endmember within a pixel. Due to the spectral similarity of the image, and the ambiguity of some burn severity endmembers, it was most probable that the endmembers mixed and overlapped among pixels. A more rigorous field study with more sample plots for verification would likely improve the accuracy of the MTMF, yet endmember overlap would probably still occur. The

benefits of the MTMF are more pronounced in the classification of a single endmember, such as soil water repellency.

The spectral classification of soil water repellency was dependent on materials exhibiting specific spectral features indicative of their presence. In locations where dense shrub had been incinerated, the ground displayed blackened, charred soil. Water repellency was often noted in the charred soils, which exhibited spectral signatures of 10% – 15% less reflectance in the SWIR portion of the spectrum than soils from non-water repellent areas. This decreased reflectance was noted in areas of high water repellency, contrary to areas classified as moderate or high burn severity, in which the reflectance values varied. Although these areas of low reflectance were not the only areas to display high water repellency, they were the only water repellent areas that could be differentiated spectrally. Even though no spectral feature was found strictly unique of water repellent soils, the lowered reflectance typical of incinerated, dense vegetation was indicative of their presence.

The narrow bandwidths of the hyperspectral imagery enabled the detection of the charred soils across the image, and their presence was best mapped using the MTMF algorithm. The success of the SAM classification varied according to the maximum spectral angle established. Various angles were experimentally used and the shift between 0.60 and 0.70 radians was the principal angle difference for under- or over-detection of endmembers. While a SAM classification with a maximum angle of 0.65 classified small portions of the image, it did not cover enough of the image to be verifiable.

The MTMF algorithm was beneficial in locating areas of high water repellency. The output of pixel abundance is a more detailed and accurate representation of the soil water repellency, because it replicates the intermittent nature of water repellency across a burned area. The resulting accuracies from the subpixel abundance representation of strong soil water repellency with the MTMF ranged from 55% to 78% (producer's accuracy) among different values of pixel abundance. The changes in accuracy indicate that with increases in subpixel abundance (lower MF threshold), the more likely it is that portions of the image classified as strongly water repellent will be overlaid by ground truth plots representing that endmember.

Although the MF score results of the MTMF can be related to a measure of subpixel abundance of an endmember, for the purpose of identifying areas of soil water repellency, we did not attempt to quantify the subpixel abundance, but instead utilized the MTMF to predict the endmembers' presence. Given the inherent spatial errors of the imagery and the field-acquired GPS data, an accurate representation of subpixel abundance value would not be practical below the 3 m pixel resolution scale. In addition, the verification of subpixel abundance values would prove difficult to verify given the scale of the 9 m x 9 m sample plots, because the area of the sample plots was meant to encompass 9 pixels (to account for inherent georegistration errors), and the soil water repellency was tested at a 1 m point level within the sample plots.

Unlike the results of the field assessment, in the spectroscopic classification the high soil water repellency was depicted primarily in high severity burn areas, even though more repellency was found in moderate severity areas during the field season. A probable reason for this is because the absence of litter and vegetation in the high severity areas allows for imaging of the soil reflectance. In the moderate severity areas, however, litter and standing vegetation, though burned, is often present, which introduces spectral interference among the image. In addition, the field classification of burn severity has a degree of subjectivity, and moderate and high burn severity classifications may have been confused in the field. Other sources of spectral interference and confusion include shade within the gullies and canyons and the presence of basalt rocks on the surface, which likely contribute to reduced reflectance; some portions of the study area were more rock-strewn than others, like the gullies and slopes of the butte. The infeasiblity scores of the MTMF were decisive for differentiating these materials from water repellent soils. On the

bottom portion of the MTMF image (Fig. 3.13) a substantial amount of high infeasibility is present on the slopes of Devil Creek Butte (2), which was observed to have a considerable covering of basalt stones across the slopes. High infeasibility is also present in the shade of Devil Creek Canyon (3), and in the high reflectance bare ground areas (1). Another important point to note is that, even though the hyperspectral imagery can discern subtle variations of spectra across the surface of the soil, it cannot detect sub-surface soil characteristics. Because fires often cause heat to migrate downward in the soil, a water repellent layer is often present at depths below the surface, and was found at depths up to 2 cm below the surface soil, primarily in areas of high severity grass. A detection of areas likely to have subsurface water repellency with the MTMF classification is possible by detecting areas of high severity grass where the layers are common, but the actual repellent layer would not be detected.

We analyzed the spectra of the burned area in search of additional spectral features that may indicate the presence of fire-induced water repellency; in particular, the lack of a clay oxide absorption band at 2.3 μm, and the indication of aliphatic hydrocarbons. After heating forest soils to various temperatures, Moody et al. (2005) found that the surface of soils heated to very high temperatures (220°-275°) exhibited cementation due to the cooking of the clay oxides within the soils. Because of the high water retention capabilities of clay minerals, the spectral signatures of soils often exhibit a noticeable dip in the spectral signature at 2.3 μm, where clay oxides are detected. If the clays were cemented in a fire due to intense heating, the clay absorption feature would be dissolved from the signature because of the removal of the water. We examined the clay absorption band in spectra from water repellent sample plots at our study area but no noticeable change in the signature was substantiated. In addition, no evidence of clay cementation in the soils was found at the study site. It was concluded that the relatively sparse cover and fuel load in the rangeland did not burn hot enough to induce clay cementation. No evidence of aliphatic hydrocarbons was observed during the analysis of the NIR and SWIR. The charring of the soils, due to the incineration of organic matter, likely muted any spectral evidence of the compounds.
This project demonstrates the potential for spectroscopy to supplement an analysis of post-fire effects on soil properties and rangeland fire dynamics through the use of classification algorithms like the SAM and MTMF. Future research can be built onto these findings to refine the analysis procedures. The SAM classification is best for classifying burn severity across the image because the output classes are more continuous in trait, and express the uniform nature of burn severity across rangelands. The MTMF proved optimal for classifying water repellency because the subpixel abundance output is indicative of the discontinous, unpredictable character of water repellency across burned rangelands. A pitfall of the hyperspectral sensor, though not unexpected, is its inability to detect sub-surface water repellency. Higher accuracy of the classifications may be obtained by implementing a more rigorous field study across the study area. While the MTMF classification algorithm is useful for depicting the presence of water repellency, the degree of repellency is difficult to detect, mainly because the burned, darkened soils within the areas of soil water repellency dominate the spectral reflectance. A future development of this research that may enhance the results could involve the migration of a spatial analysis, using GIS, in conjunction with the described spectral analysis. The addition of a spatial analysis such as kriging, or probability mapping, may better interpolate the spatial variability of soil water repellency across the study area in association with burn severity.

We conclude from this research that water repellent soils are most likely to be found in moderately high to high severity areas of rangelands. Field analysis indicated water repellent soils are likely to be found in moderate severity areas, though this is likely biased by the subjective nature of in-situ burn severity analysis, especially in moderate and high areas. This same confusion was demonstrated in the spectroscopic classification of burn severity and water repellency, but the detection of water repellency among the high severity burned, blackened soils confidently indicates it to be evident in high severity areas. Due to potential discrepancies involving the vegetation burn severity assessment, the methods used for this research could be improved upon in rangelands by examining the parameters of burn severity classes, or perhaps classifying burn severity in a different manner altogether. Though the abolition of

low, moderate, and high severity classes may go against protocol, recent literature (Doerr et al., 2006; Shakesby and Doerr, 2006) has suggested that a more comprehensive range of burn severity assessment, involving more than just the destruction of biomass, may better describe the effects of wildland fire. For example, a greater understanding of hydro-geomorphic impacts across a wider variety of fire landscapes is needed, as is the development of severity indices relating to hydrological, geomorphological, and soil changes across fire landscapes. The utilization of the MDI for assessing water repellency improved the understanding of the phenomenon throughout the burned area by quantifying the degree of repellency among burn severity classes, while the WDPT test was useful for identifying the presence of water repellent soils.

Aside from the success of the spectroscopic classifications, results of this research indicate that rangeland wildfires are dynamic in nature, and their effects on soil properties are consequential of pre-fire vegetation type and condition, fuel load abundance and previous fire history. Although numerous other factors affect fire behavior (e.g. temperature, humidity, wind, slope, aspect), the principal factors influencing the formation of water repellent soils are the presence and amount of biomass available for consumption. Results of this or a similar analysis may be useful parameters in a predictive model of erosion and debris flow susceptibility following rangeland wildfire; the results also prove beneficial for rangeland management and planning practices.

ACKNOWLEDGEMENTS

This thesis is dedicated to my Father, William W. Finley, whose legendary accomplishments and work ethic will never be matched. In addition, my Mother has given me wonderful love and encouragement over the past two years, and her mail-order brownies and banana bread have been a lifesaver. Many thanks go to my older siblings for their support over the past 2 years, especially John, whose sage advice persuaded me to pursue graduate school.

My advisor, Nancy Glenn has been fantastic, and I thank her tremendously for the help, encouragement and confidence she instilled in me while completing my thesis. Many thanks go to the rest of the committee: Glenn, Jen, and John, for their insightful input, and Terry for stepping in at the last minute. Great thanks go to Keith Weber, Laurie Lindsay and the GIS center for employing and supporting me. The ISU Geosciences department deserves great appreciation, especially Melissa for cheerfully handling my inquiries. The geosciences professors are top-notch and deserve a well-rounded appreciation for their hard work, masterful education, and genuine friendliness. In addition, Dr. James Mahar of Engineering deserves a special note for providing the "most bang for the buck" in graduate education. I would like to thank John Ash of the BLM Twin Falls Office for assisting me with field inquiries. Forest Service researchers Peter Robichaud, Charlie Luce, and Fred Pierson, were helpful in the formulation of my thesis.

I am indebted to all of the wonderful people and long-lasting friends I have met and known here at ISU and in Idaho, and will continue to bond with. Finally, I consider myself lucky and fortunate that I was allowed to conduct research in a state as unique, accommodating, and indisputably beautiful as that of Idaho.

This study was made possible by a grant from the National Aeronautics and Space Administration Goddard Space Flight Center. ISU would also like to acknowledge the Idaho Delegation for their assistance in obtaining this grant.

LITERATURE CITED

Analytical Spectral Devices, I., 2004, http://www.asdi.com/.

Aspinall, R.J., Marcus, W.A., and Boardman, J.W., 2002, Considerations in collecting, processing, and analysing high spatial resolution hyperspectral data for environmental investigations: Journal of Geographic Systems, v. 4, p. 15-29.

Bachmann, C.M., Donato, T.F., Lamela, G.M., Rhea, W.J., Bettenhausen, M.H., Fusina, R.A., Bois, K.R.D., Porter, J.H., and Truitt, B.R., 2002, Automatic Classification of Land Cover on Smith Island, VA, Using HyMAP Imagery: IEEE Transactions on Geoscience and Remote Sensing, v. 40, p. 2313-2330.

Bobbe, T., Finco, M.V., Quayle, B., and Lannon, K., 2001, Field Measurements for the Training and Validation of Burn Severity Maps from Spaceborne, Remotely Sensed Imagery: Salt Lake City, Utah, 18 pp., USDA Forest Service, Remote Sensing Applications Center, p. 18.

Britton, C.M., and Clark, R.G., 1985, Effects of fire on sagebrush and bitterbrush, *in* Durham, J., ed., Rangeland Fire Effects; A Symposium: Boise, ID, USDI-BLM, p. 22-26.

Bunting, S.C., 1985, Fire in sagebrush ecosystems: Successional changes, *in* Durham, J., ed., Rangeland Fire Effects; A Symposium: Boise, ID, USDI-BLM, p. 7-11.

Cannon, S.H., 2001, Debris-Flow Generation from Recently Burned Watersheds: Environmental & Engineering Geoscience, v. 7, p. 321-341.

Cannon, S.H., Kirkham, R., and Parise, M., 2001, Wildfire-Related Debris Flow Initiation Processes, Storm King Mountain, Colorado: Geomorphology, v. 39, p. 171-188.

Chabrillat, S., Goetz, A.F.H., Krosley, L., and Olsen, H.W., 2002, Hyperspectral images in the identification and mapping of expansive clay soils and the role of spatial resolution: Remote Sensing of Environment, v. 82, p. 432-445.

Clark, M.L., Clark, D.B., and Roberts, D.A., 2004, Small-footprint estimation of sub-canopy elevation and tree height in a tropical rain forest landscape: Remote Sensing of Environment, v. 91, p. 68-89.

Cocke, A.E., Fulé, P.Z., and Crouse, J.E., 2005, Comparison of burn severity assessments using Differenced Normalized Burn Ratio and ground data: International Journal of Wildland Fire, v. 14, p. 189-198.

Congalton, R.G., and Green, K., 1999, Assessing the accuracy of remotely sensed data: principles and practices: Boca Raton, Florida, CRC Press, 137 p.

Davis, M., and Holbeck, C., 2001, Nuts and bolts of BAER soil and watershed assessments, *in* Harmon, D., ed., Crossing Boundaries in Park Management: 11th Conference on Research and Resource Management in Parks and on Public Lands: Hancock, MI, p. 5.

DeBano, L.F., 1981, Water Repellent Soils: a state-of-the-art: Berkeley, CA, 22 pp., Pacific Southwest Forest and Range Experiment Station, p. 22.

DeBano, L.F, 2000, The role of fire and soil heating on water repellency in wildland environments: a review: Journal of Hydrology, v. 231-232, p. 195-206.

DeBano, L.F., Neary, D.G., and Pfolliott, P.F., 1998, Fire's Effects on Ecosystems: New York, John Wiley and Sons, 333 p.

Debba, P., Ruitenbeek, F.J.A.v., Meer, F.D.v.d., Carranza, E.J.M., and Stein, A., 2005, Optimal field sampling for targeting minerals using hyperspectral data: Remote Sensing of Environment, v. 99, p. 373-386.

Decagon Devices, I., 1998, URL: http://decagon.com/, accessed 06/01/05.

Dekker, L.W., and Ritsema, C.J., 1994, How water moves in a water repellent sandy soil 1. Potential and actual water repellency: Water Resources Research, v. 30, p. 2507-2517.

Dekker, L.W., and Ritsema, C.J., 2000, Wetting patterns and moisture variability in water repellent Dutch soils: Journal of Hydrology, v. 231/232, p. 148-164.

DeLuis, M., Gonzalez-Hidalgo, J.C., and Raventos, J., 2002, Effects of fire and torrential rainfall on erosion in a mediterranean gorse community: Land Degradation and Development, v. 14, p. 203-213.

Doerr, S.H., Shakesby, R.A., Blake, W.H., Chafer, C.J., Humphreys, G.S., and Wallbrink, P.J., 2006, Effects of differing wildfire severities on soil wettability and implications for hydrological response: Journal of Hydrology, v. 319, p. 295-311.

Doerr, S.H., and Thomas, A.D., 2000, The role of soil moisture in controlling soil water repellency: new evidence from forest soils in Portugal: Journal of Hydrology, v. 231/232, p. 134-147.

ESRI, I., 2005, http://www.esri.com

Fraser, R.H., and Li, Z., 2002, Estimating fire-related parameters in boreal forest using SPOT VEGETATION: Remote Sensing of Environment, p. 95-110.

Gimeno-Garcia, E., Andreu, V., and Rubio, J.L., 2004, Spatial patterns of soil temperatures during experimental fires: Geoderma, v. 118, p. 17-38.

Glenn, N.F., Mundt, J.T., Weber, K.T., Prather, T.S., Lass, L.W., and Pettingill, J., 2005, Hyperspectral data processing for repeat detection of small infestations of leafy spurge: Remote Sensing of Environment, v. 95, p. 399-412.

Holecheck, J.L., and Pieper, R.D., 2001, Range management: Principles and practices: Saddle River, NJ, Prentice Hall Inc.

Houston, D.B., 1973, Wildfires in Yellowstone National Park: Ecology, v. 54, p. 1111-1117.

Hummel, J.W., Sudduth, K.A., and Hollinger, S.E., 2001, Soil moisture and organic matter prediction of surface soils using an NIR soil sensor: Computers and electronics in agriculture, v. 32, p. 149-165.

Ice, G.G., Neary, D.G., and Adams, P.W., 2004, Effects of wildfire on soils and watershed processes: Journal of Forestry, v. 102, p. 16-20.

Iverson, R.M., 1997, The physics of debris flows: Reviews of Geophysics, v. 35, p. 245-296.

Jensen, J.R., 2000, Remote sensing of the environment, an earth resources perspective: Saddle River, NJ, Prentice Hall, Inc., 544 p.

Jensen, J.R., 2005, Introductory digital image processing: A remote sensing perspective: Upper Saddle River, NJ, Pearson Prentice Hall, 526 p.

Johnson, M., and Beschta, R., 1981, Seasonal variation of infiltration capacities of soils in Western Oregon: Corvallis, OR, 6 pp., Pacific Northwest forest and range experiment station, p. 6.

Key, C., and Benson, N., 2004, Landscape Assessment (LA) Sampling and Analysis Methods, FIREMON Landscape Assessment V4.

Kirkham, M.B., 2005, Principles of Soil and Plant Water Relations: San Diego, CA, Elsevier Academic Press, 500 p.

Knapp, P.A., 1995, Intermountain West lightning-caused fires: Climatic predictors of areas burned: Journal of Range Management, v. 48, p. 85-91.

Krammes, J.S., and Debano, L.F., 1965, Soil wettability: a neglected factor in watershed management: Water Resources Research, v. 1, p. 283-286.

Kruse, F.A., Lefkoff, A.B., Boardman, J.B., Heidebrecht, K.B., Shapiro, A.T., Barloon, P.J., and Goetz, A.F.H., 1993, The Spectral Image Processing System (SIPS) - Interactive Visualization and Analysis of Imaging Spectrometer Data: Remote Sensing of Environment, v. 44, p. 145-163.

Kruse, F.A., Richardson, L.L., and Ambrosia, V.G., 1997, Techniques developed for geologic analysis of hyperspectral data applied to near-shore hyperspectral ocean data, ERIM 4th International Conference, Remote Sensing for Marine and Coastal Environments, Volume 1: Environmental Research Institute of Michigan (ERIM), Ann Arbor, p. I-233 - I-246.

Laes, D., Mas, P., Lewis, S., Robichaud, P., and Kokaly, R., 2004, Postfire burn-severity classification of the Hayman fire, CO: Based on hyperspectral data-JFSP RFP 2001-2 Task 1: SLC, UT, Remote Sensing App. Center, p. 29.

Lewis, S.A., Robichaud, P.R., Elliot, W.J., Frazier, B.E., and Wu, J.Q., 2004, Hyperspectral remote sensing of postfire soil properties, Tenth Forest Service Remote Sensing Applications Conference: Salt Lake City, Utah, p. 9.

Lewis, S.A., Wu, J.Q., and Robichaud, P.R., 2006, Assessing burn severity and comparing soil water repellency, Hayman Fire, CO: Hydro. Proc. v. 20, p.1-16.

Lillesand, T.M., Kiefer, R.W., and Chipman, J.W., 2004, Remote Sensing and Image Interpretation: USA, John Wiley & Sons, 763 p.

Meyer, G.A., Pierce, J.L., Wood, S.H., and Hull, A.J.T., 2001, Fire, storms and erosional events in the Idaho batholith: Hydrological Processes, v. 15.

Meyer, G.A., and Wells, S.G., 1997, Fire-related sedimentation events on alluvial fans, Yellowstone National Park, U.S.A.: Journal of Sedimentary Research, v. A67, p. 776-791.

Moody, J.A., and Smith, J.D., 2005, Critical shear stress for erosion of cohesive soils subjected to temperatures typical of wildfires: Journal of Geophysical Research, v. 110, p. 1-13.

Moody, J.A., Smith, J.D., and Regan, B.W., 2005, Critical shear stress of cohesive soils subjected to temperatures typical of wildfires: Journal of Geophysical Research, v. 110, FO1004, p. 1-13.

Mundt, J.T., Glenn, N.F., Weber, K.T., Prather, T.S., Lass, L.W., and Pettingill, J., 2005, Discrimination of hoary cress and determination of its detection limits via hyperspectral image processing and accuracy assessment techniques: Remote Sensing of Environment, v. 96, p. 509-517.

Mundt, J., Glenn, N., Weber, K., Pettingill, J., 2005, Determining target detection limits and accuracy delineation using an incremental technique. Remote Sensing of Environment, in press.

Mundt, J.T., Streutker, D.R., and Glenn, N.F, 2006, Mapping sagebrush distribution using fusion of hyperspectral and lidar classifications: Photogrammetric Engineering & Remote Sensing, v. 72, p. 47-54.

NCDC, 2005, http://www.ncdc.noaa.gov/oa/ncdc.html, Accessed May 24, 2006. Okin, G.S., Roberts, D.A., Murray, B., and Okin, W.J., 2001, Practical limits on hyperspectral vegetation discrimination in arid and semiarid environments: Remote Sensing of Environment, v. 77, p. 212-225.

Noy-Meir, I., 1973, Desert Ecosystems: environment and producers: Annual Reviews in Ecological Systems, v. 4, p. 25-51.

Odion, D.C., Frost, E.J., Strittholt, J.R., Jiang, H., Dellasala, D.A., and Moritz, M.A., 2004, Patterns of fire severity and forest conditions in the Western Klamath Mountains, California: Consevation Biology, v. 18, p. 927-936.

Okin, G.S., Roberts, D.A., Murray, B., and Okin, W.J., 2001, Practical limits on hyperspectral vegetation discrimination in arid and semiarid environments: Remote Sensing of Environment, v. 77, p. 212-225.

Okin, W.J., Okin, G.S., Roberts, D.A., and Murray, B., 1999a, Multiple endmember spectral mixture analysis: application to an arid/semi-arid landscape, *in* Green, R.O., ed., The 1999 AVIRIS Workshop: Pasadena California, p. 291-300.

Okin, W.J., Okin, G.S., Roberts, D.A., and Murray, B., 1999b, Multiple endmember spectral mixture analysis: endmember choice in an arid shrubland, *in* Green, R.O., ed., The 1999 AVIRIS Workshop: Pasadena California, p. 323-332.

Palacios-Orueta, A., Pinzon, J.E., Ustin, S.L., and Roberts, D.A., 1999, Remote Sensing of Soils in the Santa Monica Mountains: II. Hierarchical Foreground and Background Analysis: Remote Sensing of Environment, v. 68, p. 138-151.

Palacios-Orueta, A., and Ustin, S.L., 1998, Remote Sensing of Soil Properties in the Santa Monica Mountains, pt. I: Spectral Analysis: Remote Sensing of Environment, v. 65, p. 170-183.

Parker-Williams, A., and Hunt Jr., R., 2004, Accuracy assessment for detection of leafy spurge with hyperspectral imagery: Journal of Range Management, v. 57, p. 106-112.

Parker-Williams, A.E., 2004, Accuracy assessment for detection of leafy spurge with hyperspectral imagery: Journal of Range Management, v. 57, p. 106-112.

Pierce, J., Meyer, G.A., and Jull, T., 2004, Fire-Induced erosion and millenial-scale climate change in northern ponderosa pine forests: Nature, v. 432, p. 87-90.

Pierson, F.B., Robichaud, P.R., and Spaeth, K.E., 2001, Spatial and temporal effects of wildfire on the hydrology of a steep rangeland watershed: Hydrological Processes, v. 15, p. 2905-2916.

Pierson, F.B., Robichaud, P.R., Spaeth, K.E., and Moffet, C., 2003, Impacts of fire on hydrology and erosion in steep mountain big sagebrush communities, First Interagency Conference on Research in the Watersheds: Benson, AZ.

Pinzon, J.E., Ustin, S.L., Castaneda, C.M., Pierce, J.F., and Costick, L.A., 1998, Robust spatial and spectral feature extraction for multispectral and hyperspectral imagery, *in* Schewel, J., ed., SPIE Int. Soc. Opt. Eng., Volume 3372: Boston, Massachusetts.

Rahman, A.F., and Gamon, J.A., 2004, Detecting biophysical properties of a semi-arid grassland and distinguishing burned from unbuned areas with hyperspectral reflectance: Journal of Arid Environments, v. 58, p. 597-610.

Raper, B., Clark, B., Matthews, M., and Aldrich, A., 1984, Early effects of a fall burn in a Western Wyoming big sagebrush-grass community, *in* Durham, J., ed., Rangeland fire effects, a symposium: Boise, ID, USDI Bureau of Land Management, p. 88-93.

Robichaud, P., Macdonald, L., Freeouf, J., Neary, D., Martin, D., and Ashmun, L., 2003, Postfire Rehabilitation of the Hayman Fire, USDA Forest Service, p. 293-314.

RSI, 2005, Environmental Systems Research Institute (ENVI) online help documentation, http://www.ittvis.com/index.asp.

SAS Institute, I., 2005, Online Documentation, http://v8doc.sas.com/sashtml/.

Scott, D.F., 1993, The hydrological effects of fire in South African mountain catchments: Journal of Hydrology, v. 150, p. 409-432.

Shakesby, R.A., Chafer, C.J., Doerr, S.H., Blake, W.H., Wallbrink, P., Humphreys, G.S., and Harrington, B.A., 2003, Fire Severity, Water Repellency Characteristics and Hydrogeomorphological Changes Following the Christmas 2001 Sydney Forest Fires: Australian Geographer, v. 34, p. 147-175.

Shakesby, R.A., and Doerr, S.H., 2006, Wildfire as a hydrological and geomorphological agent: Earth-Science Reviews, v. 74, p. 269-307.

Shinn, D.A., 1980, Historical perspectives on range burning in the Inland Pacific Northwest: Journal of Range Management, v. 33, p. 415-423.

Smith, J.K., 2000, Wildland fire in ecosystems: effects of fire on fauna: Ogden, UT, 83 pp., U.S. Department of Agriculture, Forest Service, Rocky Mountain Research Station, p. 83.
Sprague-Wheeler, D.K., 2001, The use of remote sensing imagery for evaluation of post-wildfire susceptibility to landslide and erosion hazards in the Salmon-Challis National Forest, Lemhi County, Idaho: Pocatello ID,, Idaho State University.

Steede-Terry, K., 2000, Integrating GIS and the Global Positioning System: Redlands, CA, Environmental Systems Research Institute, Inc., 95 p.

Summerfield, M.A., 1991, Global Geomorphology: London, England, Pearson Education Ltd., 537 p.

Switky, K.R., 2003, Fire monitoring handbook: Boise, ID, 274 pp., NPS Fire management program center, National Interagency Fire Center, p. 274.

Trimble Navigation, L., 2005, http://www.trimble.com/.

Tucket, T., Beard, J., Fluckiger, M., Rizvi, H., Woodcock, P., and Mahar, W., 2004, Caddy Canyon erosion debris flow and abatement, Proceedings for the 39th annual Symposium of Engineering Geology and Geotechnical Engineering: Butte, MT, 8 pp.

USDA-FSA, 2005, USDA-Farm Service Agency National Agriculture Imagery Program, http://www.apfo.usda.gov/NAIP.html.

USDA-NRCS, 2005, Owyhee, Twin Falls County, ID, Soil Taxonomy database, Volume 2005.

Ustin, S.L., Roberts, D.A., Gamon, J.A., Asner, G.P., and Green, R.O., 2004, Using imaging spectroscopy to study ecosystem processes and properties: Bioscience, v. 54, p. 523-534.

Wagtendonk, J., Root, R., and Key, C., 2004, Comparison of AVIRIS and Landsat ETM+ Detection Capabilities for Burn Severity: Remote Sensing of Environment, v. 92, p. 397-408.

West, N.E., and Hassan, M.A., 1985, Recovery of sagebrush-grass vegetation following wildfire: Journal of Range Management, v. 38, p. 131-134.

Whisenant, S.G., 1990, Changing fire frequencies on Idaho's Snake River Plains: Ecological and management implications, USDA Forest Service, Intermountain Research Station, p. 10.

Wondzell, S., and King, J., 2003, Postfire erosional processes in the Pacific Northwest and Rocky Mountain regions: Forest Ecology and Management, v. 178, p. 75-87.

Wright, H.A., 1985, Effects of fire on grasses and forbs in sagebrush-grass communities, *in* Durham, J., ed., Rangeland Fire Effects; A Symposium: Boise, ID, USDI-BLM, p. 12-21.

Young, J.A., and Evans, R.A., 1981, Demography and fire history of a western juniper stand: Journal of Range Management, v. 34, p. 501-506.

Appendix A. HyMap Georegistration Error Analysis

Table A.1. GCP locations and difference between NAIP and HyMap imagery

GCP	Image	POINT_X	POINT_Y	X Shift (meters)	Y Shift (meters)	Direction (degrees)
1	NAIP	666,102.45	4,715,075.72			
1	Hymap	666,105.87	4,715,073.63	3.42	2.09	328
2	NAIP	666,893.28	4,715,232.65			
2	Hymap	666,886.48	4,715,221.46	6.80	11.19	238
3	NAIP	666,090.55	4,714,050.23			
3	Hymap	666,091.67	4,714,049.09	1.12	1.13	313
4	NAIP	666,548.17	4,713,147.33			
4	Hymap	666,545.50	4,713,141.34	2.67	5.99	240
5	NAIP	667,160.10	4,711,880.29			
5	Hymap	667,156.15	4,711,875.03	3.95	5.26	230
6	NAIP	666,486.12	4,709,334.87			
6	Hymap	666,483.74	4,709,330.91	2.38	3.95	230
7	NAIP	666,158.87	4,708,526.93			
7	Hymap	666,158.46	4,708,522.45	0.41	4.48	265
8	NAIP	667,208.51	4,708,389.00			
8	Hymap	667,202.51	4,708,380.42	6.01	8.58	234
9	NAIP	667,645.14	4,706,835.53			
9	Hymap	667,639.29	4,706,824.72	5.86	10.81	241
10	NAIP	666,973.99	4,706,594.00			
10	Hymap	666,968.56	4,706,588.15	5.43	5.85	228
11	NAIP	667,046.15	4,705,139.67			
11	Hymap	667,043.09	4,705,131.62	3.06	8.06	250
12	NAIP	666,996.98	4,704,364.09			
12	Hymap	666,994.01	4,704,360.58	2.97	3.51	235
13	NAIP	667,904.24	4,704,083.76			
13	Hymap	667,898.02	4,704,074.44	6.22	9.32	236
14	NAIP	666,684.22	4,703,657.20			
14	Hymap	666,682.96	4,703,653.65	1.25	3.55	250
15	NAIP	667,390.52	4,702,319.32			
15	Hymap	667,388.29	4,702,312.07	2.23	7.25	252
16	NAIP	666,371.51	4,702,252.54			
16	Hymap	666,371.28	4,702,252.54	0.23	0.00	180
17	NAIP	667,313.54	4,700,577.16			
17	Hymap	667,314.21	4,700,570.66	0.67	6.51	275
18	NAIP	666,781.14	4,699,651.41			
18	Hymap	666,782.30	4,699,653.72	1.15	2.31	63
		Mean		3.10	5.55	238.22
		Standard Deviation		2.16	3.24	
		Maximum difference		6.80	11.19	
		Minimum difference		0.23	0.00	
		Range		6.57	11.19	

Assessment of the HyMap georegistration was based on measurements between 18 NAIP aerial photograph ground control points (GCP's) and their equivalent locations on HyMap image 06.

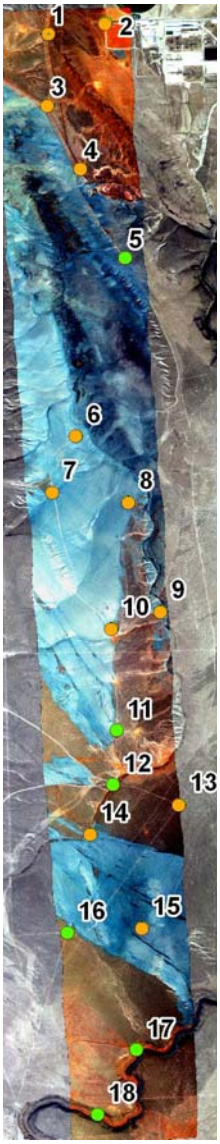

Fig. A.1. GCP's used for georegistration assessment, HyMap image 06

Appendix B. Daily Weather Observations, Castleford, Idaho

Daily weather records for Castleford, Idaho weather station obtained from National Climatic Data Center, US Department of Commerce (NCDC, 2005). Castleford is approximately 6 km east of the Clover Fire study area.

Table A.2. Weather observations, August, 2005

Year	Month	Day	Temp. (deg. F) Max.	Min.	Obs.	Precip (mm)
2005	Aug.	1	94	56	83	0
2005	Aug.	2	88	58	88	0
2005	Aug.	3	89	52	88	0
2005	Aug.	4	94	53	93	0
2005	Aug.	5	97	53	95	0
2005	Aug.	6	99	58	99	0
2005	Aug.	7	99	55	88	0
2005	Aug.	8	92	69	80	Trace
2005	Aug.	9	92	58	82	0
2005	Aug.	10	92	58	91	0
2005	Aug.	11	91	57	88	0
2005	Aug.	12	88	51	85	0
2005	Aug.	13	86	47	80	0
2005	Aug.	14	82	46	81	0
2005	Aug.	15	86	51	85	0
2005	Aug.	16	84	61	74	Trace
2005	Aug.	17	86	51	77	0
2005	Aug.	18	80	56	79	1.02
2005	Aug.	19	85	51	85	0
2005	Aug.	20	93	52	92	0
2005	Aug.	21	96	54	94	0
2005	Aug.	22	94	62	74	Trace
2005	Aug.	23	88	53	83	0
2005	Aug.	24	84	53	76	0
2005	Aug.	25	83	44	82	0
2005	Aug.	26	88	50	87	0
2005	Aug.	27	90	50	89	0
2005	Aug.	28	91	50	90	0
2005	Aug.	29	90	55	85	0
2005	Aug.	30	85	49	69	0
2005	Aug.	31	76	41	75	0
Mean:			**89.1**	**53.4**	**Total:**	**1.02**

Table A.3. Weather observations, September, 2005

Year	Month	Day	Temp. (deg. F) Max.	Min.	Obs.	Precip (mm)
2005	Sept.	1	82	41	81	0
2005	Sept.	2	93	49	92	0
2005	Sept.	3	93	51	86	0
2005	Sept.	4	86	51	83	0
2005	Sept.	5	83	48	79	0
2005	Sept.	6	82	41	81	0
2005	Sept.	7	85	49	83	0
2005	Sept.	8	90	52	77	0
2005	Sept.	9	83	52	77	0
2005	Sept.	10	77	34	57	Trace
2005	Sept.	11	66	34	65	0

2005	Sept.	12	69	44	67	0
2005	Sept.	13	70	33	68	0
2005	Sept.	14	74	39	73	0
2005	Sept.	15	80	48	79	0
2005	Sept.	16	79	45	75	0
2005	Sept.	17	77	48	63	Trace
2005	Sept.	18	70	38	68	0
2005	Sept.	19	76	38	75	0
2005	Sept.	20	79	42	76	0
2005	Sept.	21	78	54	71	0
2005	Sept.	22	79	41	N/A	0
2005	Sept.	23	77	47	70	0
2005	Sept.	24	68	43	55	0
2005	Sept.	25	62	34	62	0
2005	Sept.	26	73	35	70	0
2005	Sept.	27	70	49	66	1.8
2005	Sept.	28	71	39	69	0
2005	Sept.	29	77	37	76	0
2005	Sept.	30	81	45	79	0
Mean:			**77.7**	**43.4**	**Total:**	**1.8**

Table A.4. Weather observations, October, 2005

Year	Month	Day	Temp. (deg. F) Max.	Min.	Obs.	Precip (mm)
2005	Oct.	1	84	48	81	0
2005	Oct.	2	80	41	53	1.8
2005	Oct.	3	57	38	52	Trace
2005	Oct.	4	53	36	50	0.5
2005	Oct.	5	55	27	54	0
2005	Oct.	6	64	28	62	0
2005	Oct.	7	68	33	66	0
2005	Oct.	8	66	46	58	0
2005	Oct.	9	60	39	58	0
2005	Oct.	10	61	32	59	0
2005	Oct.	11	60	31	56	0
2005	Oct.	12	60	42	58	0
2005	Oct.	13	72	33	69	0
2005	Oct.	14	80	38	78	0
2005	Oct.	15	80	52	62	0
2005	Oct.	16	63	42	61	0
2005	Oct.	17	61	38	59	0
2005	Oct.	18	72	35	68	0
2005	Oct.	19	69	46	66	0
2005	Oct.	20	67	42	61	0
2005	Oct.	21	63	35	61	0
2005	Oct.	22	65	33	63	0
2005	Oct.	23	69	35	67	0
2005	Oct.	24	74	37	73	0
2005	Oct.	25	73	40	65	0
2005	Oct.	26	67	48	61	0
2005	Oct.	27	61	42	45	0.76
2005	Oct.	28	55	35	53	3.05
2005	Oct.	29	55	35	52	0.25
2005	Oct.	30	52	30	48	0
2005	Oct.	31	55	27	54	0
Mean:			**65.2**	**37.5**	**Total:**	**6.36**

Appendix C: Additional Image Processing

The efficiency of spectroscopy is demonstrated in its ability to transfer spectra among multiple images in order to classify them without undertaking all of the pre-processing steps required for the initial image classification (PPI & n-DV endmember identification). After conducting the primary image analysis on image 6, the other images were mosaicked together for more efficient processing. Listed below are the image analysis and classification results of mosaicked images 5, 6, and 7, of section A; images 3 and 4 of section B, and images 1 and 2 of section C. Prior to conducting the mosaics, the images were MNF-transformed and saved as 125-band MNF files. After the images were mosaicked, a mask was applied to the image to isolate the burned areas. A SAM classification of burn severity and a MTMF classification of water repellency were conducted on each mosaicked image. Prior to the classification of water repellency, the reflectance images were subset to the SWIR portions of the image (bands 65-125), and the remaining 61 bands were MNF-transformed.

As was the case in image 6, higher accuracies may have been obtained for the MTMF classification of high water repellency had a more complete field assessment been conducted. The classifications do serve to indicate those areas most likely to exhibit soil water repellency, while the infeasibility scores are useful for identifying areas of false positives.

Section A

A SAM classification of burn severity and a MTMF classification of high water repellency were conducted on the mosaicked images 5, 6, and 7 (Fig. A.2 A), comprising section A. The extreme pixel endmembers identified in image 6 were used as training endmembers for burn severity classes. Several sample plots in images 5 and 7 were used as supplemental training sites in order for the classification to completely cover the mosaicked image. Bare ground was not included in the burn severity classification of the mosaicked image because of a lack of ground truth plots outside of image 6 representing bare ground. An error matrix was calculated for the classification using 54 field-collected sample plots from section A (plots used for training were not used as ground truth) as reference. The classification resulted in 66% overall accuracy, and a Kappa coefficient of 0.56 (Table A.5). As with the other classifications, the burn severity classes of moderate and high shrub were confused, as is evident by the lower producer's accuracy. The high severity grass had low accuracy as well, but the primary reason is likely because there were only 3 sample plots available for reference sites in that class, which were confused in themselves with high severity shrub. The accuracies of low severity grass and shrub, and high severity shrub were actually higher for the mosaicked image classification of section A. The probable reason for this is because the ground truth sample plots added to the accuracy assessment for the classified mosaic consisted mainly of these classes, and their presence beneath the correctly classified area increased the accuracy of that class.

The MTMF classification of burn severity detected highly water repellent soils across 12.5% of the burned area when a pixel abundance of 100% was used for presence/absence detection (Table A.6 A). A total of 8 positive reference ground truth plots and 10 negative reference plots were used for the accuracy assessment. When the threshold was lowered to a percentage of material identified within the pixel (Table A.6 B, C), the overall accuracies of the classification increased from 33% to 61% at MF score thresholds of 0.5 and 0.3. Slight reflectance differences among the mosaicked images resulted in over-classification of the bottom portion of the image (Fig. A.2 B) on Devil Creek Butte, but the results still serve to pinpoint areas susceptible to increased sedimentation following the fire.

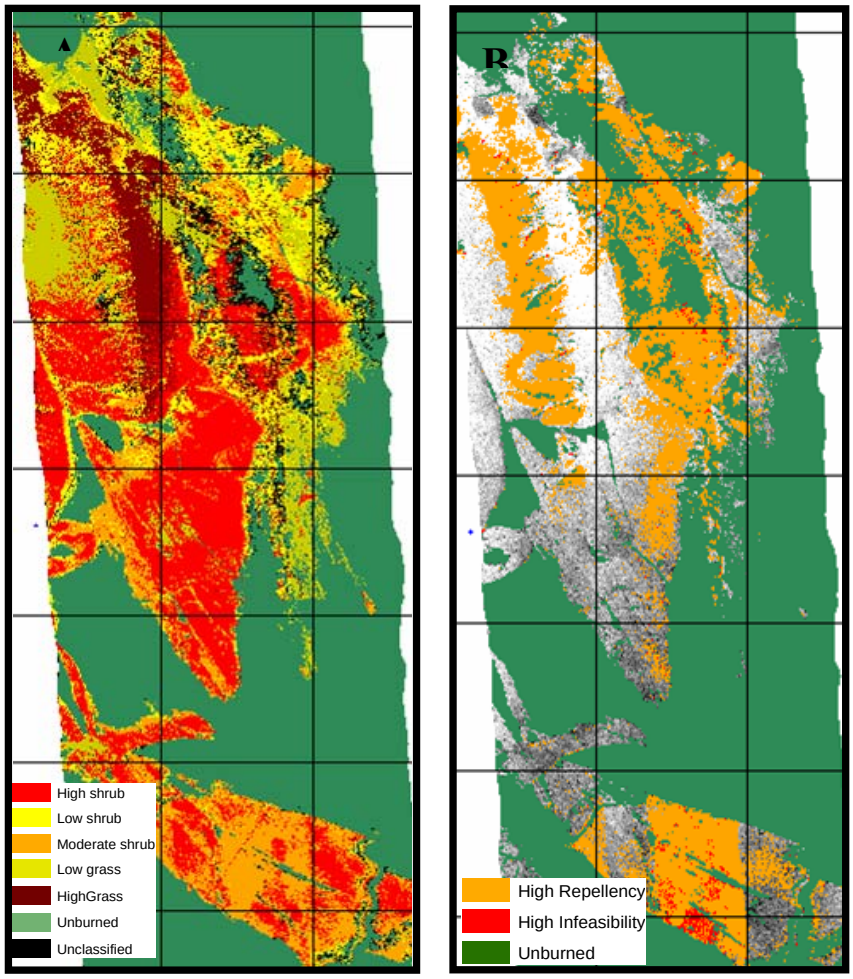

Figure A.2. A. SAM burn severity classification, section A. B. MTMF classification of fire-induced high water repellency, MF score threshold = 0.65-2.0. Infeasibility scores (red) greater than 20. Note: 1 square = 2 km

Table A.5. SAM burn severity classification error matrix, section A

Error Matrix, SAM Burn Severity Classification, Image 5, 6, & 7 Mosaic						
Overall Accuracy = (205/312) 66%						
Kappa Coefficient = 0.56						
Ground Truth (pixels)						
Class	**Low Severity Shrub**	**Moderate Severity Shrub**	**High Severity Shrub**	**Low Severity Grass**	**High Severity Grass**	**Total**
Unclassified	0	6	0	0	0	6
Low Severity Shrub	64	13	5	7	0	89
Moderate Severity Shrub	2	45	20	0	0	67
High Severity Shrub	5	12	50	0	0	67
Low Severity Grass	0	5	1	35	10	51
High Severity Grass	0	2	18	1	11	32
Total	71	83	94	43	21	312

Class	Commission (%)	Omission (%)	Producer's Accuracy (%)	User's Accuracy (%)
Low Severity Shrub	28.09	9.86	90.14	71.91
Moderate Severity Shrub	32.84	45.78	54.22	67.16
High Severity Shrub	25.37	46.81	53.19	74.63
Low Severity Grass	31.37	18.6	81.4	68.63
High Severity Grass	65.63	47.62	52.38	34.38

Table A.6. Presence/absence error matrices of MTMF classification of highly water repellent soils, Section A: A. MF = 1-2.0; B. MF = 0.5 – 2.0; C. MF = .3-2.0

A. MF score threshold = 1.0-2.0 (189,351 pixels) 12.5% of burned area			
MTMF Class	Reference Positive	Reference Negative	User's Accuracy
Classified Positive	3	6	33%
Classified Negative	6	3	33%
Producer's Accuracy	33%	33%	**33%**

B. MF score threshold = 0.5-2.0 (679,134 pixels) 45% of burned area			
MTMF Class	Reference Positive	Reference Negative	User's Accuracy
Classified Positive	5	4	56%
Classified Negative	3	6	67%
Producer's Accuracy	63%	60%	**61%**

C. MF score threshold = 0.3-2.0 (993,927 pixels) 66% of burned area			
MTMF Class	Reference Positive	Reference Negative	User's Accuracy
Classified Positive	5	4	56%
Classified Negative	3	6	67%
Producer's Accuracy	63%	60%	**61%**

Section B

A SAM classification of burn severity was conducted on mosaicked images 3 and 4 (Fig. A.3). The SAM classification used 23 extreme pixel classes representing burn severity categories as endmembers; these were identified on image 4 using the PPI and n-DV endmember identification technique. A maximum angle of 1.0 radian was utilized for the classification. 25 sample plots were utilized for accuracy assessment of the classifications. The SAM classification of burn severity had an overall accuracy of 60% and a kappa coefficient of 0.50 (Table A.7). The burned grass areas were classified accurately in the image, while the moderate and high shrub areas were confused.

A MTMF classification of highly water repellent soils was conducted on the mosaicked images 3 and 4 (Fig. A.4). The MNF-transformed spectra of 2 known water repellent sample plots in section B were input as endmembers in the classification. The presence/absence error matrices of the classification are listed in Table A.8 (A, B, C). For the accuracy assessment of the MTMF classification, 11 positive reference plots were used and 8 negative reference plots. The overall accuracies of the MTMF classifications increased by 10% each time the MF score threshold was lowered to include greater pixel abundance. The infeasibility scores of 20 or higher (Fig. A.4) indicate most false positives to be within the very high and low reflectance areas, like the access roads, and rock-strewn slopes.

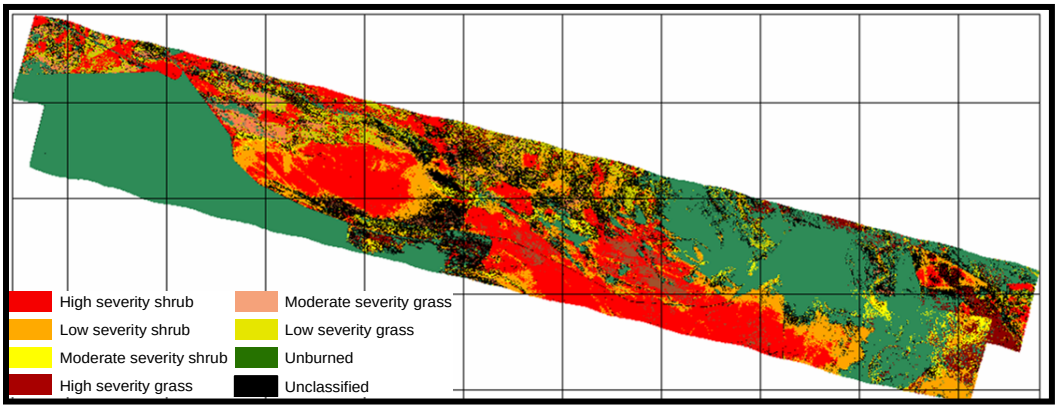

Figure A.3. SAM burn severity classification, section B. 1 square=2 km

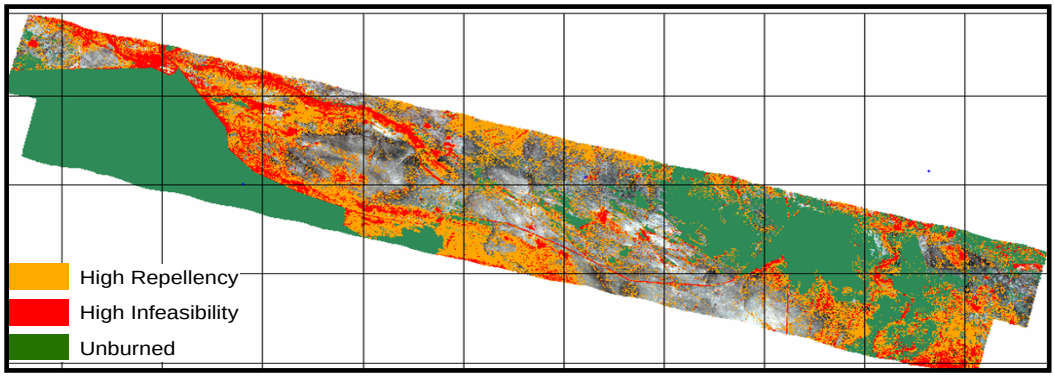

Figure A.4. MTMF classification of fire-induced high water repellency, MF score threshold = 0.65-2.0. Infeasibility scores (red) greater than 20.

Table A.7. SAM burn severity classification error matrix, section B

Error Matrix, SAM Burn Severity Classification, Image 3 & 4 Mosaic							
Overall Accuracy = (131/225) 60%							
Kappa Coefficient = 0.50							
Ground Truth (pixels)							
Class	**Low Severity Shrub**	**Moderate Severity Shrub**	**High Severity Shrub**	**Low Severity Grass**	**Moderate Severity Grass**	**High Severity Grass**	**Total**
Unclassified	5	7	7	17	1	0	37
Low Severity Shrub	13	1	0	0	0	0	14
Moderate Severity Shrub	5	33	9	0	0	0	47
High Severity Shrub	0	20	23	0	0	0	43
Low Severity Grass	0	2	0	38	0	0	40
Moderate Severity Grass	0	8	0	6	16	0	30
High Severity Grass	1	5	0	0	0	8	14
Total	24	76	39	61	17	8	225

Class	Commission (%)	Omission (%)	Producer's Accuracy (%)	User's Accuracy (%)
Low Severity Shrub	7.14	45.83	54.17	92.86
Moderate Severity Shrub	29.79	56.58	43.42	70.21
High Severity Shrub	46.51	41.03	58.97	53.49
Low Severity Grass	5	37.7	62.3	95
Moderate Severity Grass	46.67	5.88	94.12	53.33
High Severity Grass	42.86	0	100	57.14

Table A.8 A, B, C. Presence/absence error matrices of MTMF classification of highly water repellent soils, Section B

A. MTMF score threshold = 1.0-2.0 (142,662 pixels) 3.4% of burned area			
MTMF Class	Reference Positive	Reference Negative	User's Accuracy
Classified Positive	5	6	45%
Classified Negative	6	2	25%
Producer's Accuracy	45%	25%	**37%**

B. MTMF score threshold = 0.5-2.0 (680,674 pixels) 17% of burned area			
MTMF Class	Reference Positive	Reference Negative	User's Accuracy
Classified Positive	5	6	54%
Classified Negative	6	2	33%
Producer's Accuracy	64%	25%	**47%**

C. MTMF score threshold = 0.3-2.0 (1,103,054 pixels) 27% of burned area			
MTMF Class	Reference Positive	Reference Negative	User's Accuracy
Classified Positive	7	4	64%
Classified Negative	4	4	50%
Producer's Accuracy	64%	50%	**58%**

Section C

The field data collection in section C was inadequate for a robust classification, because heavy wind storms had transported large amounts of soil and litter away from the study site, leaving very different conditions than those at the time of image acquisition. These storms resulted in ground conditions that were not representative of conditions in the imagery. Because of this deficiency, the classifications of section C could not be substantially assessed for accuracy.

The field conditions in section C also made it difficult to differentiate high and moderate severity shrub from high and moderate severity grass areas, so the burn severity of the section only differentiated low, moderate and high burn severity. Burn severity endmembers from section B were transferred to section C for the supervised classification. Several of the training sites from the field were input for endmember identification as well. The SAM burn severity classification (Fig. A.5 A) was conducted with a maximum angle of 1 radian. After the classification, an error matrix was calculated for the classification using the field-assessed sample plots (excluding those that were input as training sites). The general burn severity classification of low, moderate and high severity produced a surprisingly high accuracy of 75%. The presented high accuracy may be slightly misleading, however, because the number of training sites for error assessment only totaled 2 for high severity, 3 for moderate severity, 5 for low severity, and 1 for bare ground. Table A.9 lists the error matrix values for the SAM burn severity classification.

Table A.9. SAM burn severity classification error matrix, section C

Error Matrix, SAM Burn Severity Classification, Image 1 & 2 Mosaic					
Overall Accuracy = (117/155) 75% **Kappa Coefficient = 0.66**					
Ground Truth (pixels)					
Class	**High Severity**	**Moderate Severity**	**Low Severity**	**Bare Ground**	**Total**
Unclassified	0	0	2	0	2
High Severity	30	10	1	0	41
Moderate Severity	3	36	14	2	55
Low Severity	0	0	38	0	38
Bare Ground	0	0	6	13	19
Total	33	46	61	15	155
Class	**Commission (%)**	**Omission (%)**	**Producer's Accuracy (%)**	**User's Accuracy (%)**	
High Severity	26.83	9.09	90.91	73.17	
Moderate Severity	34.55	21.74	78.26	65.45	
Low Severity	0	37.7	62.3	100	
Bare Ground	31.58	13.33	86.67	68.42	

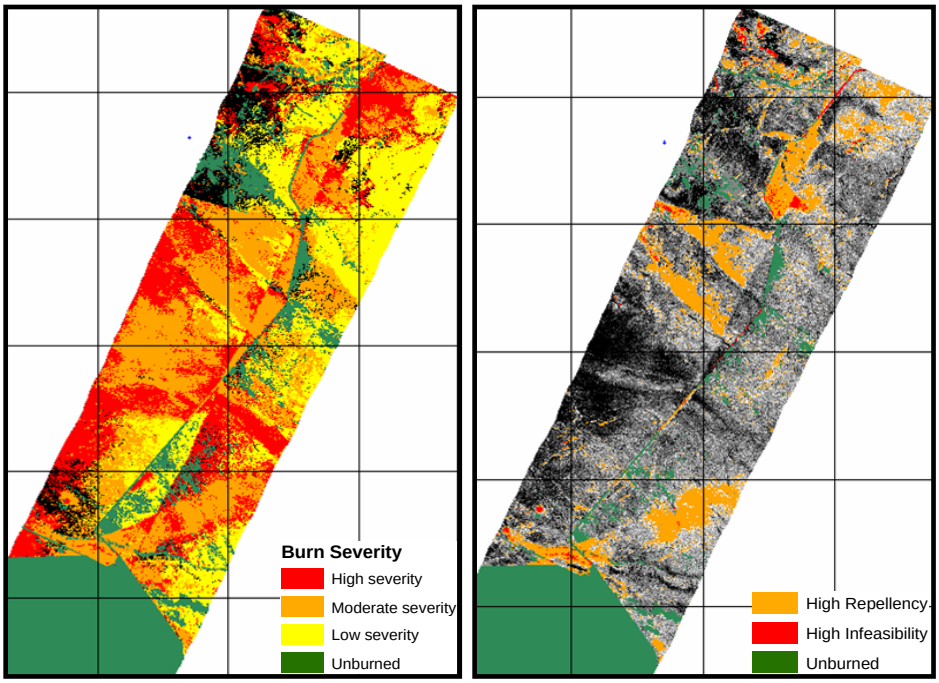

Figure A.5 A (left). SAM burn severity classification, section C.
Figure A.5 B (right). MTMF classification of soil water repellency, section C (MF score threshold 0.65-2.0). 1 square equals 2 km.

The lack of strong water repellency in Section C during field sampling was likely due to damage and dispersion of soil by the windstorms. A MTMF classification of water repellent soils was conducted on the mosaicked images of section C using the spectral endmembers of highly water repellent training sites assessed in section B. Due to the lack of field data, the MTMF could not be verified, but served as an indicator of areas most likely to exhibit soil water repellency (Fig. A.5 B). The MTMF classification detected 3.5% of the burned portion of section C to have highly water repellent soils, when a MF score threshold of 0.65-2 was used.

Appendix D. NAIP Aerial Photography Classification of Vegetation

To verify the areas being classified as shrub and/or grass, a supervised classification of the 2004 USDA National Agriculture Imagery Program (NAIP) true color ortho-photograph was employed to identify areas of shrub, grass, and bare ground, and used as a supplemental endmember identification layer. Because the HyMap imagery of the burned area appeared quite homogeneous and spectrally similar, it was difficult to remotely identify which of the burned areas were of grass, shrub, or a mixed shrub and grass area, especially in severely burned areas. For this reason, the NAIP classification was utilized to identify those areas.

The countywide NAIP images, which were flown in the summer of 2004, were obtained as MR SID compressed image files, subset to the study section areas with ArcGIS, and converted to TIFF format for use in ENVI. In ENVI, an interactive histogram stretch of the RGB brightness values allowed for the differentiation of the green shrub areas, and the higher reflectance, yellow grass areas, as well as areas of bare ground (Fig 1A). Regions of Interest (ROI's) were drawn among 3 classes: High reflectance bare ground, green sagebrush/shrub, and senesced yellow grass**.** Because the imagery was acquired during the summer, the majority of the grass had already reached senescence, allowing accurate detection after adjusting the RGB values.

A SAM classification was conducted of the subset image (Fig. 1B) using digitized ROI's as training areas. A maximum SAM angle of 1 radian was used for the grass and shrub classes, and a SAM angle of 2.5 was used for the bare ground class. The larger angle was used for the bare ground area because they tended to be under-classified, and grouped, or committed to, the grass areas. A comparison of Figure 1A and Figure 1B demonstrates the tendency for the bare ground to be under-classified.

Although the images contained features other than burned vegetation (asphalt, buildings, rock), they were not separated into different classes, because ENVI was unable to differentiate the dark reflectance of rock and asphalt from the shrub areas, and the buildings were inapplicable to the study. The accuracy of the vegetation classification was assessed with ground truth data from the field-collected sample plots of unburned or low severity areas, where the vegetation type was confidently assessed in the field, and the dominant vegetation group identified. The error matrix (Table A.10) indicates an overall accuracy of 90% and a Kappa coefficient of 0.78.

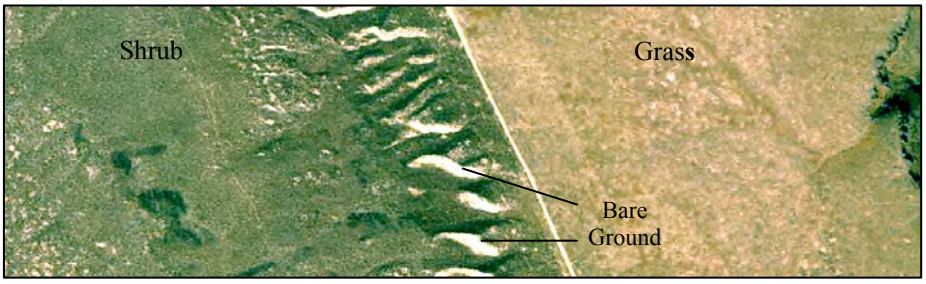

Fig A.6 A. Summer 2004 (pre-fire) NAIP aerial imagery utilized for validation of vegetation specific burn severity.

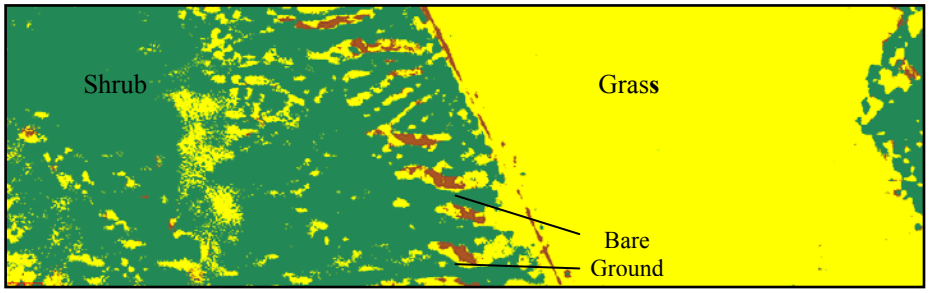

Fig A.6 B. SAM classification of the summer 2004 (pre-fire) NAIP aerial imagery. Yellow = grass, green = shrub, brown = bare ground.

Error Matrix, SAM Vegetation Classification				
Overall Accuracy = (25376/28265) 90% **Kappa Coefficient = 0.7804**				
Ground Truth (pixels)				
Class	**Bare Ground**	**Grass**	**Shrub**	**Total**
Unclassified	0	0	0	0
Bare Ground	4830	1585	62	6477
Grass	12	18427	648	19087
Shrub	392	190	2119	2701
Total	5234	20202	2829	28265
	Ground Truth (%)			
Class	**Bare Ground**	**Grass**	**Shrub**	**Total**
Unclassified	0	0	0	0
Bare Ground	92.28	7.85	2.19	22.92
Grass	0.23	91.21	22.91	67.53
Shrub	7.49	0.94	74.9	9.56
Total	100	100	100	100
Class	**Commission (%)**	**Omission (%)**	**Producers Accuracy (%)**	**Users Accuracy (%)**
Bare Ground	25.43	7.72	92.28	74.57
Grass	3.46	8.79	91.21	96.54
Shrub	21.55	25.1	74.9	78.45

Appendix E. GeoXT Customized GPS Data Collection Forms

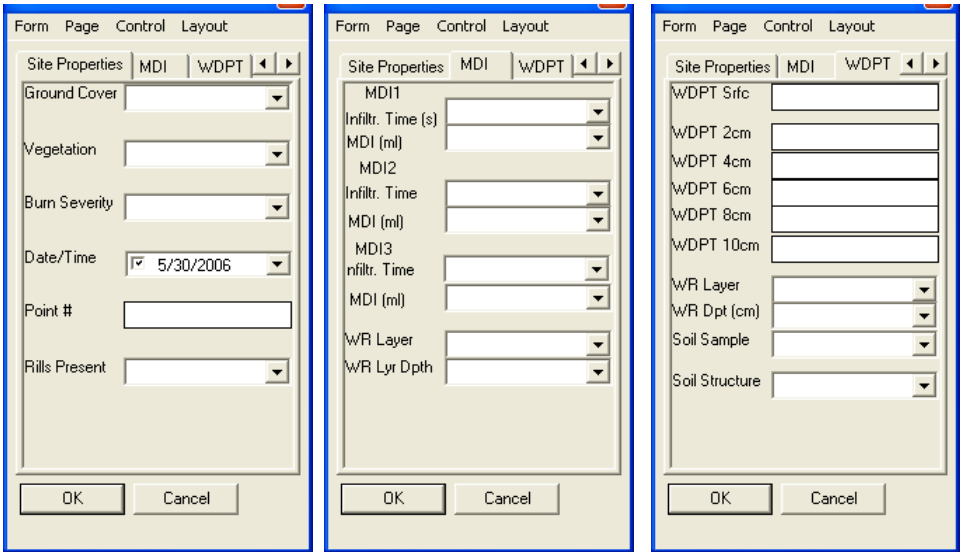

Figure A.7. Customized GeoXT data collection forms

Customized GPS data collection forms were created in ArcPad 6 (ESRI, 2005). The forms included drop-down menus and data entry boxes for the purpose of inputting data values assessed in the field.

Appendix F. Field Data

235 sample points were collected throughout sections A, B, and C. Tables A.11-A.13 list the burn severity and soil water repellency information recorded at each point. The water repellency information was recorded with the Water Drop Penetration Test (WDPT) and the Mini-Disc Infiltrometer (MDI).

Table A.11. Burn severity and soil water repellency field data, Section A.

Point	Vegetation	Severity	WDPT (seconds)				MDI (ml/min)
			Surface	2 cm	4 cm	6 cm	
1	Shrub	Unburned	0	0	0	0	4.00
2	Shrub	Unburned	0	0	0	0	6.33
3	Shrub	Unburned	30	0	0	0	6.67
4	Shrub	Unburned	0	0	0	0	8.00
5	Shrub	Unburned	0	0	0	0	9.00
6	Shrub	Unburned	0	0	0	0	10.00
7	Shrub	Unburned	0	0	0	0	10.00
8	Shrub	Unburned	2	0	0	0	10.33
9	Shrub	Unburned	0	0	0	0	10.33
10	Shrub	Unburned	0	0	0	0	13.67
11	Shrub	Unburned	0	0	0	0	13.67
12	Shrub	Unburned	0	0	0	0	16.67
13	Shrub	Low	360	0	0	0	4.67
14	Shrub	Low	360	0	0	0	5.33
15	Shrub	Low	0	0	0	0	5.33
16	Shrub	Low	0	0	0	0	6.33
17	Shrub	Low	0	0	0	0	6.33
18	Shrub	Low	360	0	0	0	7.00
19	Shrub	Low	0	0	0	0	7.00
20	Shrub	Low	0	0	0	0	7.33
21	Shrub	Low	30	0	0	0	7.67
22	Shrub	Low	0	0	0	0	7.67
23	Shrub	Low	5	0	0	0	7.67
24	Shrub	Low	0	0	0	0	8.67
25	Shrub	Low	0	0	0	0	9.00
26	Shrub	Moderate	360	360	0	0	1.00
27	Shrub	Moderate	360	360	5	0	2.33
28	Shrub	Moderate	360	60	0	0	2.67
29	Shrub	Moderate	60	60	45	0	3.00
30	Shrub	Moderate	360	10	5	0	3.00
31	Shrub	Moderate	360	30	0	0	3.00
32	Shrub	Moderate	30	360	5	0	3.33
33	Shrub	Moderate	30	360	60	5	3.67
34	Shrub	Moderate	360	30	0	0	4.00
35	Shrub	Moderate	360	10	0	0	4.67
36	Shrub	Moderate	120	0	0	0	4.67
37	Shrub	Moderate	360	10	0	0	5.00
38	Shrub	Moderate	60	0	0	0	5.67
39	Shrub	Moderate	360	15	10	0	6.00
40	Shrub	Moderate	360	110	30	5	6.00
41	Shrub	Moderate	360	30	0	0	6.00
42	Shrub	Moderate	60	0	0	0	6.00
43	Shrub	Moderate	10	0	0	0	6.67
44	Shrub	Moderate	360	13	15	15	6.67
45	Shrub	Moderate	360	60	5	0	7.33
46	Shrub	Moderate	60	0	0	0	7.33
47	Shrub	Moderate	60	45	5	0	7.67

48	Shrub	Moderate	360	30	0	0	8.00
49	Shrub	Moderate	120	5	0	0	8.33
50	Shrub	Moderate	360	15	0	0	3.00
51	Shrub	Moderate	30	0	0	0	4.00
52	Shrub	Moderate	20	0	0	0	4.67
53	Shrub	Moderate	360	60	10	0	4.67
54	Shrub	Moderate	30	0	0	0	5.33
55	Shrub	Moderate	60	5	0	0	8.00
56	Shrub	Moderate	60	5	0	0	8.00
57	Shrub	Moderate	15	0	0	0	8.33
58	Shrub	High	360	30	0	0	2.33
59	Shrub	High	360	360	0	0	2.33
60	Shrub	High	360	60	0	0	2.33
61	Shrub	High	360	360	30	0	3.00
62	Shrub	High	360	60	0	0	4.00
63	Shrub	High	60	0	0	0	4.00
64	Shrub	High	60	5	0	0	4.67
65	Shrub	High	360	30	0	0	4.67
66	Shrub	High	360	30	0	0	4.67
67	Shrub	High	360	360	0	0	4.67
68	Shrub	High	360	30	0	0	5.00
69	Shrub	High	0	0	0	0	5.33
70	Shrub	High	60	5	0	0	5.67
71	Shrub	High	30	0	0	0	5.67
72	Shrub	High	360	30	0	0	5.67
73	Shrub	High	5	0	0	0	5.67
74	Shrub	High	0	0	0	0	6.33
75	Shrub	High	0	0	0	0	6.67
76	Shrub	High	360	360	0	0	6.67
77	Shrub	High	30	0	0	0	7.33
78	Shrub	High	0	0	0	0	7.67
79	Shrub	High	30	0	0	0	7.67
80	Shrub	High	0	0	0	0	9.00
81	Shrub	High	30	0	0	0	9.33
82	Shrub	High	0	0	0	0	9.33
83	Shrub	High	0	0	0	0	10.00
84	Shrub	High	0	0	0	0	12.00
85	Shrub	High	10	0	0	0	15.00
86	Grass	Unburned	10	0	0	0	5.33
87	Grass	Unburned	2	0	0	0	8.00
88	Grass	Unburned	2	0	0	0	12.00
89	Grass	Low	0	0	0	0	4.33
90	Grass	Low	15	0	0	0	4.33
91	Grass	Low	30	0	0	0	6.33
92	Grass	Low	0	60	0	0	7.00
93	Grass	Low	0	0	0	0	9.67
94	Grass	Moderate	120	5	0	0	0.00
95	Grass	Moderate	360	25	0	0	2.00
96	Grass	Moderate	360	60	5	0	3.67
97	Grass	Moderate	360	20	0	0	4.00
98	Grass	Moderate	120	5	0	0	5.33
99	Grass	Moderate	360	360	30	0	6.00
100	Grass	Moderate	90	0	0	0	6.00
101	Grass	Moderate	30	0	0	0	6.33
102	Grass	Moderate	0	5	0	0	7.33

103	Grass	Moderate	0	0	0	0	8.00
104	Grass	High	60	0	0	0	5.33
105	Grass	High	360	30	20	0	5.67
106	Grass	High	0	360	60	0	5.67
107	Grass	High	5	60	0	0	6.67
108	Grass	High	60	0	0	0	6.67
109	Grass	High	5	120	0	0	7.33
110	Grass	High	0	0	0	0	7.33
111	Grass	High	0	120	0	0	7.67
112	Grass	High	10	360	0	0	8.00
113	Grass	High	15	60	0	0	9.00
114	Grass	High	0	90	0	0	9.00
115	Grass	High	0	60	0	0	9.33
116	Grass	High	0	120	0	0	9.67
117	Grass	High	0	0	0	0	10.33
118	Grass	High	0	0	0	0	11.33
119	Grass	High	10	15	10	0	13.00

Table A.12. Burn severity and soil water repellency field data, Section B.

			WDPT				
Point	**Vegetation**	**Severity**	**Surface**	**2 cm**	**4 cm**	**6 cm**	**MDI (ml/min)**
1	Shrub	Low	0	0	0	0	4.00
2	Shrub	Low	0	0	0	0	4.33
3	Shrub	Low	20	3	0	0	3.33
4	Shrub	Low	0	0	0	0	7.67
5	Shrub	Low	0	0	0	0	6.33
6	Shrub	Low	0	0	0	0	5.67
7	Shrub	Low	0	0	0	0	8.33
8	Shrub	Low	0	0	0	0	10.33
9	Shrub	Low	0	0	0	0	8.33
10	Shrub	Low	0	0	0	0	9.00
11	Shrub	Low	0	0	0	0	8.33
12	Shrub	Low	0	0	0	0	11.67
13	Shrub	Low	0	0	0	0	6.33
14	Shrub	Low	0	0	0	0	9.00
15	Shrub	Low	0	0	0	0	9.33
16	Shrub	Low	0	0	0	0	12.67
17	Shrub	Low	0	0	0	0	5.33
18	Shrub	Low	20	0	0	0	6.00
19	Shrub	Moderate	30	0	0	0	4.00
20	Shrub	Moderate	60	0	0	0	4.67
21	Shrub	Moderate	60	30	0	0	1.00
22	Shrub	Moderate	30	0	0	0	2.00
23	Shrub	Moderate	360	360	10	0	1.67
24	Shrub	Moderate	0	0	0	0	4.33
25	Shrub	Moderate	360	0	0	0	2.00
26	Shrub	Moderate	0	0	0	0	6.33
27	Shrub	Moderate	360	30	0	0	1.67
28	Shrub	Moderate	60	0	0	0	4.67
29	Shrub	Moderate	60	0	0	0	6.33

30	Shrub	Moderate	360	5	0	0	1.67
31	Shrub	Moderate	60	10	0	0	3.33
32	Shrub	High	15	0	0	0	6.00
33	Shrub	High	360	0	0	0	3.33
34	Shrub	High	0	0	0	0	4.00
35	Shrub	High	60	0	0	0	5.67
36	Shrub	High	0	0	0	0	6.33
37	Shrub	High	60	0	0	0	8.33
38	Shrub	High	0	0	0	0	4.00
39	Shrub	High	0	0	0	0	7.00
40	Shrub	High	360	5	0	0	3.67
41	Shrub	Moderate	30	0	0	0	8.33
42	Shrub	Moderate	360	0	0	0	6.33
43	Shrub	Moderate	0	0	0	0	4.00
44	Shrub	High	30	0	0	0	5.00
45	Shrub	High	360	0	0	0	1.33
46	Shrub	High	30	0	0	0	2.67
47	Shrub	Moderate	60	10	0	0	3.33
48	Shrub	Moderate	360	60	0	0	3.33
49	Shrub	Moderate	120	60	0	0	1.67
50	Shrub	Moderate	360	0	0	0	4.67
51	Shrub	Moderate	60	0	0	0	4.67
52	Shrub	Moderate	60	0	0	0	3.67
53	Shrub	High	360	30	0	0	1.67
54	Shrub	High	360	0	0	0	4.67
55	Grass	Unburned	5	0	0	0	5.67
56	Grass	Unburned	5	0	0	0	6.33
57	Grass	Unburned	0	0	0	0	5.00
58	Grass	Unburned	0	0	0	0	3.67
59	Grass	Unburned	0	0	0	0	2.67
60	Grass	Unburned	0	0	0	0	3.00
61	Grass	Unburned	0	0	0	0	2.67
62	Grass	Unburned	0	0	0	0	2.67
63	Grass	Low	0	0	0	0	6.67
64	Grass	Low	0	0	0	0	3.00
65	Grass	Low	0	0	0	0	3.67
66	Grass	Moderate	120	5	0	0	5.00
67	Grass	Moderate	360	10	0	0	2.33
68	Grass	Moderate	5	0	0	0	5.33
69	Grass	Moderate	360	15	0	0	5.00
70	Grass	Moderate	120	60	0	0	0.67
71	Grass	Moderate	360	60	0	0	1.33
72	Grass	Low	0	0	0	0	4.00
73	Grass	Low	0	0	0	0	7.33
74	Grass	Low	0	0	0	0	5.00
75	Grass	Low	0	0	0	0	4.67
76	Grass	Low	0	0	0	0	2.33
77	Grass	Low	0	0	0	0	4.00
78	Grass	High	0	30	0	0	4.00

79	Grass	High	30	60	0	0	4.33
80	Grass	High	0	30	0	0	3.67
81	Grass	Unburned	15	0	0	0	6.67

Table A.13. Burn severity and soil water repellency field data, Section C.

Point	Vegetation	Severity	WDPT Surface	2 cm	4 cm	6 cm	MDI (ml/min)
1	Shrub	Low	0	0	0	0	4.33
2	Shrub	Low	0	0	0	0	4.67
3	Shrub	Low	0	0	0	0	5.33
4	Shrub	Low	0	0	0	0	4.00
5	Shrub	Low	0	0	0	0	7.67
6	Shrub	Low	0	0	0	0	4.00
7	Shrub	Moderate	60	10	0	0	3.33
8	Shrub	Moderate	360	60	0	0	3.33
9	Shrub	Moderate	120	60	0	0	1.67
10	Shrub	Moderate	360	0	0	0	4.67
11	Shrub	Moderate	60	0	0	0	4.67
12	Shrub	Moderate	60	0	0	0	3.67
13	Shrub	High	360	30	0	0	1.67
14	Shrub	High	360	0	0	0	4.67
15	Shrub	Low	0	0	0	0	5.67
16	Shrub	Low	0	0	0	0	3.67
17	Shrub	Low	0	0	0	0	5.67
18	Shrub	Low	0	0	0	0	3.00
19	Shrub	Moderate	30	0	0	0	4.33
20	Shrub	Moderate	30	0	0	0	3.67
21	Shrub	Moderate	0	0	0	0	4.33
22	Shrub	Moderate	360	30	5	0	5.00
23	Shrub	Moderate	60	10	0	0	2.67
24	Grass	Low	0	0	0	0	4.67
25	Grass	Low	0	0	0	0	2.33
26	Grass	Low	0	0	0	0	4.00
27	Grass	High	30	0	0	0	4.00
28	Grass	High	30	0	0	0	4.33
29	Grass	High	30	0	0	0	3.67
30	Grass	Low	0	0	0	0	5.67
31	Grass	Low	0	0	0	0	8.00
32	Grass	Low	0	0	0	0	5.67
33	Grass	Low	0	0	0	0	6.67
34	Grass	Low	0	0	0	0	6.00
35	Grass	Low	360	0	0	0	3.67